Material Characterization of Cardiovascular Biomaterials using an Inverse Finite Element Method

by

Miriam Nightingale

A thesis submitted to the

Faculty of Graduate and Postdoctoral Studies

in partial fulfillment of the requirements for the degree of

Master of Applied Science in Biomedical Engineering

The Ottawa-Carleton Institute for Biomedical Engineering

University of Ottawa

Ottawa, Canada

May, 2017

© Miriam Nightingale, Ottawa, Canada, 2017

Abstract

Being able to accurately model soft tissue behaviour, such as that of heart valvular tissue, is essential for developing effective numerical simulations of in-vivo conditions and determining patient-specific care options. Although several analytical material models, based on strain energy functions, have been successful in predicting soft tissue behaviour, complications arise when these models are implemented into finite element (FE) programs due to the incorporation of a penalty parameter for numerically enforcing material incompressibility. Specifically, material parameters determined through non-FE methods may no longer produce a material behaviour that reflects the experimental behaviour once they are used in an FE analysis. Based on commercial finite element software LS-DYNA, an inverse methodology was developed in MATLAB to simultaneously optimize the material parameters and the penalty parameter for the Guccione strain energy model. The methodology produced accurate predictions of the material behaviour under planar equibiaxial testing for five biomaterials used in heart valve cusp replacements.

Table of Contents

Abstract ii

List of Figures vi

List of Tables ix

1 Introduction 1

1.1 Soft tissue 2

1.2 Objective 6

1.3 Contributions 7

1.3.1 Modeling biaxial testing of soft tissue using an explicit solver 7

1.3.2 Novel approach for determining the material parameters using an inverse finite element approach 8

1.4 Thesis organization 9

2 Literature review 11

2.1 Material characteristics of soft tissue 12

2.2 A theoretical framework 13

2.3 Strain energy functions 16

2.3.1 The Neo-Hookean model 17

2.3.2 The Fung model 17

2.3.3 The Guccione model 18

2.3.4 The Holzafel, Gasser, and Ogden model 19

2.4 Determining the value of material parameters 20
2.4.1 Uniaxial and biaxial testing 21
2.4.2 Solid and hollow cylinders 23
2.4.3 Indentation 24
2.4.4 Inverse finite element method 25
2.5 Evaluating predictive capabilities of material models 26
2.6 Potential for improvements 27
3 Experimental and FE model set up 28
3.1 Experimental testing 28
3.1.1 Experimental Green strain and Second Piola-Kirchoff (P-K) membrane tension 30
3.2 FE model 33
3.2.1 Simulated Green strain and Cauchy stress 34
3.2.2 Initial run 35
3.2.3 Error Function 40
4 Optimization 44
4.1 Initial runs 44
4.2 Optimization with *fmincon* 47
4.2.1 Constraints on the material parameters 48
4.2.2 Upper and lower bounds used with *fmincon* 51
5 Results and discussion 58

5.1 Optimization of material constants 58

5.1.1 Two-constant Optimization 59

5.1.2 Five-constant Optimization 64

5.2 Effects of actual sample thickness 69

5.3 Analyzing a quarter of the elements in the FE model 71

5.4 Program capabilities 74

5.4.1 Importance of initial guesses 79

5.5 Individual roles of Guccione's strain energy material parameters 81

6 Conclusion and future work 88

6.1 Summary of findings 88

6.2 Future work 90

References 92

Appendix A: Simulated Material Responses 96

Appendix B: MATLAB Programs 103

List of Figures

Figure 1.1: Schematic Stress-Strain curve for skin with diagram showing collagen fiber arrangement..... 4

Figure 1.2 Typical material behaviour curves for biological soft tissue [7]. Biaxial testing is usually either force-controlled or displacement-controlled. 5

Figure 3.1**:** Sample from fresh porcine AV leaflet and tissue sample testing set up [7]. 29

Figure 3.2: Experimental results for planar biaxial testing averaged over the nine experimental protocols for the five materials [7]..... 33

Figure 3.3: Example brick element used in LS-DYNA, the material properties in nodes 1 to 2 direction relate to the material properties along the fibres while the cross fibre material properties are applied in the nodes 1 to 4 directions..... 37

Figure 3.4: Geometry of material sample 39

Figure 3.5: The comparison of simulated responses through the optimization of c and K ($cK=P$) for the material SJM when implementing just point difference error (left) versus point difference and curvature ratios (right)..... 42

Figure 3.6: Diagram showing how curve ratio was determined in the error function. 42

Figure 3.7: Comparison of the simulated responses for the material GPP using the last third of the data set (left) versus three quarters of the data set (right) to calculate curvature for the error. 43

Figure 4.1: Optimized simulated material behaviour for CC using the *fmincon* function only for two constant optimization. 45

Figure 4.2: Effect on the simulated response from a change of constant c for SJM. 46

Figure 4.3: Effect on the simulated response from a change in constant K for SJM..... 46

Figure 4.4: The constraints for a problem using *fmincon* in MATLAB [23]. 47

Figure 4.5: The simulated material response of SJM (left) using the upper bound C value and PC(right) using the lower bound, which had the largest and smallest experimental responses respectively. 52

Figure 4.6: The effects on the material response from a change at high *K* values for the material SJM. 53

Figure 5.1: FE model of GPP showing y-axis displacement for equibiaxial testing 59

Figure 5.2: Simulated and experimental response of GPP through the optimization of *c* and *K*. 61

Figure 5.3: Simulated and experimental responses for APP through the optimization of *c* and *K*. 63

Figure 5.4: Comparison of the simulated response through two-constant (left) and five-constant optimization (right) for SJM. 67

Figure 5.5: Simulated response for GPP using a 1 mm undeformed thickness (left) versus 0.2 mm thickness (right) through the optimization of *c* and *K*. 70

Figure 5.6: Comparison of the simulated responses for GPP using all elements (left) versus only a quarter of the elements (right) through the optimization of *c* and *K*. 73

Figure 5.7: Comparison of the simulated responses for APP using all elements (left) versus aquarter of the elements (right) through the optimization of *c* and *K*. 74

Figure 5.8: Comparison of the experimental and analytically derived responses (left) and the experimental and LS-DYNA simulated responses (right) for APP [7]. 77

Figure 5.9: Simulated response from two constant optimization with a manual increase in the optimized *K* from ~$5x10^8$ to $8x10^8$ for SJM (left) and ~$9x10^8$ to $2x10^9$ for APP (right). 78

Figure 5.10: Simulated response for APP through two constant optimization from starting c of $9x10^{-4}$ MPa. 80

Figure 5.11: Comparison of simulated response of CC with a change of $1x10^{-3}$ in *c*. 83

Figure 5.12: Comparison between simulated response of CC for different b_1. 84

Figure 5.13: Comparison between simulated response of CC for different b_2. 85

Figure 5.14: Comparison of simulated responses of CC with a change in b_3. 86

Figure 5.15: Comparison of the simulated response through two constant optimization of CC with a change in *K*. 87

Figure A.1: Simulated response for GPP through the optimization of *c* and *K*. 96

Figure A.2:Simulated response for PC through the optimization of *c* and *K*. 96

Figure A.3: Simulated response for CC through the optimization of *c* and *K*. 97

Figure A.4: Simulated response for APP through the optimization of *c* and *K*. 97

Figure A.5: Simulated response for SJM through the optimization of *c* and *K*. 98

Figure A.6: Simulated response for GPP through the optimization of all five parameters. 99

Figure A.7: Simulated response for PC through the optimization of all five parameters. 100

Figure A.8: Simulated response for CC through the optimization of all five parameters. 100

Figure A.9:Simulated response for APP through the optimization of all five parameters. 101

Figure A.10:Simulated response for SJM through the optimization of all five parameters. 102

List of Tables

Table 5.1: Optimized material constants from the two-constant optimization program 60

Table 5.2: Optimized material constants from the five-constant optimization program 65

1 Introduction

With the increase in the aging population across the world, there will only be more instances of age-related illnesses. By 2030, it is projected that a quarter of the population in the developed world will be above 60 years of age, with one in six people being over 60 globally [1]. This demographic shift will produce a significant burden on healthcare especially for countries with public healthcare systems such as Canada. The need to maximize the efficiency of these systems, such as increasing the use of preventive medicine, minimizing wait times, and increasing surgery success rate becomes apparent.

A recent focus in the biomedical engineering field has been to maximize the efficiencies of medical procedures through numerically simulating in-vivo conditions. Many surgery procedures like heart valve repair involve trial and error, with the surgeon performing multiple modifications on the geometry of the valve then testing its functionality [2]. The success rate of this procedure relies heavily on the experience of the surgeon. However, if there was a way to already know the geometry that would restore functionality before the surgery, this technically difficult procedure could become straightforward with a surgeon only needing to follow a predetermined set of steps. Being able to effectively simulate in-vivo conditions would allow several valve geometry scenarios to be tested and the appropriate modification chosen before surgery. This addition could potentially lead to a decrease in surgery time and an increase in success rate. Heart valve repair surgery is just one example of a medical procedure that could be improved with the ability to simulate in-vivo conditions. In general, such ability could be used as either a diagnostic tool or to evaluate surgical intervention, allowing for less invasive surgeries with higher success rates.

For a simulated model to be representative of the physical object, and therefore to be useful, there needs to be confidence that it will behave in the same way as the object in real life would under the same conditions. Four main criteria must be considered for an accurate model: the object's geometry, its boundary conditions and loading, and its material behaviour. Having the appropriate geometry, with a focus in patient specific geometry, is essential given how closely tied shape and functionality are in the human body. Boundary conditions as well as loading that reflect patient specific in-vivo conditions again play an important role. Indeed, changes in boundary and load conditions, such as an increase in blood pressure over an extended period of time, can have significant effects on an organ's function. A simulated material must also behave as the physical material does in vivo to be effective. Discrepancies between how the material physically responds to an external force and how the simulated model predicts how the material will behave can have grave consequences. For example, if aortic tissue is simulated to be more elastic than seen in vivo, this could lead to inaccurate predictions of the amount of stress that would cause rupture. Although to effectively simulate in-vivo conditions geometry, boundary conditions, loading and material behaviour must be considered, this thesis will focus only on accurately predicting material behaviour in simulated models, specifically predicting hyperelastic anisotropic soft tissue behaviour.

1.1 Soft tissue

Soft tissue is an all-encompassing term for any biological tissue that is not mineralized i.e. does not have a firm extracellular matrix like bone or cartilage [3]. This definition includes a wide variety of tissues such as tendons, muscles, skin, fat and blood vessel, each with their own composition and function. Although soft tissue can be many different specific materials, the composition of soft tissue can generally be described as a fibre-reinforced composite [4].

The material behaviour of soft tissue is mainly dictated by the amount and position of collagen and elastin in the tissue [4]. Collagen and elastin are both proteins found in the extracellular matrix [4]. Collagen is responsible for supporting loads in most soft tissues while elastin allows the material to stretch under stress. The composition of elastin and collagen varies between soft tissues depending on function. Tendons are the connective tissue between bones and muscle. The collagen in tendons is arranged in parallel fibres to support the transfer of load from muscle to bone [5]. Since tendons' main function is to support, their compositions contains ~80% collagen by dry weight and less than 3% elastin making them the stiffest of soft tissues [4]. In comparison, aortic tissue has some of the highest percentages of elastin, accounting for ~45% of dry weight and collagen for ~30% [4]. The high elastin content could be due to the aorta having to withstand the pulsatile flow of blood, with the aorta regularly experiencing large changes in cross-sectional area.

Still, there are some common material characteristics experienced across soft tissues. Soft tissues generally display non-linear behaviour. Unlike typical engineering materials such as steel which begins experiencing plastic deformation at 0.2% of its undeformed length, soft tissue can undergo large deformations during regular in-vivo conditions while still maintaining its original shape. Tendons for example can experience deformations around 2.5% of their undeformed length during typical loading [6]. Materials that experience large elastic (i.e. recoverable) deformations upon loading are considered as hyperelastic materials.

The nonlinear mechanical behaviour of soft tissues can be explained as follows. In many soft tissues, the collagen fibres are not straight but appear wavy or crimped when unloaded. When there is a load placed on the soft tissue, the collagen fibres begin to straighten, causing the material to deform while not actually stretching the collagen or having it bear load, except

through the contribution of the stretchier elastin. The stress on the material only begins to significantly increase once the collagen is straight and bearing the load. The uncrimping effect causes the material to become stiffer as deformation increases. The non-linear stress-strain relationship for skin is illustrated in Figure 1.1.

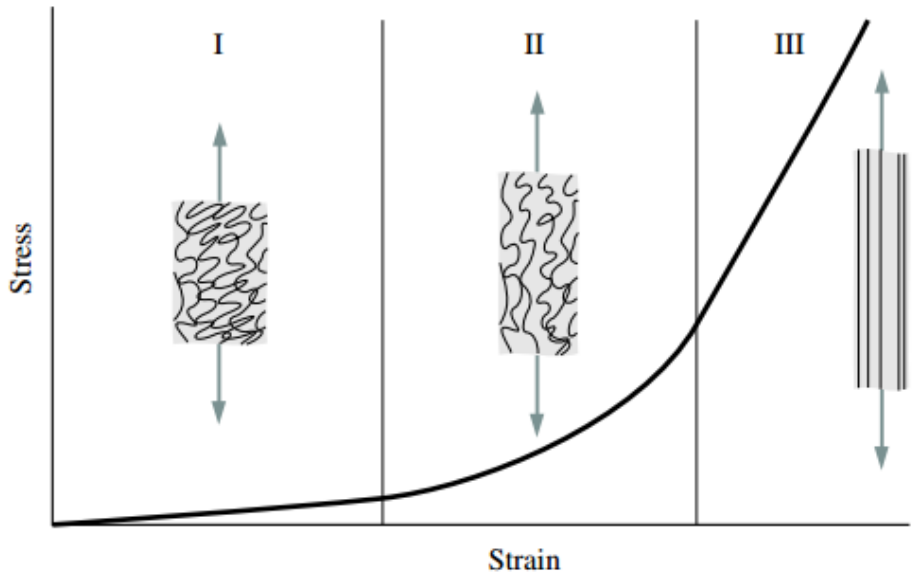

Figure 1.1: Schematic Stress-Strain curve for skin with diagram showing collagen fiber arrangement

Due to the fibre arrangements of collagen in soft tissue, the mechanical behaviour of the material varies depending on the direction of the load. As mentioned above, collagen is the main load bearing and stiffest component of soft tissue, therefore soft tissue will experience less deformation from the same load if that load is applied along the collagen fibres versus in the cross-fibre direction [4]. In Figure 1.1, the collagen fibres in the skin appear to be in one direction; however, in physical soft tissue there is less of a defined structure. Although the collagen fibres in soft tissue do have a preferred direction usually along the main load path, there

are collagen fibres in other orientations to counteract other less dominating loads such as shearing [4]. This structure of fibre arrangements would have the mechanical behaviour of the soft tissue varying with almost every small change in orientation. It is generally unrealistic to model soft tissue as a purely anisotropic material and account for every change in orientation; instead material models of soft tissue generally consider the material to be transversely isotropic. As seen in Figure 1.2, soft tissue material may be described along two directions; the main collagen fibre direction and the cross-fibre direction. The mechanical behaviour across the width and thickness of the fibres is assumed to be the same.

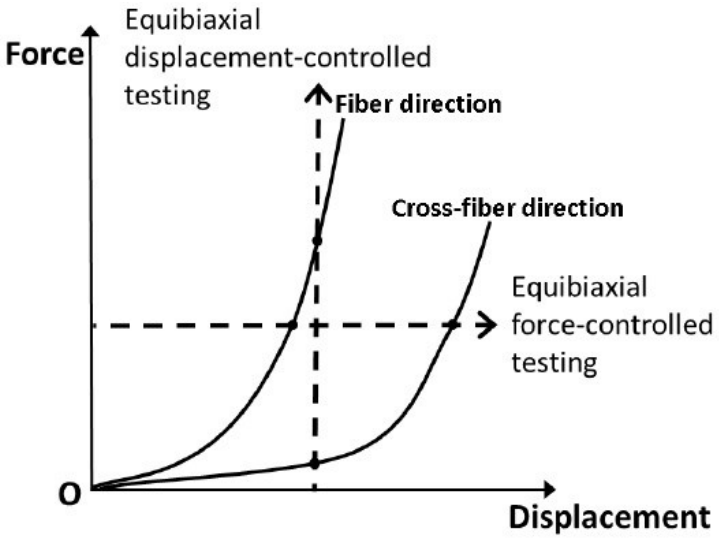

Figure 1.2 Typical material behaviour curves for biological soft tissue [7]. Biaxial testing is usually either force-controlled or displacement-controlled.

When attempting to numerically simulate soft tissue behaviour, hyperelasticity and anisotropy significantly complicate the process. Whereas with metals in the elastic range, the material behaviour can generally be defined mathematically by a stiffness or elastic modulus, this way of describing soft tissue is impractical. Even with the assumption of transverse isotropy,

the stiffness of soft tissue takes the form of a fourth order-tensor [8], and is dependent on strains. Therefore, a need has arisen to develop accurate mathematical models to describe soft tissue for the purpose of simulating and modeling in-vivo conditions.

1.2 Objective

In recent years, there has been a significant amount of research in attempting to determine material models for predicting soft tissue behaviour. Hyperelastic materials can be described by a so-called strain energy function, such that stress is the partial derivative of the strain energy function with respect to strain. Several strain energy models have been developed with a series of material parameters that are material-specific [9]. These material parameters have been determined analytically through numerical regression with some success; however, pure analytical models are limited in their application (simple shapes such as flat membranes or cylinders) and must generally be transferred into a finite element (FE) model to be considered practical. However, issues arise when analytically optimized material parameters produce reasonable material behaviour when compared with experimental results, but produce simulated responses that no longer reflect the material's experimental behaviour once implemented into FE models.

The purpose of this thesis was to develop an optimization program for determining material parameters to produce an FE-simulated response that would reasonably reflect the experimental material behaviour of soft tissue. Thus the new optimized material constants could be used to predict soft tissue behaviour and simulate in vivo conditions in FE programs.

1.3 Contributions

The following contributions are presented in this thesis:

1.3.1 Modeling biaxial testing of soft tissue using an explicit solver

When performing a dynamic FE analysis, like the simulated planar biaxial test presented in this thesis, the needed equilibrium equations can be integrated in the time domain using either implicit or explicit methods to determine displacements [10]. For the explicit method, the equilibrium equations at a time t, with already known displacements, are used to determine displacements at time $t + \Delta t$ [11]. The implicit method, on the other hand, determines the displacements at time $t + \Delta t$ from equilibrium equations at a time t, with unknown displacements [11]. Therefore, when using the implicit method, the equilibrium equations must be solved at each time step making it computationally demanding compared to the explicit method [10].

Common implicit methods are considered unconditionally stable as the time step size Δt is chosen to satisfy accuracy and convergence considerations [10]. Common explicit methods, such as the central difference method, are only conditionally stable unlike the implicit method: the time step size must be smaller or equal to a critical time step to avoid losing stability in the system [11]. This can lead to the solver picking small time steps, making implicit methods typically more desirable [11].

However, with nonlinear responses such as the case with soft tissue behaviour, explicit methods become preferred for solving equilibrium equations. Implicit methods like the trapezoidal rule, that are stable in linear analysis become unstable for nonlinear analysis especially over a long response time or when there are large deformations, and they can produce

unrealistic displacements [11]. On the other hand, the non-linearity of soft tissue works in favour of the explicit solvers because the critical time step needed for stability is inversely proportional to the square root of the elastic modulus of the material [10]. This means that soft tissue with low elastic moduli and large deformations may produce larger time steps for analysis, thereby mitigating the drawback of explicit solving methods.

Most inverse finite element models for soft tissue use implicit methods in their mostly static analyses. However, one of the eventual applications of the present work includes the FE analysis of heart valves, which feature large deformations of hyperelastic anisotropic materials, contact issues, in dynamics. Such characteristics are typically better handled by explicit FE solvers.

In this thesis, the FE analyses modelled equibiaxial tests. Experimentally determined displacements were applied in two orthogonal directions to a square tissue sample. The tissue's samples edges were aligned with the fibre and cross-fibre direction. LS-DYNA (LS-DYNA R8.1.0; LSTC, Livermore, CA, USA), the FE commercial software used in this thesis, is widely trusted for instance by the automotive industry to simulate crashes between multiple cars, as well as air-bag deployments.

1.3.2 Novel approach for determining the material parameters using an inverse finite element approach

Strain energy functions are used to describe the material behaviour of soft tissues. For this thesis, the material parameters for a specific strain energy function were optimized through an inverse finite element method started from user-inputted guesses. Given that the effectiveness of any optimization algorithm is generally heavily reliant on determining an appropriate starting point, an initial set of 25 runs of finite element simulations was implemented using variations in two

material parameters. This allowed the error between the simulated and experimental responses to be "pre-minimized" even before the implementation of the MATLAB optimization function fmincon, and greatly increased the chances of the program producing an accurate simulated response. A scalar error function was also introduced for the optimization process; it included not only the point-by-point difference between the simulated and experimental responses, but also the error between the curvatures in the stress-strain curves as well. This addition was found to increase the chances of the optimized parameters producing realistic material behaviour.

The so-called Lagrange multiplier P is a penalty term added to the strain energy model to enforce incompressibility in most, if not all finite element implementations [12]. It is current practice to assume a large P, usually in the region of 10^3c-10^4c where c is the scaling constant in the strain energy model [12]. The other constants of the strain model are then optimized using this assumed value of P. However, in this thesis, the Lagrange multiplier was not kept at a constant value but optimized as an additional material parameter of the strain energy model used in combination with commercial finite element code LS-DYNA. This approach allowed for the P value to vary depending on the material being tested, thus developing a more robust, versatile and automated program for the identification of material constants. A new range of acceptable P values was proposed in replacement of the traditionally assumed one for use in LS-DYNA modeling.

1.4 Thesis organization

The remainder of the thesis is organized as follows:

Chapter 2 provides an overview of the process behind establishing a soft tissue material model; the different methods currently available are discussed and gaps in the current research are identified.

Chapter 3 provides an overview of the procedure for determining the experimental material behaviour data used in this thesis, how the optimization program simulates the experimental conditions in LS-DYNA and how it compares the determined simulated response with the experimental one.

Chapter 4 discusses the optimization process for determining the material parameters from FE simulations, in a so-called inverse method process.

Chapter 5 details the results of this research and discusses the capabilities of the optimization program that was devised and of the material parameters that were outputted.

Chapter 6 presents the conclusion of this research and provides recommendations for future work.

Appendix A presents the simulated material responses for all the materials tested for both the two- and five-constant optimization methods.

Appendix B details the MATLAB code of the optimization program for the five-constant optimization method.

2 Literature review

The material behaviour of soft tissue is often described through continuum-based constitutive models. The continuum hypothesis assumes the general behaviour of the overall material can be approximated using averaged local behaviour. This allows for the material to be described by an overall continuous or piece-wise continuous function based on the properties of many smaller homogenous elements. This assumption holds when the size of the microstructure is significantly smaller than the size of the material sample being modelled i.e. $\delta << l$, where δ is the characteristic length of the microstructure and l is the length of the sample [8]. For soft tissue material, the diameter of the collagen fibres would be on the order of micrometers, whereas the thickness of the material samples would be in millimetres, giving the ratio of δ/l on the order of 10^{-3}. The continuum hypothesis is thought to be applicable with a ratio of $\delta/l < 0.01$ thus it is reasonable to use a continuum model for soft tissue characterization [8].

In the context of material characterization, constitutive models describe the behaviour of a material when exposed to external loading through mathematical relations. There are five general steps to developing a constitutive model for a material: 1) Delineate general characteristics of the material; 2) Establish appropriate theoretical framework; 3) Identify a specific functional form for the relation; 4) Calculate the values of the material parameters; 5) Evaluate the predictive capability of the final relation [8]. There is a general consensus in the biomedical engineering field on the properties of soft tissues as well as the theoretical framework for modeling; however, there are many variants for determining material models and evaluating the material's parameters. This literature review will discuss these different aspects.

2.1 Material characteristics of soft tissue

The first step for developing a constitutive model would be defining the characteristics of the material for the loading conditions of interest. Some defining characteristics would be: determining whether the material has elastic deformation, is isotropic or anisotropic, or the phase (e.g. solid or liquid). The material of interest in this case is biological soft tissue or materials with soft tissue-like properties. As mentioned previously, soft tissue is a solid material with elastic behaviour defined as hyperelastic, it is generically quantified based on a strain energy function instead of directly relating the stress and strain through the material's stiffness [8]. This is because typical linear elastic models cannot accurately describe large, anisotropic deformations experienced by soft tissue. Soft tissue can also be defined as homogeneous through the application of the continuum hypothesis; therefore, it is assumed the material's response is uniform regardless of position within the material, or at least away from attachments or end conditions. Material classification also involves defining kinematic constraints, mainly if the material is incompressible [8]. Due to its large water content (70% or more), soft tissue would be described as nearly incompressible except under extreme pressure or velocity [8]. Given that the material samples being examined in the experimental or analytical tests are under physiological conditions, these extreme conditions would not be present. Although no material can be truly incompressible, for example soft tissue's volume can shrink/expand due to temperature change, the constitutive material model currently being defined is for stress-strain relation, the effects from thermal stress and other external forces are considered negligible [8]. With these characteristics in mind, a theoretical framework for the material model can be determined.

2.2 A theoretical framework

As mentioned, hyperelastic material models are generally described through a strain energy function *W*, defined as the quantity of recoverable energy stored in the material as it deforms [8]

For determining a strain energy model, the conservation of energy must first be examined. The first law states that the total energy of the material, internal and kinetic, must be equal to the work being done on the material from external forces and heat being added, with respect to time. The scalar energy equation can then be described as

$$\rho_o \frac{d\varepsilon}{dt} = \boldsymbol{P}^T : \frac{d\boldsymbol{F}}{dt} - \nabla_o \cdot \boldsymbol{q_o} + \rho_o g \tag{2.1}$$

where ρ_o is the (scalar) mass density of the material, ε is the (scalar) internal energy density per unit mass, $\boldsymbol{P}$ is the first Piola-Kirchoff stress tensor, the : sign represents the double dot product (yielding a scalar from two tensors), $\boldsymbol{F}$ is the transformation gradient tensor of the deformed state with respect to the undeformed state, ∇_o is the del operator, q_o is the heat flux vector, both are with respect to the undeformed state, the dot product is the regular scalar product, and g is the (scalar) heat addition per unit mass. The internal energy of the material can be broken down into an equation relating to the scalar Helmholtz potential ψ, and (scalar) entropy η, such that $\varepsilon = \psi + \eta T$ where T is temperature. Thus, the second law of thermal dynamics for the material can be rewritten as the Clausius-Duhem equation [13]

$$-\rho_o \left(\frac{d\psi}{dt} + \eta \frac{dT}{dt}\right) + \boldsymbol{P}^T : \frac{d\boldsymbol{F}}{dt} - \frac{1}{T}\boldsymbol{q_o} \cdot \nabla_o T \geq 0 \tag{2.2}$$

From Equation (2.2), it can be seen that the Helmholtz potential, entropy, stress, deformation and heat flux would all need to be determined to develop a constitutive model for material behaviour. However, given that the material model being developed is only analyzing the behaviour of soft

tissue in isothermal conditions, the temperature is assumed to be constant and there is no heat flux. Therefore, the second law can then be reduced to

$$-\rho_o \frac{d\psi}{dt} + \boldsymbol{P}^T : \frac{d\boldsymbol{F}}{dt} \geq 0 \tag{2.3}$$

The energy of the material then relates to Helmholtz potential, stress, and deformation. If the inequality in Equation (2.3) is replaced with an equality as the material is assumed to have a reversible elastic response, then the internal energy/Helmholtz potential can be related to the deformation of the material.

$$\frac{\boldsymbol{d\psi}}{\boldsymbol{dt}} = \frac{\boldsymbol{d\psi}}{\boldsymbol{dF}} : \frac{\boldsymbol{dF}}{\boldsymbol{dt}} \tag{2.4}$$

where

$$\frac{\boldsymbol{dF}}{\boldsymbol{dt}} = \boldsymbol{L} \cdot \boldsymbol{F} \tag{2.5}$$

$\boldsymbol{L}$ is the velocity gradient tensor of the material as it deforms [8]. Thus Equation (2.3) becomes

$$\left(-\rho_o \frac{d\psi}{d\boldsymbol{F}} + \boldsymbol{P}^T\right) : \frac{d\boldsymbol{F}}{dt} = 0 \; \forall \; \boldsymbol{F} \tag{2.6}$$

Since $\frac{d\boldsymbol{F}}{dt}$ could be any set of tensors, a sufficient condition for this equation to hold is to have the part in the brackets equated to zero. Therefore, the first Piola-Kirchoff stress tensor is directly relatable to the Helmholtz potential, and is not an independent constitutive function.

$$\boldsymbol{P}^T = \rho_o \frac{d\psi}{d\boldsymbol{F}} \text{ or } \boldsymbol{P} = \rho_o \frac{d\psi}{d\boldsymbol{F}^T} \tag{2.7}$$

From Equation (2.7) it can be seen that isothermal hyperelastic behaviour of a homogeneous material can be described by one constitutive function $\psi = \psi(\boldsymbol{F})$, therefore the strain energy

function $W = W(\boldsymbol{F})$ can also be used to describe this type of material, as strain energy can be related to the Helmholtz potential through the first law, for isothermal loading conditions.

$$\rho_o \psi(\boldsymbol{F}) = W(\boldsymbol{F}) \tag{2.8}$$

Where strain energy is in per unit volume, Helmholtz potential is defined as per unit mass. Thus strain energy can relate stress and the transformation gradient tensor $\boldsymbol{F}$ for hyperelastic models. Therefore, it is important to describe the strain energy in terms of $\boldsymbol{F}$, but in ways that excludes rigid body motion. It is also more convenient to develop a strain energy model that relates the 2nd Piola-Kirchoff stress tensor $\boldsymbol{S}$, and the Green strain tensor $\boldsymbol{E}$, as the experimental behaviour of hyperelastic materials are generally defined by these parameters. $\boldsymbol{F}$ can be decomposed such that $\boldsymbol{F} = \boldsymbol{R} \cdot \boldsymbol{U}$; where tensor $\boldsymbol{R}$ accounts for the rigid body motion and tensor $\boldsymbol{U}$ defines the deformation within the body. Hence, it is more beneficial to define deformation in terms of the right Cauchy-Green deformation tensor $\boldsymbol{C}$, as it only relates to deformation within the body/material instead of the transformation gradient, $\boldsymbol{F}$ [8]. $\boldsymbol{C}$ is also symmetric by definition

$$\boldsymbol{C} = \boldsymbol{F}^T \cdot \boldsymbol{F} = \boldsymbol{U}^T \cdot \boldsymbol{R}^T \cdot \boldsymbol{R} \cdot \boldsymbol{U} = \boldsymbol{U}^2 \tag{2.9}$$

Then, Equation (2.7) becomes

$$\boldsymbol{P} = 2\frac{\partial W}{\partial \boldsymbol{C}} \cdot \boldsymbol{F}^T \tag{2.10}$$

The 2nd P-K stress tensor relates to the 1st P-K stress tensor through the inverse transpose of the transformation gradient [8],

$$\boldsymbol{S} = \boldsymbol{P} \cdot \boldsymbol{F}^{-T} \tag{2.11}$$

Thus Equation (2.10) becomes

$$\boldsymbol{S} = 2\frac{\partial W}{\partial \boldsymbol{C}} \tag{2.12}$$

The right Cauchy-Green tensor can be related to the Green strain tensor such that

$$\boldsymbol{E} = \frac{1}{2}(\boldsymbol{C} - \boldsymbol{I}) \tag{2.13}$$

Therefore, through the strain energy function, the relationship between the 2nd P-K stress tensor and the Green strain tensor can be determined as

$$\boldsymbol{S} = \frac{\partial W}{\partial \boldsymbol{E}} \tag{2.14}$$

This equation is the base on which analytical models for hyperelastic materials are developed. The next step in developing a material model is to determine an appropriate form of the strain energy function for analyzing soft tissue.

2.3 Strain energy functions

There are currently several strain energy functions in the literature that can be used to develop an analytical hyperelastic material model. These models are generally described as pseudo-elastic because in reality soft tissues are not truly elastic as they exhibit hysteresis [8]. Fung initially proposed separating the loading and unloading curves of soft tissue material and treating them as different elastic materials, therefore eliminating the need to rely on past loading for current tissue behaviour [14]. This assumption is now applied to most soft tissue modelling and all the models that will be discussed. The main models being discussed in this section will be Neo-Hookean, Fung's, Guccione's and Holzapfel-Gasser-Ogden's strain energy models. The strain energy equations can be modified for 2-D as well as 3-D analysis. The following models will be presented in their 3-D form with the exception of the Fung model.

2.3.1 The Neo-Hookean model

The Neo-Hookean model is the simplest strain energy model; it describes the behaviour of rubber, and takes a form that is closest to typical stress-strain relationship seen in many metals [8]. Assuming incompressibility:

$$W_{NH} = \boldsymbol{c_1}(\mathrm{tr}\boldsymbol{C} - 3) \tag{2.15}$$

where

$$\mathrm{tr}\boldsymbol{C} = 2(E_{11} + E_{22} + E_{33}) + 3 \tag{2.16}$$

and E_{11}, E_{22}, and E_{33} are the Green strains in the fibre, and two cross-fibre directions. The Neo-Hookean model only has one material constant and displays a linear relationship between the Cauchy stress and right Cauchy-Green deformation, hence the name that is in reference to Hooke's Law [8]. The Neo-Hookean has been shown to describe the isothermal behaviour of rubber for up to 30% deformation whereas Hooke's Law only applies for linear elastic behaviour of engineering metals, generally up to 0.2% strain [8]. However the Neo-Hookean model only describes behaviour for isotropic materials, and therefore cannot be used to describe most soft tissue materials [8].

2.3.2 The Fung model

The Fung strain energy model was initially developed to describe the behaviour of skin tissue; however, it has also been determined that variations of this model can reliably describe other soft tissue behaviour such as heart valvular tissue [15]. The following is the generalized pseudo-elastic 2-D Fung strain energy model [16]. The strain energy function takes on an exponential form

$$W_F = \frac{c_1}{2}[\exp(Q_F) - 1] \quad \textbf{(2.17)}$$

where Q_F is a quadratic function of the two principal strains of the material and shear strain.

$$Q_F = c_2E_{11}^2 + c_3E_{22}^2 + 2c_4E_{11}E_{22} + c_5E_{12}^2 + 2c_6E_{11}E_{12} + 2c_7E_{22}E_{12} \quad \textbf{(2.18)}$$

E_{11} is the Green strain along the fibre direction of the soft tissue while E_{22} is the Green strain in the cross-fibre direction. Shear strains E_{12} and E_{21} are equal because the Green strain tensor is symmetric by definition. The Fung model assumes soft tissue to be orthotropic and contains seven material constants; c_1 is a scaling factor usually in terms of membrane tension (N/m) or stress (N/m^2) while the other six constants are dimensionless. These parameters have no direct physical meaning.

2.3.3 The Guccione model

The Guccione model was developed through the study of the behaviour of the left ventricular myocardium tissue as a thick-walled cylinder [17]. This strain energy function assumes the material to be transversely isotropic with the plane of isotropy being normal to the fibre direction [17]. The strain energy model equation is the same exponential form as proposed by Fung but with a new form of Q to describe this new condition [17].

$$W_G = \frac{c_1}{2}[\exp(Q_G) - 1] \quad \textbf{(2.19)}$$

where,

$$Q_G = c_2E_{11}^2 + c_3(E_{22}^2 + E_{33}^2) + 2c_4E_{12}^2 \qquad E_{12} = E_{21} \quad \textbf{(2.20)}$$

The Guccione model can be implemented for 2-D incompressible applications by defining E_{33} in terms of E_{11} and E_{22}.

$$E_{33} = \frac{1}{2}\left(\frac{1}{(2E_{11}+1)(2E_{22}+1)} - 1\right) \quad \textbf{(2.21)}$$

The meaning of the strains is the same as in Fung's model. There are four constants in Guccione's model for strain energy. c_1 is a scaling factor for the stress with the same dimensions as the scaling factor in the Fung model, while the other 3 are dimensionless coefficients that are used to implement the different material's symmetries [17]. Changing c_2 and c_3 modifies the stiffness in the fibre and cross-fibre directions, respectively [17]. c_4 modifies the shear properties of the material in the fibre/cross-fibre plane [17].

2.3.4 The Holzafel, Gasser, and Ogden model

The Holzafel, Gasser, and Ogden (HGO) strain energy function was developed to model arterial behaviour [18]. While the Fung and Guccione models are considered phenomenological, i.e. not derived directly from first principles and the material's microstructure, the HGO model was developed from theory regarding the mechanics of fibre-reinforced composites [18]. The HGO strain energy function assumes the material to be orthotropic and was determined by modeling an artery as a thick-walled cylinder, with two families of collagen arranged in helices along its length [18]. The model is made from different layers with separated strain-energy functions [18]. Each layer is considered a composite with the collagen fibres acting as reinforcement. As each layer displays similar mechanical behaviour the same strain energy function was used but with different material constants [18]. The HGO model is split into two parts: the strain energy stored from isotropic deformations (the mechanical response from the non-collagenous matrix), and the strain energy from anisotropic deformations from the collagen fibres [18]. The 3-D HGO strain energy equation for a layer of material is shown:

$$W_{HGO} = \frac{c_1}{2}(trC - 3) + \frac{c_2}{2c_3}(\exp(c_3 Q_1) - 1 + \exp(c_3 Q_2) - 1) \quad \textbf{(2.22)}$$

where

$$Q_1 = ((\boldsymbol{C}:\boldsymbol{A_1}) - 1)^2,\ Q_2 = ((\boldsymbol{C}:\boldsymbol{A_2}) - 1)^2 \tag{2.23}$$

and

$$\boldsymbol{A_1} = \begin{bmatrix} cos^2 \propto & cos \propto sin \propto & 0 \\ cos \propto sin \propto & sin^2 \propto & 0 \\ 0 & 0 & 0 \end{bmatrix},\ \boldsymbol{A_2} = \begin{bmatrix} cos^2 \propto & -cos \propto sin \propto & 0 \\ -cos \propto sin \propto & sin^2 \propto & 0 \\ 0 & 0 & 0 \end{bmatrix} \tag{2.24}$$

$\boldsymbol{C}$ denotes the right Cauchy-Green tensor, while $Q_1$and Q_2 relate to the strain energy from the two different collagen families in the model using tensors $\boldsymbol{A_1}$ and $\boldsymbol{A_2}$ to characterize the structure for the collagen [18]. $\propto$ is the angle between the collagen fibers and the circumferential direction of the artery, leaving the HGO strain energy function with three material parameters to be determined. Although implementing fibre mechanics into the strain energy model could be seen to produce a more accurate function that should reflect the behaviour of the material, this does increase the computation costs, and thus Fung and Guccione's strain energy models are still more favourable for describing soft tissue [9]. In addition, angle $\propto$ is often turned into a material constant for better accuracy, or to avoid the experimental expense of determining fibre orientation and distribution, turning the HGO model back into a phenomenological one.

2.4 Determining the value of material parameters

The material specific constants/parameters can rarely be determined purely from theory, therefore experimental data from soft tissue testing are generally required to ascertain them. For instance, an analytical model may be developed to predict the deformation of the material under loading with the same testing conditions as found in the experiment. The estimation of material parameters is generally done through numerical regressions from overdetermined equations i.e. having more data points than unknown material parameters [8]. The final result is an analytical

soft tissue model that closely resembles the behaviour of the actual soft tissue under certain loading conditions. The experimental data can be taken from any number of experimental tests such as uniaxial, biaxial, solid/hollow cylinders, or indentation testing. From these experimental results, the Green Strains and the 2nd Piola-Kirchoff or Cauchy Stresses can be defined and used to estimate the material parameters. Material parameters can be determined either analytically or numerically. Analytically, as defined in this thesis, is when the material parameters are determined directly through the strain energy function and an experimental data set using numerical regression. Therefore, these parameters are implemented in an analytical material model. On the other hand, numerical material parameters are determined through an inverse FE method, and are implemented in a simulated model through FE analysis.

2.4.1 Uniaxial and biaxial testing

As the name suggests, uniaxial testing is when a displacement or force is applied along the length of the material. The material sample is generally thin and rectangular, with a large length to width ratio and constant thickness [8]. For biaxial testing, loading (either displacement or force) is applied to both the length and the width of a thin rectangular material with a constant thickness [8]. Uniaxial and biaxial testing are useful for determining the behaviour of soft tissue because it can be assumed that within a central region of the sample, i.e. away from where the material is attached to the testing device, the material has homogeneous properties and the stress and strain fields are also homogeneous [8]. If shear deformations can be neglected, e.g. in the case of biaxial testing along and perpendicular to the fibre direction, the stretch ratios, $\lambda_1, \lambda_2, \lambda_3$ are determined such that:

$$x_1 = \lambda_1 X_1 \quad \textbf{(2.25)}$$

$$x_2 = \lambda_2 X_2 \quad \textbf{(2.26)}$$

$$x_3 = \lambda_3 X_3 \tag{2.27}$$

where X_1, X_2, X_3 is the unloaded reference location of the material and x_1, x_2, x_3 is the location after deformation. Given the incompressibility of the materials being tested, the determinant of the deformation gradient, $\det \boldsymbol{F} = 1$, and λ_3 can be calculated from the other two stretch ratios.

$$\lambda_3 = \frac{1}{(\lambda_1 \lambda_2)}. \tag{2.28}$$

Therefore, only those two components from the biaxial test are needed to determine the deformation gradient tensor $\boldsymbol{F}$. The first Piola-Kirchoff stress can be determined experimentally from the applied force used on the material divided by the undeformed thickness and undeformed dimension perpendicular to the application of the force [8]. From Equations (2.11) and (2.13), the Green Strains and 2nd P-K/Cauchy stresses can be calculated from the biaxial test of the material in both planar directions.

For uniaxial testing, only one stretch ratio is determined, therefore following the same method as above, the Green Strains and P-K Stresses can be calculated for this one direction only. Uniaxial testing can be suitable for determining isotropic material behaviour or if the condition of interest for the material behaviour is along only one axis. However, given that soft tissues are generally anisotropic, the cross-fibre direction of the soft tissue will behave differently than the fibre direction for the same loads. Therefore, biaxial testing will give more general and useful results (from a constitutive perspective) that better reflects the material's behaviour, while uniaxial testing should generally be used for qualitative results [8].

2.4.2 Solid and hollow cylinders

While biaxial testing can probe the general behaviour of a material under planar tension, if the soft tissue in question is usually under different in vivo forces, then a different type of testing is needed to assess these stress conditions. When determining the behaviour of arterial tissue, treating the material as a pressurized cylinder would be a more appropriate model and testing as such would produce a response that better reflects the typical in vivo behaviour of the material. Having a solid cylinder model for the soft tissue allows for the measurement of extension and torsion of the cylinder, while a thick-walled circular tube allows for the measurements of extension, torsion, and inflation [8]. Testing a hollow tube material sample would allow various displacements or forces and moments to be applied to the ends of the tube, as well as pressure to be applied inside the tube. A solid cylinder being tested would experience the same type of condition but without the applied pressure on the inside.

The deformed position of a material particle of a hollow cylinder can be described as:

$$r = r(R) \tag{2.29}$$

$$\theta = \Theta + \gamma Z \tag{2.30}$$

$$z = \Lambda Z \tag{2.31}$$

where R,Θ, Z is the undeformed reference location of the same particle [8]. γ and Λ are the twist and axial stretch per unit of undeformed length, respectively [8]. The deformation gradient can then be determined from these three equations. Assuming material incompressibility allows for the need of only one measured radial position in the material's wall as long as the undeformed radii and axial stretch ratio is known [8], according to

$$r^2 - r_1^2 = \frac{1}{\Lambda}(R^2 - R_1^2)\,. \tag{2.32}$$

where r_1 and R_1 are the inner radii of a hollow cylinder for the deformed and undeformed states respectively. From the deformation gradient and calculating the 1st Piola-Kirchoff stresses, the experimental Green Strains and 2nd Piola-Kirchoff stresses can be determined. As with uniaxial and biaxial testing, this measurement of deformation happens away from where the sample is fixed so there are only radial and longitudinal variations in the material, no axial curvature [8].

2.4.3 Indentation

Indentation is a relatively new experimental method for soft tissue testing developed to combat the difficulties of tensile and compressive testing. Given the geometrical irregularities of soft tissue, complications can arise from compressive testing due to the need for a uniform test sample [19]. The grips used in tensile testing to secure the sample can cause slipping and tearing of tissue during testing [19]. Material testing using indentations can be a good alternative as it minimizes the sample preparation, damage done during testing, and can even be performed in vivo [19].

Indentation testing involves pressing a material sample with an indenter under a known applied force, and recording the displacement of the sample under the indenter [20]. From this displacement, the properties of the material, such as stiffness, may be determined. The indenter tip can vary in size and can have a number of different geometries such as hemi-spheres, cones, cylinders or pyramids [19]. The models for determining material characterization are greatly affected by the indentation tip geometry [19]. The Hertz model is one example of a material model that can be used to estimate a material's elastic modulus, E, from an experimental nanoindentation test [20].

$$E = \frac{3(1-\nu^2)}{4FR^{1/2}\delta^{3/2}} \quad \textbf{(2.33)}$$

F denotes the force applied from the indenter to the material, while δ and R are respectively the indentation depth and indenter's radius, and v is the Poisson's ratio of the material being tested [20].

Although indentation experiments provide a less invasive and simpler procedure compared to some other experimental testing methods, indentation has a few drawbacks that must be addressed before it can become a widely used method for describing soft tissue material. Most indentation material models only allow for uniaxial testing as the behaviour of the material can only be determined in the direction of the indenter. For this reason, most models assume the material to be isotropic. Experimental results from micro-indentation testing often cannot be linked to current material constitutive models, such as the analytical models defined above, and rely on describing material properties in general terms like the elastic modulus as in the Hertz model [20]. As a result, the current material models from indentation testing are not as adequately equipped as those derived from other experimental testing methods to accurately describe the hyperelastic anisotropic behaviour of soft tissue material.

2.4.4 Inverse finite element method

The inverse finite element (FE) approach for determining material behaviour arose from the complications of applying a material model, developed analytically, to a finite element analysis. Finite element programs such as LS-DYNA, ABAQUS, etc. often add penalty parameters to ensure incompressibility in the material [12]. These extra parameters have been shown to cause the simulated behaviour of the material in the FE program to become dramatically different from the experimental behaviour, even when using the material parameters that were found through analytical means determined from the same experimental results. This phenomenon will be

amply illustrated in the thesis as well. Still, being able to accurately depict material behaviour in FE programs is crucial because it allows for the accurate simulation of in-vivo conditions.

The inverse FE approach consists of determining the material parameters by iterative optimization from FE analysis [21,22]. It requires a material model, such as neo-Hookean or Fung, to be applied to an FE geometry. Oftentimes, the FE program already has a hyperelastic material model in its toolbox. The experimental test conditions are simulated in the FE analysis and the results are compared with those from the experimental testing. The effect of the incompressibility parameter used in the FE program is taken into account during the optimization of the constants. By using FE analysis directly, by the end of the optimization process, the material parameters determined will be the parameters that would produce the behaviour that closely resembles that observed in the experiment in the FE program being used. This approach also allows for the simulating of materials with complex geometries, whereas the purely analytical method usually has the material geometries in thin rectangles or hollow tubes which does not reflect the shape the material would have in vivo.

2.5 Evaluating predictive capabilities of material models

The final step in forming a constitutive material model is to evaluate the predictive capabilities of the model under a variety of other loading conditions. A material model is of little practicality if it can only describe material behaviour for one specific loading scenario. Therefore, after the material constants are optimized, the accuracy of the final material model should be tested by attempting to simulate complex boundary problems that were not integral to the formulation of the material model. These simulated results must then be compared with known measurements to determine the effectiveness of the model. This step would generally be implemented using powerful numerical methods such as FE analysis. This would be another reason why determining

material constants through inverse FE methods could be more favourable than other methods. The material model would already have incorporated the incompressibility parameter and have been tested to accurately predict material behaviour in the FE program in some loading cases.

2.6 Potential for improvements

The current (bio)medical research trend is towards providing patient-specific care, with less invasive methods. Although the current state of research for modeling soft tissue behaviour is still at designing a general material modeling process, there is a need to keep this trend in mind. At present, the experimental soft tissue behaviour is often determined from porcine, bovine, or synthetic material using external testing apparatus requiring large samples. Human soft tissue behaviour could display different material characteristics than seen in these other tissue samples. There is also a difference in material properties of soft tissue tested in vivo versus ex vivo, which is how most tissue is now tested. Current material models often only provide information on material behaviour from tension or compression loading. Effects due to bending or shear, which may also exist in physiological conditions, need to be further explored.

There is also little research or information on the effective range of the penalty term to ensure incompressibility; yet it is essential for the implementation of material models in FE programs. More research into determining the acceptable range of such parameters as well as the effects of the other material parameters on this acceptable range and vice-versa would greatly aid in the ability to produce accurate simulated material models, and is necessary for the goal of patient-specific simulated models. This is the topic of the present thesis.

3 Experimental and FE model set up

Please note that the experimental work, as described in Section 3.1, was not part of this thesis, which focused on FE modeling aspects and material characterization. The material behaviour of five different biomaterials under planar biaxial testing was simulated through FE modeling. The simulated mechanical response was compared with the known material response from the experimental planar biaxial testing under the same conditions. From a set of initial material parameters, the parameters were optimized to produce a simulated material response similar to the experimental behaviour of the material.

3.1 Experimental testing

The experimental material behaviour was taken from [7]. Five aortic valve (AV) cusp replacement materials were tested; 1) fresh autologous porcine pericardium (APP), 2) glutaraldehyde fixed porcine pericardium (GPP), 3) St Jude Medical pericardial patch (SJM; St Jude Medical, St Paul, Minnesota, USA), 4) CardioCel patch (CC; Admedus, Minneapolis, Minnesota, USA, and 5) Fresh porcine AV leaflets (PC) obtained from adult pigs [7]. The AV leaflets were stored in a saline solution at 4^{o} C until testing [7]. For the GPP sample, the 0.6% glutaraldehyde solution was applied 20 minutes before testing [7].

Nine samples of the cusp replacement materials were tested. Six samples of PC, taken from the belly region of each of AV leaflets from two porcine hearts, were also tested [7]. Each sample was cut to form a 6.5x6.5 mm^2 square with the direction of the fibres aligned or perpendicular to the edges as seen in Figure 3.1 [7]. An electronic thickness gauge (Model 700-118-20, Mitutoyo, Japan) was used to determine each sample's thickness from an average of three measurements in three locations [7]. The samples were then mounted with four tungsten

rakes, each fitted with five 0.7 mm spaced tines, on the 5-N capacity biaxial testing equipment (Biotester, CellScale, Waterloo, Canada) [7].

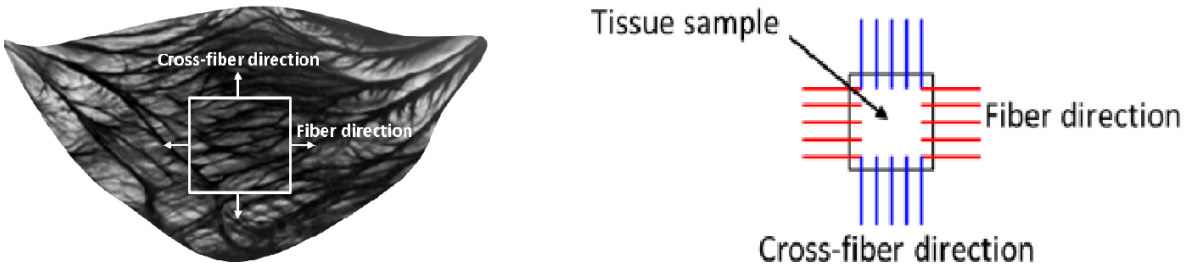

Figure 3.1: Sample from fresh porcine AV leaflet and tissue sample testing set up [7].

Each material was subjected to 10 preloading cycles with a maximum displacement determined from preliminary testing, followed by nine experimental protocols [7] with different ratios of displacements applied in the fibre and cross-fibre directions. Strains were determined for each sample by visually tracking a 9 by 9 node grid in the centre of the sample through each protocol [7]. Only the central region of the sample was used because stress concentration and potential tissue tearing around attachment sites can result in less strain than would normally be calculated, therefore not reflecting the typical strain behaviour that would be present in the material [7]. After each experimental protocol, this grid was examined to determine a region of homogeneous strains [7]. 4 nodes were selected from this sub-region, and the deformation components from the centre of these nodes were used to determine the material's experimental behaviour [7]. Each test was implemented using displacement-controlled protocols approximating force-controlled protocols, to better explore the range of deformation of the materials (see Fig. 1.2) [7].

3.1.1 Experimental Green strain and Second Piola-Kirchoff (P-K) membrane tension

Through image tracking, the experimental mechanical response for each sample was determined in terms of Second Piola-Kirchoff (P-K) membrane tension and Green strain. The experimental data were taken from the equibiaxial protocol resulting in shear strains of 0 for the simulated response and minimum experimental shear strains. Before deformation, the sample's dimensions can be defined as $-L_1/2 \leq X_1 \leq L_1/2$, $-L_2/2 \leq X_2 \leq L_2/2$, and $-H/2 \leq X_3 \leq H/2$, with H being the undeformed thickness. X_1, X_2, X_3 is defined as the location of a material particle in the undeformed material [7]. As the material sample begins to deform during the testing, the same particle can be mapped to a new set of coordinates, x_1, x_2, x_3, such that:

$$x_1 = \lambda_1 X_1 \tag{3.1}$$

$$x_2 = \lambda_2 X_2 \tag{3.2}$$

$$x_3 = ({}^{h}/_{H})X_3 \tag{3.3}$$

The stretch ratios along the two axes; λ_1 (along fibres) and λ_2 (across fibres), were monitored through the biaxial testing machine as were the forces applied in each direction, f_1 and f_2 [7]. Both the stretch ratios were taken from the centre of the already defined four node homogeneous sub-region of the sample [7]. The deformed thickness of the sample can be defined by the undeformed thickness as:

$$h = {}^{H}/_{J_{2D}} \tag{3.4}$$

where

$$J_{2D} = \lambda_1 \lambda_1 \tag{3.5}$$

This is because the determinant of the transformation gradient tensor $\boldsymbol{F}=\frac{\partial x}{\partial X}$, associated with planar biaxial testing was set to equal one, as all the materials were assumed to be

incompressible due to their large water content [7]. The Cartesian components of $\boldsymbol{F}$ can then be defined as:

$$\boldsymbol{F} = \begin{bmatrix} \lambda_1 & 0 & 0 \\ 0 & \lambda_2 & 0 \\ 0 & 0 & {}^{1}/_{J_{2D}} \end{bmatrix} \tag{3.6}$$

From the transformation gradients, the experimental Green strain can be determined.

$$\boldsymbol{E} = \begin{bmatrix} \lambda_1^2 - 1 & 0 & 0 \\ 0 & \lambda_2^2 - 1 & 0 \\ 0 & 0 & \frac{1}{J_{2D}^2} - 1 \end{bmatrix} \tag{3.7}$$

E_{33} was not considered for the experimental or simulated response in this thesis, as the interest was in how the material deformed along the planar axes and not through the thickness. For determining the second P-K stress membrane tension, the first P-K stress tensor $\boldsymbol{P}$ was first defined [7]. Since f_1 and f_2 were the only external forces applied to the sample in direction 1 (fibre) and 2 (cross-fibre), $\boldsymbol{P}$ becomes:

$$\boldsymbol{P} = \begin{bmatrix} \frac{f_1}{HL_2} & 0 & 0 \\ 0 & \frac{f_2}{HL_1} & 0 \\ 0 & 0 & 0 \end{bmatrix} \tag{3.8}$$

From the first P-K stress tensor and the transformation gradient, the experimental second P-K stress tensor was determined through Equation (2.11) or

$$\mathbf{S} = \frac{1}{HJ_{2D}} \begin{bmatrix} \frac{\lambda_2 f_1}{L_2} & 0 & 0 \\ 0 & \frac{\lambda_1 f_2}{L_1} & 0 \\ 0 & 0 & 0 \end{bmatrix} \tag{3.9}$$

The second P-K stress tensor can be converted into membrane tension if it is assumed that the components of the stress tensor do not vary significantly throughout the thickness of the material [7]. This allows for the second P-K membrane tension to be independent of the thickness of the sample.

$$\boldsymbol{T^s} = H\boldsymbol{S} \tag{3.10}$$

or

$$\boldsymbol{T^s} = \begin{bmatrix} \frac{\lambda_2 f_1}{L_2 J_{2D}} & 0 & 0 \\ 0 & \frac{\lambda_1 f_2}{L_1 J_{2D}} & 0 \\ 0 & 0 & 0 \end{bmatrix} \tag{3.11}$$

Although the second P-K membrane tension has no physical meaning, many groups in the literature use it, along with Green strains, to describe soft tissue behaviour [7]. However, the optimization program designed outputs the simulated response in Cauchy stress versus Green strain because LS-DYNA calculates the Cauchy stress as part of its soft tissue material toolbox. Therefore, the experimental second P-K membrane tension is converted into Cauchy stress in the program. Figure 3.2 contains the final experimental responses for the five biomaterials.

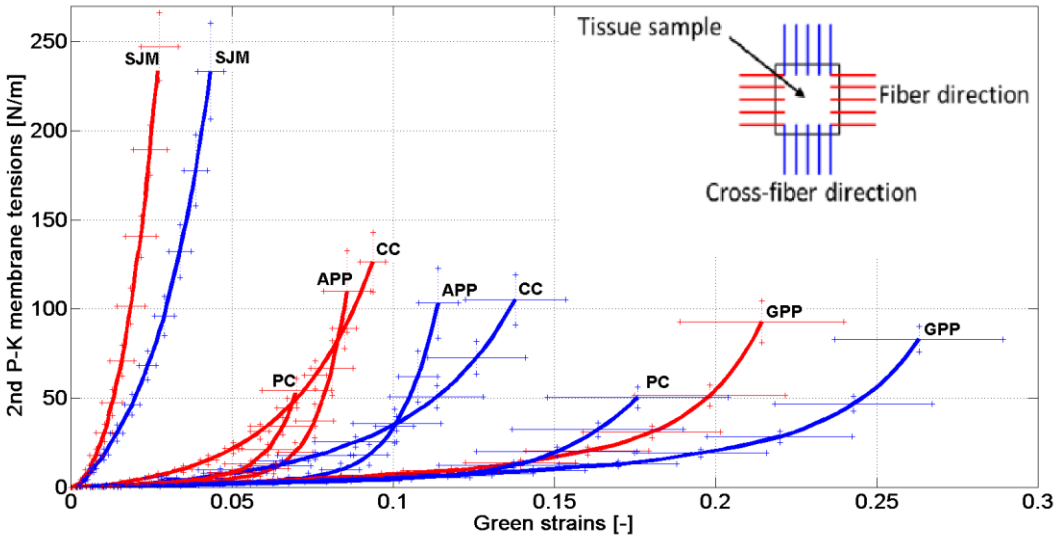

Figure 3.2: Experimental results for planar biaxial testing averaged over the nine experimental protocols for the five materials **[7]**.

3.2 FE model

A MATLAB program was written to determine the optimized material constants to produce a simulated mechanical response similar to the experimental one. Using initial user inputted constants and experimental conditions, the MATLAB program creates and launches an LS-DYNA input file to simulate a planar biaxial. The FE model was representative of the central region of the experimental samples. LS-DYNA (used as a black box) runs the simulated test and outputs Green strains and Cauchy stresses from that test. These results are read by the MATLAB program and compared with the experimental response. The program then iteratively modifies the material constants for the least discrepancy between the simulated and experimental results (optimization process). The MATLAB program code for optimizing all five constants is found in Appendix B. LS-DYNA was chosen as the FE program because it is one of the few programs that can implement dynamic analysis for hyperplastic anisotropic materials.

3.2.1 Simulated Green strain and Cauchy stress

In this program, LS-DYNA enforced the strain energy material model with the inputted material constants to determine the material's behaviour. This allowed for constants to completely reflect the effects of LS-DYNA on the material's behaviour by incorporating the incompressibility term (the *P* factor) in the FE strain energy model.

The Guccione strain energy model was used as the analytical strain energy model for determining the material's simulated behaviour. The Guccione model was chosen for its robustness as well as the fact that it is already part of the LS-DYNA tool box which allows it to be directly implanted by the FE program. The Guccione model used in this program contained five material constants, four being similar to the analytical version of the strain energy model (see Equations (2.19) and(2.20)) whereas the fifth constant, *P*, is the incompressibility factor such that $I_3 - 1 \cong 0$ to numerically enforce the material's incompressibility. The simulated Green Strain for the strain energy model was determined from the experimental stretch ratios.

$$W = \frac{c}{2}[\exp(Q) - 1] + \frac{1}{2}P(I_3 - 1) \quad \textbf{(3.12)}$$

where,

$$Q = b_1E_{11}^2 + b_2(E_{22}^2 + E_{33}^2 + 2E_{23}^2) + 2b_3(E_{12}^2 + E_{13}^2) \quad \textbf{(3.13)}$$

Indices 1, 2 and 3 refer to the fibre, cross-fibre and thickness directions of the sample, respectively. The Guccione strain energy model was also chosen because it has been shown to produce similar material constants and simulated results from equibiaxial planar testing only instead of general biaxial testing [7]. This made the implementation of the MATLAB program easier, as only the experimental response from the equibiaxial testing needed to be considered. The simulated material response was expected (and verified) to show negligible shear

deformation, because the simulated testing in LS-DYNA was equibiaxial and the material's preferred axes (fibres and cross-fibres) were aligned with the coordinate axes for all the samples [8]. Therefore, the Green strains could be simply expressed in terms of the simulated stretch ratios, such that

$$E_{11(LS-DYNA)} = \frac{1}{2}(\lambda_1^2 - 1) \quad \textbf{(3.14)}$$

$$E_{22(LS-DYNA)} = \frac{1}{2}(\lambda_2^2 - 1) \quad \textbf{(3.15)}$$

$$E_{12} = E_{13} = E_{23} = 0 \quad \textbf{(3.16)}$$

LS-DYNA derives the simulated Cauchy stresses from the second P-K stresses which are determined from the partial derivatives of the strain energy equation with respect to the Green strains. With the assumption that the components of the second P-K stress tensor did not vary significantly throughout the thickness, and that there was no shear deformation in the material sample, the simulated second P-K membrane tension were determined as

$$T_{11}^{(S)} = \frac{\partial W}{E_{11}} \quad \textbf{(3.17)}$$

$$T_{22}^{(S)} = \frac{\partial W}{E_{22}} \quad \textbf{(3.18)}$$

$$T_{12}^{(S)} = \frac{\partial W}{E_{12}} = 0 \quad \textbf{(3.19)}$$

3.2.2 Initial run

The experimental data of the material being characterized had to be loaded in the MATLAB program folder before it could be run. As implemented, the data needed to be in a MAT file with the experimental Green strains, E_{11}, E_{22} and second P-K membrane tensions, $T_{11}^{(S)}$, $T_{22}^{(S)}$ in a row of columns in that order. When the program runs, the experimental results in the file are split into their respective variables. A dialog box opens asking the user to enter new parameters, with the

options yes or no. If yes, the program opens another dialog box with options to input the initial material constants, if the user chooses no the program finishes. The input dialog box allows the user to set the initial guesses for the Guccione constants of c, b_1, b_2, b_3. The initial K value, where $P=cK$, is determined from a predetermined acceptable range (as discussed later). The input dialog box also gives options for setting the LS-DYNA planar biaxial testing conditions, allowing the user to set the dimensions of the material sample, duration of loading, and number of elements in the model. The units for the size are set in millimetres and the Guccione constant c units are set for Mega-Pascals, this is because the default units for LS-DYNA are Newtons and millimeters; therefore, the simulated stresses and c are also in MPa. The program also initially defines how many times LS-DYNA will save the results during the analysis; 20 was chosen as a reasonable number of saves but this can be changed manually in the program code.

The program then converts the experimental 2nd P-K membrane tensions into Cauchy stresses to be compared with the simulated Cauchy stresses when they become available after simulation. If there is very little to no shear deformation, as seen in this loading case, then the relationship between Cauchy stresses and second P-K membrane tensions can be defined as:

$$T_{11exp}^{(t)} = (T_{11exp}^{(S)} \times \lambda_{1exp}^2) \times 10^{-3}/H \quad \textbf{(3.20)}$$

$$T_{22exp}^{(t)} = (T_{22exp}^{(S)} \times \lambda_{2exp}^2) \times 10^{-3}/H \quad \textbf{(3.21)}$$

where

$$\lambda_{1exp} = \sqrt{(2E_{11exp} + 1)} \quad \textbf{(3.22)}$$

$$\lambda_{2exp} = \sqrt{(2E_{22exp} + 1)} \quad \textbf{(3.23)}$$

The Cauchy membrane tensions are divided by the thickness and multiplied by 10^{-3} to become Cauchy stresses in MPa. The experimental stretch ratios are determined from the experimental Green strains.

The program then creates the material sample that will be tested using the information provided by the user. Based on the length, thickness and number of elements, the program determines the number and position of nodes and elements. The material sample is meshed with brick elements with 8 nodes as defined in Figure 3.3. The numbering of the nodes in the brick element determines the order and coordinates of each node and element in the model. Direction 1 or the fibres direction is defined along the direction of node 1 to 2. Direction 2 or the cross-fibre direction is defined along the direction of node 1 to 4.

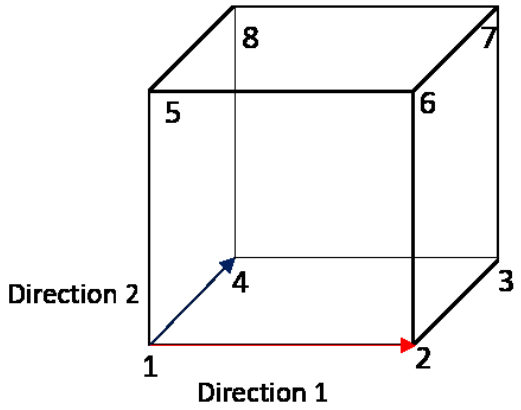

Figure 3.3: Example brick element used in LS-DYNA, the material properties in nodes 1 to 2 direction relate to the material properties along the fibres while the cross fibre material properties are applied in the nodes 1 to 4 directions.

An LS-DYNA input file is then created from MATLAB for the simulated biaxial test. LS-DYNA has a structured input file template, which can be found in the MATLAB code in Appendix B. The input file sets the duration of the analysis based on the user inputted duration of

load application. LS-DYNA saves the results at evenly spaced times over the load duration. The input file defines the material properties for each part in the analysis. In this case, there is only one part in the model, the sample itself. LS-DYNA has several material models in its toolbox. The material model chosen for this analysis was MAT_HEART_TISSUE + which is LS-DYNA's hyperplastic transversely isotropic material model, taking the form of the Guccione strain energy model. The addition of the "+" to the material model allows the material parameters to have up to twenty significant digits instead of the standard ten. The input file defines the material parameters in the LS-DYNA's material model as user inputted material constants. The elements in the simulated model are defined as solid brick elements with a constant stress within each element. The next section of the input file imports the nodes and elements of the sample from MATLAB into LS-DYNA. Boundary conditions are then applied to the sample's geometry as shown in Figure 3.4. The origin of the sample, bottom left front corner is defined as fixed in all directions. The other corner node is fixed along directions 1 and 2, but free to change in thickness. Side 1 is fixed along the y-axis while side 4 is fixed along the x-axis. The displacements along the direction 1 for side 2 and along direction 2 for side 3 are defined by the load curves 1 and 2 respectively.

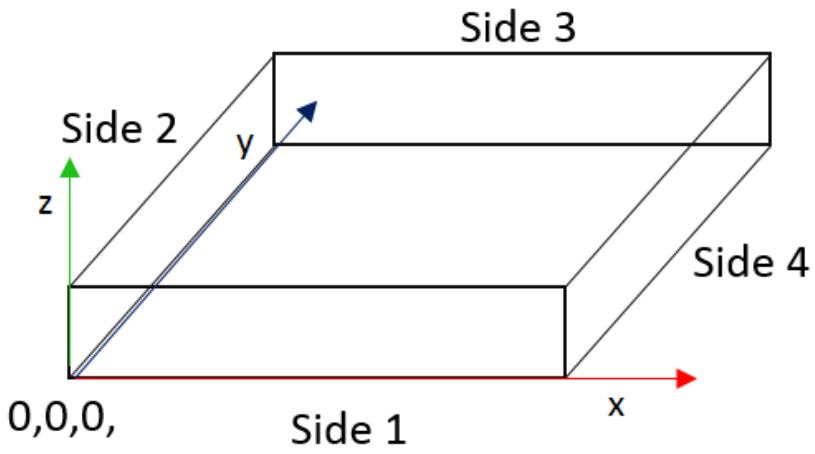

Figure 3.4: Geometry of material sample

To simulate planar biaxial testing, two load curves are applied in LS-DYNA, one for each direction, defined according to the experimental stretch ratios and converted into displacements as functions of time. The number of points on the load curves corresponds to the number of experimental stretch ratios recorded. For each stretch ratio, the displacement is determined and plotted for that point in time. The final part of the input file ensures that the post-processing of the results does not begin until the FE analysis is complete. A file called "disk8" is created by LS-DYNA at the beginning of the analysis and stays open for the whole duration of the analysis. At every second, the program checks to see if there is still a "disk8" file, and the post processing of the results only begins when the program no longer detects a "disk8" file. LS-DYNA saves the simulated results in a d3plot file.

After the simulated analysis has run, the results need to be converted into a format that can be compared with the experimental Green strains and Cauchy stresses. The MATLAB program begins the post processing by opening the d3plot file and extracting the specific results needed i.e. the Green strains and Cauchy stresses in directions 1 and 2 for the 20 times the results

were saved. The values are placed in text files. There is an option at this stage to change the amount of elements in the sample used to extract the simulated results. The default is all elements in the model are kept to extract the simulated results. However, this can be manually switched in the code to have only a quarter of the elements in the sample used. If only a quarter of the elements are chosen, the program is designed in a way that those elements are from the central region of the sample. As in the experiment, the material near where the loads are applied can behave differently than what is expected due to stress concentrations. Letting the user to decide if the results are from the whole sample versus a central region, allows more control and can mitigate any potentially unrealistic element deformation that could affect the results.

The text files for the results are then each read and converted into a matrix with the calculated simulated Green strains or Cauchy stresses in each element, for the 20 times the results were saved. These results are then averaged over all the elements for each of the 20 saves. The simulated results are then resampled over a spline to produce the same number of points as the experimental results, and the simulated and experimental results are plotted together on a graph for visual comparison in the fibre and cross-fibre directions. The scales of the axes are set to be the minimum of the experimental results to double the maximum value of the experimental results. An error function was also developed for a numerical comparison between the simulated and experimental results. This error was also used as the metric to be minimized through the optimization of the material constants.

3.2.3 Error Function

For the optimization of the material constants, a scalar error function was developed. There are two parts to the error function; the difference between the experimental results and the simulated

results on a point to point basis, as well as the difference between the ratio of curvature for both the fibre (x) and cross-fibre (y) directions.

$$Error = 100xerr + 100x\left(xcurve\ ratio_{(LS-DYNA)} - xcurve\ ratio_{(exp)}\right) + 100x\left(ycurve\ ratio_{(LS-DYNA)} - ycurve\ ratio_{(exp)}\right) \quad \textbf{(3.24)}$$

where

$$err = \frac{norm(\sum(E_{ij(LS-DYNA)} - E_{ij(\exp)})^2 + (T^{(t)}_{ij(LS-DYNA)} - T^{(t)}_{ij(\exp)})^2}{norm(\sum E^2_{ij(\exp)} + T^{(t)}_{ij(exp)}{}^2)} \quad \textbf{(3.25)}$$

$$curve\ ratio = \frac{norm(curvelength_{AB})}{norm\ (distance\ between\ AB)} \quad \textbf{(3.26)}$$

The ij in Equation (3.25) denotes the fibre or cross-fibre direction of the Green strain or Cauchy stress. A and B in Equation (3.26) represent two arbitrary points on the curves. Theoretically, the experimental Green strain should be the same as the simulated strain because the experimental stretch ratios derived from the experimental Green strain were applied to the simulated sample as the displacement and the simulated Green strain was calculated from these displacements. However, the error between the simulated and experimental Green strain was still included to determine if there are differences due to boundary effects or elements becoming distorted.

The curvature aspect was added to mitigate unrealistic results that appeared in the simulated behaviour that would still give a relatively small error based on point by point differences between the results. As seen in Figure 3.5, the addition of curvature produces simulated material responses that better reflect the material's experimental behaviour than just having an error between the points.

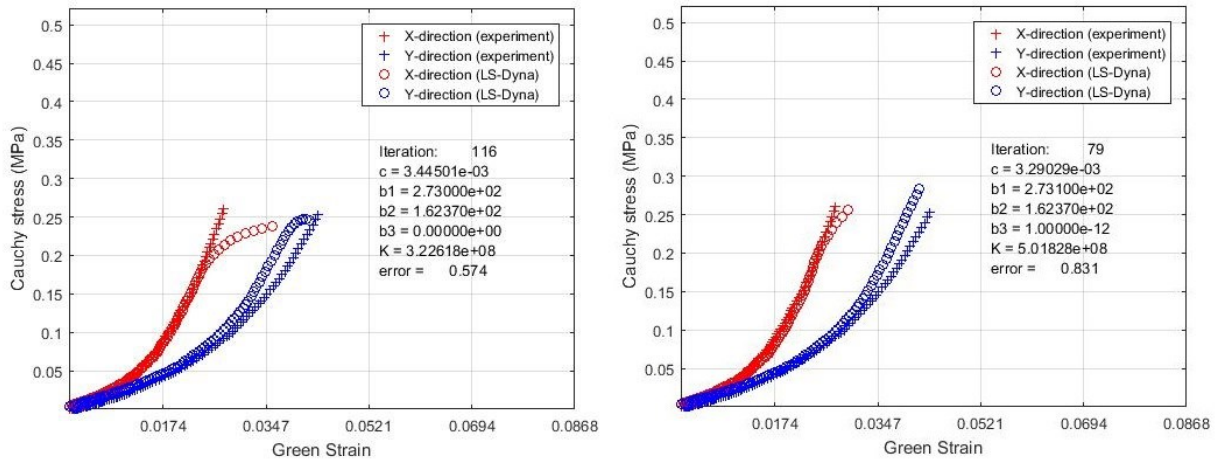

Figure 3.5: The comparison of simulated responses through the optimization of c and K ($cK=P$) for the material SJM when implementing just point difference error (left) versus point difference and curvature ratios (right).

The assessment of curvature of the simulated responses in Equation (3.26) is a ratio of the length of the curve between two points A and B on the curve and the direct distance between those two points as shown in Figure 3.6.

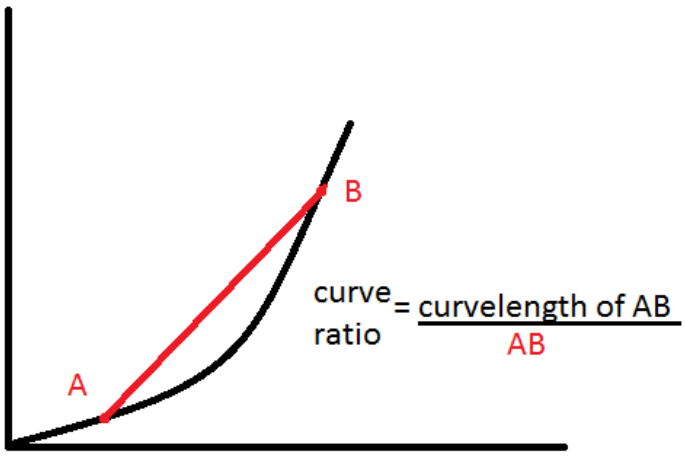

Figure 3.6: Diagram showing how curve ratio was determined in the error function.

For this thesis, the curvature was assessed from the last third of the resampled simulated data sets as it was determined that this area is where the results begin to diverge from typical soft tissue behaviour. The last third of the data set was also chosen because it produced more realistic results that better reflected the experimental behaviour during optimization than other ranges of the data sets. The difference in material responses using the last third of the date sets vs three-quarters of the sets can be seen in Figure 3.7.

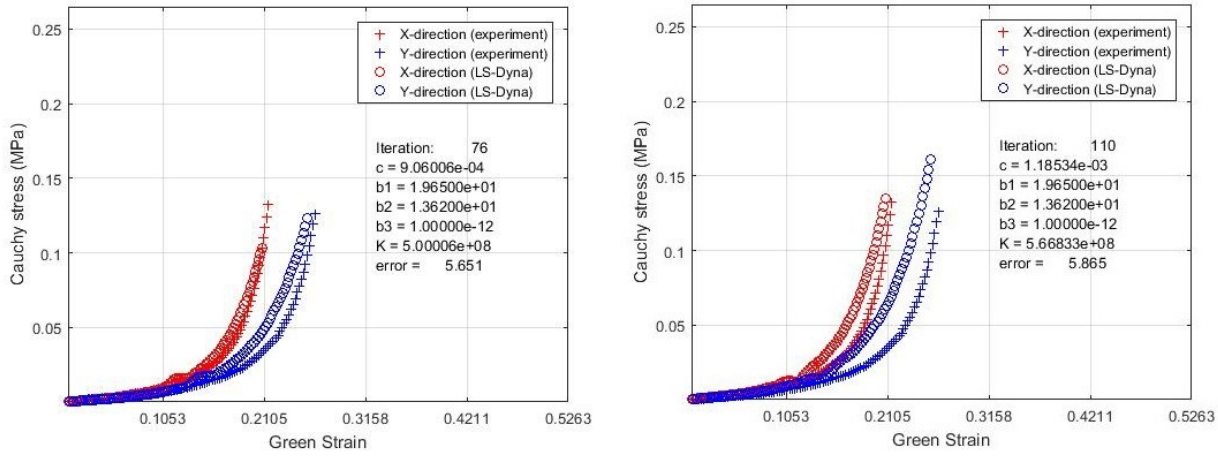

Figure 3.7: Comparison of the simulated responses for the material GPP using the last third of the data set (left) versus three quarters of the data set (right) to calculate curvature for the error.

The function chosen, from the MATLAB toolbox, for optimizing the material constants required the minimized function to be scalar; therefore, the error function was made up of the calculated norm of the point to point and the curvature ratio error.

4 Optimization

The optimization of the material constants for the Guccione model in LS-DYNA was achieved in two steps; an initial set of 25 runs using set variations of the material parameters *c* and *K*, followed by further optimization through *fmincon*, an optimization function from MATLAB's toolbox. Two programs were developed; one only optimizing the *c* and *K* constants, and the other optimizing all five material parameters.

4.1 Initial runs

Before the optimization through *fmincon*, the sample was made to undergo 25 runs of the program with different *c* and *K* values. After each run, the simulated material behaviour was compared to the experimental material behaviour. At the end of these initial runs, the combination of constants *c* and *K* with the lowest error was selected by the program as the initial guesses for the optimization through *fmincon*. Five variations of *c* and *K* were tested in combination for the initial runs:

$$c = [initialC, \quad initialCx10^{-1}, \quad initialCx10^{1}, \; initialCx10^{-\frac{1}{2}}, \quad initialCx10^{\frac{1}{2}}]$$

where $initialC$ is the user inputted constant *c*, and

$$K = [2x10^{7}, \quad 10^{8}, \quad 6x10^{7}, \quad 5x10^{8}, \quad 9x10^{8}]$$

The *K* values variations were from a range of predetermined acceptable *K* values for LS-DYNA, as will be detailed below. The other three constants b_1, b_2, b_3 remained constant as the user's initial inputted values throughout this process.

The reason for including these initial runs before using the *fmincon* function was that *fmincon* did not cater to large difference between the initial constants being optimized and the

final constants that would produce desired simulated results. Therefore, without these initial runs, the ability for *fmincon* to produce an acceptable simulated material behaviour was very dependent on the user's initial inputted constant values.

Determining one starting *K* value that would produce reasonable results for a variety of soft tissue material was also an issue. Figure 4.1 is the results of the optimization of the CC patch using just *fmincon*. As can be seen, the simulated material behaviour is not an accurate representation of the material's actual behaviour and could not be used for reliable in-vivo simulations.

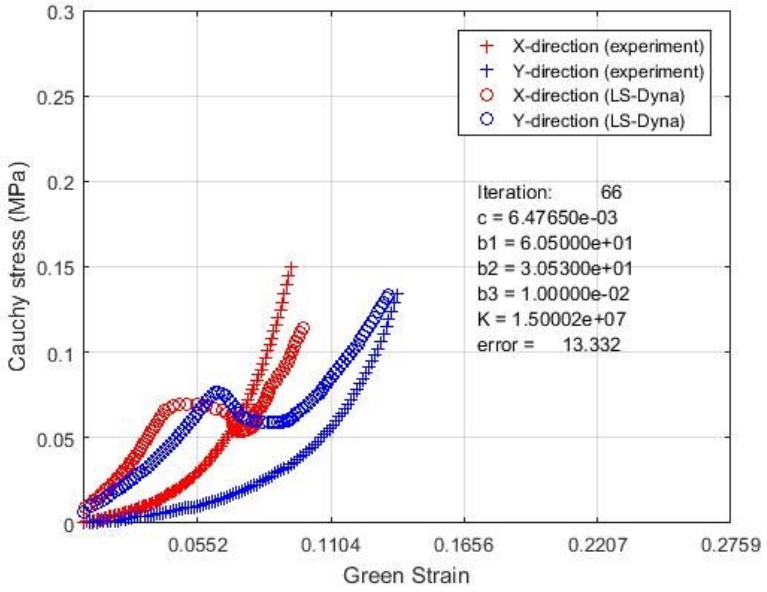

Figure 4.1: Optimized simulated material behaviour for CC using the *fmincon* function only for two constant optimization.

Therefore, a method was needed to have the initial guesses for the material constants closer to unknown desired material parameters. As seen in Figure 4.2 and Figure 4.3, of the five

material constants, differences in *c* and *K* were found to have the greatest effect on the resulting simulated material behaviour often producing large variations in results.

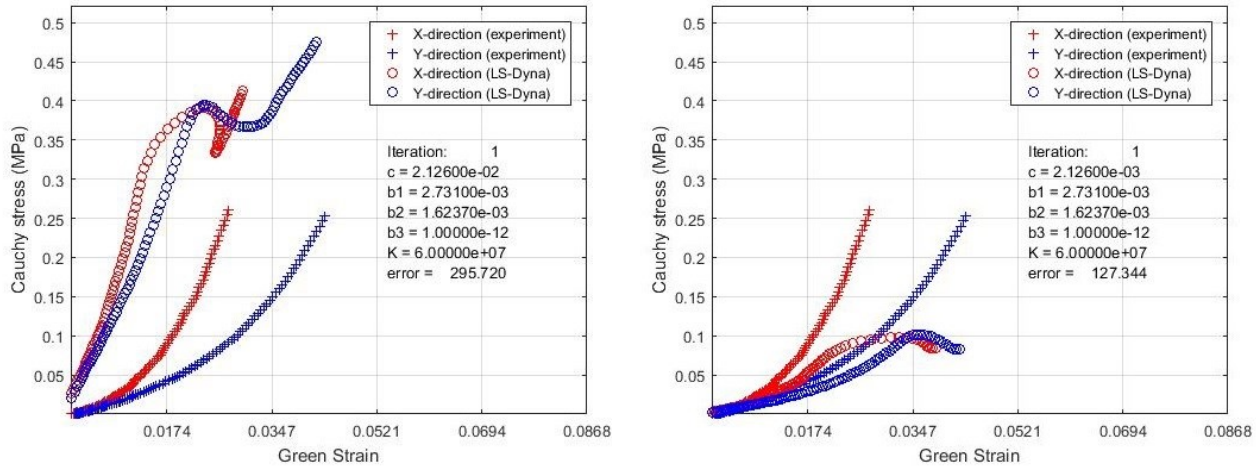

Figure 4.2: Effect on the simulated response from a change of constant *c* for SJM.

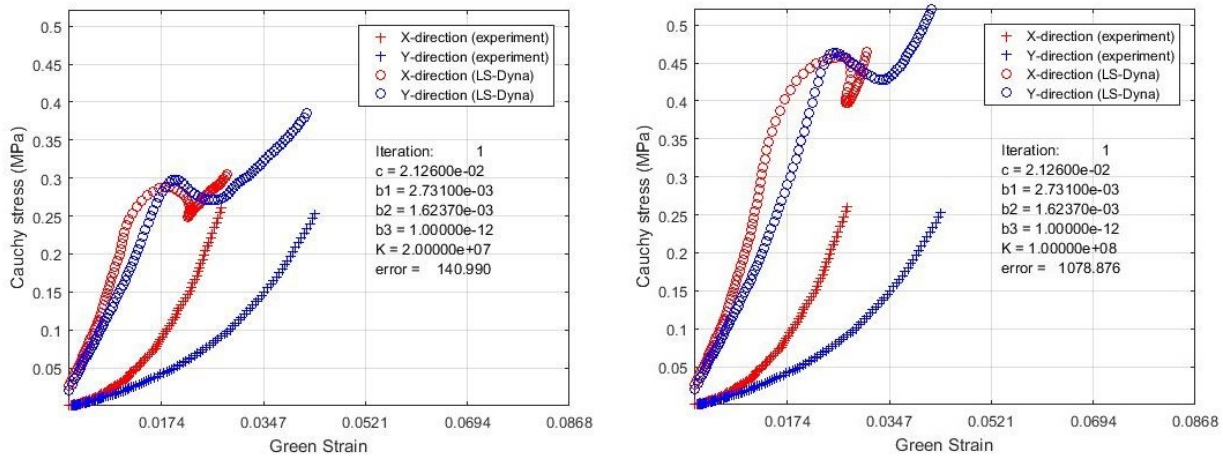

Figure 4.3: Effect on the simulated response from a change in constant *K* for SJM.

With this realization, the testing of various *c* and *K* values before *fmincon* was implemented in an attempt to bring the initial guesses for *fmincon* closer to the desired unknown constants. Testing a range of *c* values created a buffer and allowed for the program to still

produce acceptable results if there was a larger difference between the user's inputted *c* constant and the desired unknown *c*. Having this initial set of cycles also allowed for greater versatility in the materials being tested as it allowed for the range of constant *K* to be narrowed down before the optimization through *fmincon*. Having an appropriate *K* value as an initial guess for *fmincon* was the difference between the optimization program producing a simulated material behaviour that represented the experimental behaviour versus producing a result that was nonsensical.

Implementing the initial 25 runs greatly helped to develop a more reliable program and minimize the run time of *fmincon* as the error in the simulated behaviour was significantly decreased prior to optimization through *fmincon*.

4.2 Optimization with *fmincon*

fmincon, as mentioned, is an optimization function from MATLAB's toolbox. It is designed to find the minimum of a constrained nonlinear multivariable function. The function being minimized must be a scalar and is defined by a series of specific constraints as seen in Figure 4.4.

$$\min_{x} f(x) \text{ such that } \begin{cases} c(x) \le 0 \\ ceq(x) = 0 \\ A \cdot x \le b \\ Aeq \cdot x = beq \\ lb \le x \le ub, \end{cases}$$

Figure 4.4: The constraints for a problem using *fmincon* in MATLAB **[23]**.

In this case, $f(x)$ would be the error function in the program and x would be the five material parameters in a vector. A and Aeq are matrices and implement linear constraints, while

c(*x*) and *ceq*(*x*) are functions for implementing non-linear constraints, and *b* and *beq* are vectors [23]. *lb* and *ub* are the upper and lower bounds that the program must adhere to for the material constants and can either come in the form of vectors of matrices [23].

4.2.1 Constraints on the material parameters

The material constants of any material model need to ensure the convexity of the strain energy function as it is necessary for the stability and accuracy of the simulated results [24]. A function's Hessian is required be positive definite for the function to be convex [25]. Hence the constraints for the convexity of the Guccione model can be determined through applying this condition to the Hessian of the strain energy function. The Hessian for this function is a fourth order elastic tensor and is also called the tangent modulus [26]. It is defined as the second derivative of the strain energy function with respect to the Green strain [26]. For the in-plane stress conditions seen in planar biaxial testing, the component of the Hessian can be determined from:

$$\boldsymbol{H_{2D}} = \frac{\partial^2 W}{\partial^2 E_{2D}} = \begin{bmatrix} C_{11} & C_{12} & C_{14} \\ C_{12} & C_{22} & C_{24} \\ C_{14} & C_{24} & C_{44} \end{bmatrix} = \begin{bmatrix} \frac{\partial^2 W}{\partial^2 E_{11}} & \frac{\partial^2 W}{\partial E_{11}\partial E_{22}} & \frac{\partial^2 W}{\partial E_{11}\partial E_{12}} \\ \frac{\partial^2 W}{\partial E_{11}\partial E_{22}} & \frac{\partial^2 W}{\partial^2 E_{22}} & \frac{\partial^2 W}{\partial E_{22}\partial E_{12}} \\ \frac{\partial^2 W}{\partial E_{11}\partial E_{12}} & \frac{\partial^2 W}{\partial E_{22}\partial E_{12}} & \frac{\partial^2 W}{\partial^2 E_{12}} \end{bmatrix} \quad \textbf{(4.1)}$$

For $\boldsymbol{H}_{2D}$ (which is both symmetric and real), to be positive definite, all of its eigenvalues must also be positive [26]. Only the positivity of the eigenvalue of $\boldsymbol{H}_{2D}$ need be checked, since through the spectral theorem all the eigenvalues are already determined to be real, because $\boldsymbol{H}_{2D}$ is represented by a Hermitian matrix [26]. Two methods were used to determine conditions for the positivity of the eigenvalues, and both sets of constraints were implemented in this program for further robustness [7]. The first method, Descartes' rule of alternating signs, states that the

number of positive roots of a single variable polynomial ordered by descending exponents of variables with real coefficients, is equal or less by an even number to the number of sign differences between consecutive nonzero coefficients [26]. Therefore, if the form of this characteristic polynomial is:

$$X^3 - [C_{11} + C_{22} + C_{44}]X^2 + [C_{11}C_{22} + C_{11}C_{44} + C_{22}C_{44} - C_{12}^2 - C_{14}^2 - C_{24}^2]X + [C_{11}C_{24}^2 + C_{22}C_{14}^2 + C_{44}C_{12}^2 - C_{11}C_{22}C_{44} - 2C_{12}C_{14}C_{24}] = 0 \quad \textbf{(4.2)}$$

For the eigenvalues to be positive, there must three positive roots. Given this polynomial, there needs to be three sign differences. Hence the conditions for the Hessian to be positive definite, and in turn the strain energy function to be convex, using the Descartes' rule are:

$$-C_{11} - C_{22} - C_{44} < 0 \quad \textbf{(4.3)}$$

$$C_{12}^2 + C_{14}^2 + C_{24}^2 - C_{11}C_{22} - C_{11}C_{44} - C_{22}C_{44} < 0 \quad \textbf{(4.4)}$$

$$C_{11}C_{24}^2 + C_{22}C_{14}^2 + C_{44}C_{12}^2 - C_{11}C_{22}C_{44} - 2C_{12}C_{14}C_{24} < 0 \quad \textbf{(4.5)}$$

The second method for ensuring convexity is the Sylvester's criterion which states that a matrix is positive definite if and only if all the determinants are positive [26]. For a Hermitian matrix, if the leading principal minors are all positive, then the matrix will be positive definite [26]. The *k*-th principal leading minor can be found from the determinant of the upper-left *k* by *k* submatrix. Therefore, if the Hessian were to be reduced to an upper triangle matrix, while maintaining the same sign for the determinant, then the *k*th leading principal minor would be the product of its diagonal elements until row *k* and the Sylvester's criterion can be used to determine the conditions for the diagonal elements to be positive [26]. The Hessian can be reduced to an upper triangular matrix:

$$\begin{bmatrix} C_{11} & C_{12} & C_{14} \\ 0 & -\frac{(C_{12}^2 - C_{11}C_{22})}{C_{11}} & \frac{(C_{11}C_{24} - C_{12}C_{14})}{C_{11}} \\ 0 & 0 & \frac{C_{11}C_{24}^2 + C_{22}C_{14}^2 + C_{44}C_{12}^2 - C_{11}C_{22}C_{44} - 2C_{12}C_{14}C_{24}}{(C_{12}^2 - C_{11}C_{22})} \end{bmatrix} \quad \textbf{(4.6)}$$

Then, to ensure that the diagonal elements are positive which in turn ensures the eigenvalues are also positive, the conditions for the Hessian must be:

$$-C_{11} < 0 \quad \textbf{(4.7)}$$

$$C_{12}^2 - C_{11}C_{22} < 0 \quad \textbf{(4.8)}$$

$$C_{11}C_{24}^2 + C_{22}C_{14}^2 + C_{44}C_{12}^2 - C_{11}C_{22}C_{44} - 2C_{12}C_{14}C_{24} < 0 \quad \textbf{(4.9)}$$

When these five different conditions are applied specifically to the Guccione strain energy model, the constraints on the material parameters to ensure convexity as least at the origin are:

$$-b_1 - b_2 < 0 \quad \textbf{(4.10)}$$

$$-b_1 - 3b_2 - b_3 < 0 \quad \textbf{(4.11)}$$

$$-b_2^2 - 2b_1b_2 < 0 \quad \textbf{(4.12)}$$

$$-b_2^2 - 2b_1b_2 - b_1b_3 - 3b_2b_3 < 0 \quad \textbf{(4.13)}$$

$$-b_3b_2^2 - 2b_1b_2b_3 < 0 \quad \textbf{(4.14)}$$

In addition, because strain energy needs to remain positive, $-c < 0$ was also enforced. The convexity constraints were enforced within *fmincon* through the program optimizing all five material constants, where *K* was treated as an additional material constant. The two-constant optimization program used the analytically determined b_1, b_2, and b_3 for the whole process. Therefore, it was assumed these constants fit within the constraints as convexity would have been enforced during the analytical determination of the material parameters.

4.2.2 Upper and lower bounds used with *fmincon*

The upper and lower bounds for the material constants for *fmincon* were defined as

$$10^{-5} \leq c \leq 9 \times 10^{-2}$$

$$0 \leq b_1, b_2 \leq inf$$

$$-inf \leq b_3 \leq inf$$

$$1.5 \times 10^{7} \leq K \leq 10^{9}$$

The bounds for each constant must encompass enough of a range for a variety of soft-tissue materials with various hyperelastic behaviours to be modelled. However, unrestricted bounds or too large of a range can lead to the program producing unrealistic results or can even cause LS-DYNA to a crash.

The bounds for constant *c* were restricted to numbers that, when paired with the *K* values within their separate bounds, would produce results within the ranges of behaviour seen from the five materials being tested. As shown in Figure 4.5, a *c* value higher than 9×10^{-2} MPa, even when paired with a low *K*, produced a simulated material behaviour far stiffer than the experimental material behaviour of any of the materials tested. It can also be seen from Figure 4.5 that the opposite happens. For a *c* value less than 10^{-5} MPa to produce a result within the same scale as the materials' experimental behaviours, the corresponding *K* value would have to be higher than the upper bound of the *K*.

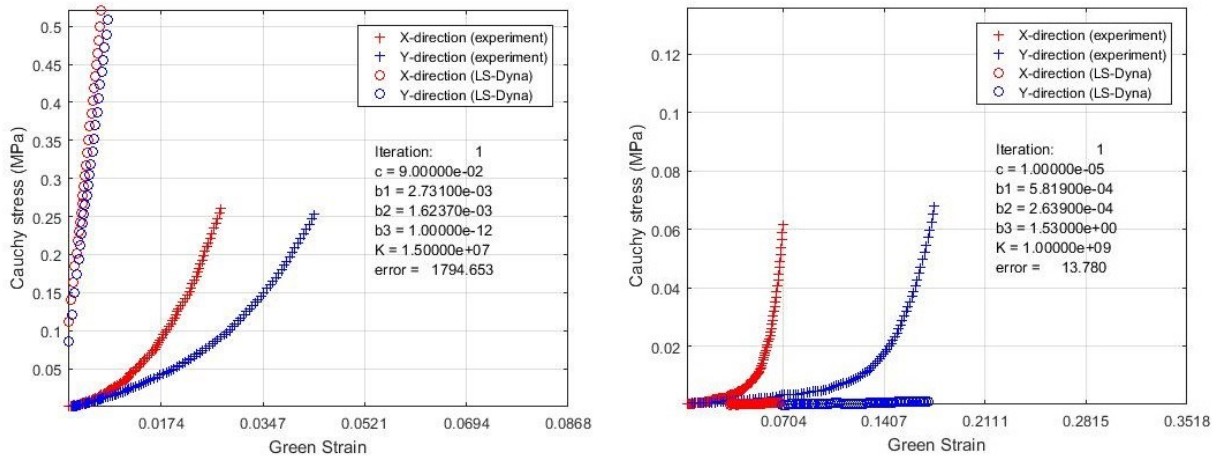

Figure 4.5: The simulated material response of SJM (left) using the upper bound C value and PC(right) using the lower bound, which had the largest and smallest experimental responses respectively**.**

The constants b_1 and b_2 were given the same bounds; the lower bound of 0 was implemented as having one of these constants negative would sometimes cause issues with the LS-DYNA computations. An upper bound of infinity allows for the increased versatility of materials being tested as it allows for stiffer material behaviours to be simulated through this program. This is also the reason for the unconstrained range of b_3.

The lower-bound constraint on constant K was set as such because of computational issues that arose from LS-DYNA attempting to analyze a material's behaviour with a K less than 1.5×10^7. For the FE analyses associated with the optimization of the material constants, time-wise load curves were applied over a short period of time. The program allows the user to input the loading duration with a typical duration being 0.01 seconds. Throughout this load duration, LS-DYNA saves its results multiple times. In addition, LS-DYNA automatically determined its time step for time integration from the size of the smallest elements in the material sample divided by the speed of sound. The speed of sound of a material is dependent on the stiffness of

the material and therefore the size of these time steps are related to the material parameters chosen by the optimization tool. Normal time step ranges are between 0.01-0.1 microseconds. However, when a material's K value decreased to a critical amount like below $1.5x10^7$, this in turn increased the stiffness of the material to the point that the calculated time step was greater than the full duration of loading, thus leading to an error during the program's post processing when the program attempted to access results that did not exist. For the upper bound of K, the length of the time steps would decrease as a higher value of K would imply a lower stiffness in the material. This in turn would lead to a decrease in the time step, and thus an increase in the computation time. In itself, higher computation time is not a reason to constrain K; however, the effects on material behaviour from the changes in the K value decrease to a point where at very high values of K such as greater than 10^9 there is little to no change in the material's simulated behaviour. This can be seen in Figure 4.6 illustrating the effects of changing K values on the material's simulated behaviour for Ks in various ranges.

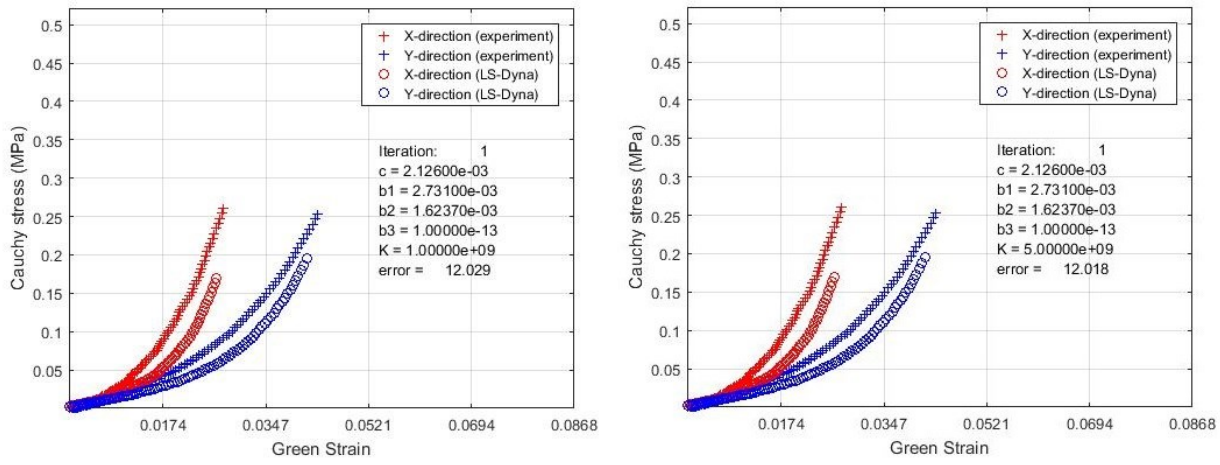

Figure 4.6: The effects on the material response from a change at high K values for the material SJM.

The *fmincon* optimization tool is a gradient-based method for finding the minimum of a constrained function, assuming both the function being minimized and the functions of the constraints are continuous and have continuous first derivatives [23]. *fmincon* has a set of different options to customize this optimization process. These options include the type of algorithm used for the optimization, the maximum evaluations of the function allowed, the type of finite difference used to estimate the gradient, and the tolerances for function values.

The type of algorithm chosen for the *fmincon* tool was the interior point algorithm. The interior point algorithm tries to find the constraint minimum of a function through solving a series of equally constrained approximate minimization problems [23]. If the original function being optimized were to take the form:

$$\min f(x), \text{ where } ceq(x) = 0 \text{ and } c(x) \leq 0 \qquad \textbf{(4.15)}$$

then the approximate problem for each $\mu > 0$, that *fmincon* attempts to optimize would be

$$\min f_\mu(x, s) = \min f(x) - \mu \sum_i \ln(s_i), \text{where } ceq(x) = 0 \text{ and } c(x) + s = 0 \qquad \textbf{(4.16)}$$

The assumption is that it is easier to solve this approximation than the original problem. As μ approaches 0 the minimum of f_μ should also approach the minimum of the original function. In Equation (4.16), s_i denotes the stack variable; the number of stack variables is the same as the number of inequality constraints in $c(x)$. In this specific case, there are three. Stack variables are also always greater than 0 to keep $\ln(s_i)$ bounded. For each iteration of *fmincon*, this approximate problem is solved using one of two steps; the direct step or the conjugate step method. The direct step method attempts to satisfy the Karush Kuhn Tucker (KKT) conditions for the approximate problem through linear approximation. The KKT conditions are

$$\nabla_x L(x, \lambda) = 0 \tag{4.17}$$

$$\lambda_{ci} c_i(x) = 0 \; \forall \; i \tag{4.18}$$

where ∇_x denotes the gradient of the function being optimized and L is the Lagrange function. The direct step $(\Delta x, \Delta s)$ equation develops from attempting to solve the KKT conditions using the linearized Lagrangian as

$$\begin{bmatrix} H & 0 & J_{ceq}^T & J_c^T \\ 0 & S\Lambda & 0 & -S \\ J_{ceq} & 0 & I & 0 \\ J_c & -S & 0 & I \end{bmatrix} \begin{bmatrix} \Delta x \\ \Delta s \\ -\Delta y \\ -\Delta \lambda \end{bmatrix} = -\begin{bmatrix} \nabla f - J_{ceq}^T y - J_c^T \lambda \\ S\lambda - \mu e \\ ceq(x) \\ c(x) + s \end{bmatrix} \tag{4.19}$$

where,

$$H = \nabla^2 f(x) + \sum_i \lambda_i \nabla^2 c_i(x) + \sum_j \lambda_j \nabla^2 ceq_j(x) \tag{4.20}$$

and H denotes the Hessian of the Lagrangian f_μ. J_c and J_{ceq} are the Jacobians of $c(x)$ and $ceq(x)$ respectively. S denotes the diagonal of s, while Λ is the diagonal of λ. λ and y are the Lagrange multiplier vectors associated with $c(x)$ and $ceq(x)$, respectively, and e is a vector of ones the same size as $c(x)$.

If direct step does not work, as in a case where the equation is not locally convex or if the projected Hessian is not positive definite, then *fmincon* attempts to solve the approximate problem with the conjugate step method using a trust region. A trust region is a region of x where an approximate solution reasonably reflects the behaviour of an original function. For the conjugate step, *fmincon* adjusts both x and s in the approximate solution with s always being greater than 0. This approach used a trust region to minimize a quadratic approximation which would display the same behaviour as the approximate problem in that specific trust region. This quadratic approximation is subjected to the linear constraints of the function being optimized.

For the radius of the trust region, *fmincon* approximates the solution for the KKT conditions using least-squares, and with λ assumed positive, to determine the Lagrange multiplier:

$$\nabla_x \mathrm{L} = \nabla_x f(x) + \sum_i \lambda_i \nabla c_i(x) + \sum_j y_j \nabla ceq_j(x) = 0 \quad \textbf{(4.21)}$$

With the Lagrange multiplier approximated, *fmincon* can now take a step $(\Delta x, \Delta s)$ to solve the approximate problem through the quadratic approximation with s being assumed to be positive:

$$min = \nabla f^T \Delta x + \frac{1}{2} \Delta x^T \nabla^2_{xx} L \Delta x + \mu e^T S^{-1} \Delta s + \frac{1}{2} \Delta s^T S^{-1} \Lambda \Delta s \quad \textbf{(4.22)}$$

Equation (4.22) is also subjected to the linearized constraints within the trust region:

$$c(x) + J_c \Delta x + \Delta s = 0 \quad \textbf{(4.23)}$$

$$ceq(x) + J_{ceq} \Delta x = 0 \quad \textbf{(4.24)}$$

After each iteration, either through the direct or conjugate step approach, *fmincon* determines if this step decreases the merit function:

$$f_\mu(x, s) + v \, \|ceq(x), c(x) + s\| \quad \textbf{(4.25)}$$

where, to force the feasibility of the solution, *fmincon* may increase v with each iteration. If the step does not decrease the merit function, then that step is rejected and a new step is attempted. The step is also rejected if the original function or non-linear constraint function returns a complex value, infinity, NaN, or an error at the current *x* value [27]. This optimization process continues until the difference between the original function's value at the current iteration and the value at the previous iteration is smaller than the function tolerance set in the program or if the attempted step is smaller than the step tolerance [28].

The other options to customize *fmincon* for this program included allowing the program to only attempt to evaluate the error function 5,000 times, and having a function tolerance of 10^{-6} as a stopping criteria, to keep the computations within reasonable accuracy and running time. The finite difference method used to estimate the gradient of the error function was set to the central method as it produced better results than the default forward option. However, the central method doubled the number of function evaluations.

Weights were also applied to each of the material constants as it was found that *fmincon* applied only a small change in the constants between iterations. Since each material constant was on a different scale from another, adding weights to each of the constants to have them all at the same levels of magnitude for the *fmincon* optimization was found to produce results which better reflected the material's experimental behaviour, especially when all five constants were being optimized. The final weights were

$$weightC = 10^2$$

$$weightb = 10^5$$

$$weightK = 10^{14}$$

Each constant was divided by their corresponding weight before the optimization processes. Weightb was used for both constants b_1 and b_2, while b_3 did not have a weight added because for most of the materials b_3 was near 0 and fluctuations of b_3 were found to have little impact on the material's behaviour.

5 Results and Discussion

From the programs developed, material constants were optimized to produce a mechanical response that would reflect the experimental response for five biomaterials during planar biaxial testing. Two programs were implemented: one optimized only the c and K constants, while the other optimized all five constants c, b_1, b_2, b_3. and K. This was to determine the effects of varying the material constants and establish whether or not the five-constant optimization was necessary to produce an accurate simulated response. The effects of the material sample's thickness on the optimized constants and simulated mechanical response were also explored. Lastly, the simulated mechanical response was compared when implementing all the elements of the FE model versus a quarter of the elements to determine if there were any effects from the end conditions in the FE simulations.

5.1 Optimization of material constants

The optimization programs were designed on the assumption that the user would already have analytically determined material parameters c, b_1, b_2, b_3, and wish to further optimize these constants to improve the accuracy of the analytical model's material behaviour for implementation LS-DYNA. The programs were not fully automated, requiring initial guesses for these four material parameters. For the optimization of the two and the five material parameters, the initial guesses were taken from [7] as derived using the Guccione model from the same equibiaxial experimental data that were used for the experimental response in this thesis [7]. The user inputted information required for the programs also included the dimensions of the sample, load duration, and number of elements in the model. For this analysis, the dimensions of the sample were assumed to be 5 mm for length and width with a 1 mm thickness. Load duration was set to 0.01 seconds, and the number of elements set was 10 along the length and width of the

sample, with 2 elements making up the thickness. An example of the FE model showing y-axis displacement for one of the biomaterials can be seen in Figure 5.1. These initial parameter guesses and experimental conditions were kept constant throughout this analysis aside from determining the effects of thickness.

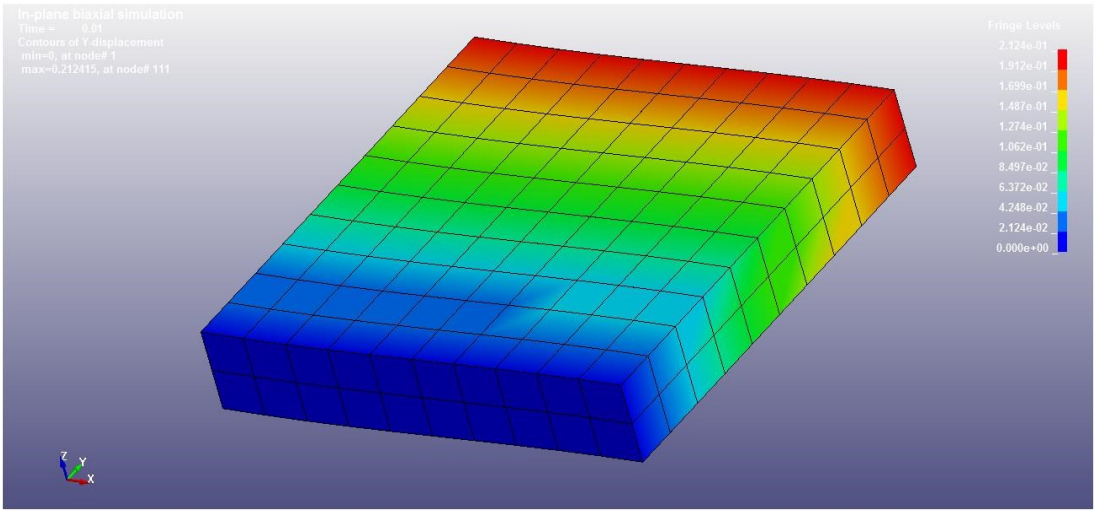

Figure 5.1: FE model of GPP showing y-axis displacement for equibiaxial testing

5.1.1 Two-constant Optimization

The simulated mechanical responses for the five biomaterials (GPP, PC, CC, APP, and SJM) were first attempted in LS-DYNA through the optimization of constants *c* and *K*, while the other parameters remained constant. The resulting optimized constants for each material and their corresponding errors upon convergence can be found in Table 5.1. The graphs showing the simulated and experimental material behaviour for all 5 materials can be found in Appendix A.

Table 5.1: Optimized material constants from the two-constant optimization program

Material	**GPP**	**PC**	**CC**	**APP**	**SJM**
Analytical c (MPa)	$9x10^{-4}$	$9x10^{-4}$	$2.01x10^{-3}$	$9x10^{-4}$	$4.89x10^{-3}$
Optimized c (MPa)	$9.060x10^{-4}$	$3.694x10^{-4}$	$1.188x10^{-3}$	$5.005x10^{-4}$	$3.290x10^{-3}$
Analytical b_1 (-)	19.65	58.19	60.50	80.88	273.10
Analytical b_2 (-)	13.62	26.39	30.53	43.46	162.37
Analytical b_3 (-)	$1x10^{-12}$	1.53	0.01	$1x10^{-12}$	$1x10^{-12}$
Optimized K ($P=cK$) (-)	$5x10^{8}$	$8.893x10^{8}$	$9x10^{8}$	$9.201x10^{8}$	$5.018x10^{8}$
Op Error (with curvature, %)	5.651	1.598	1.509	3.324	0.831

The largest discrepancy between the simulated response and the experimental response was for the material GPP with an error of 5.651%. The final simulated material behaviour from the optimization of c and K can be seen alongside the experimental material response in Figure 5.2. Even with the highest error, the simulated response for GPP is visually a good representation of how the material would behave in planar biaxial testing. The simulated response displays the same exponential shape as the experimental results; both exhibiting increasing Green strain or deformation while maintaining low Cauchy stresses first, then followed by the Cauchy stresses rapidly increasing as the Green strain continues to increase. Both the experimental and simulated responses experience a change in rate of increase of Cauchy stress at around the same Green strain.

However, there are a few discrepancies that account for the error, for instance the simulated response in the fibre direction predicts lower Cauchy Stresses at the higher Green strains than seen in the experimental material behaviour. For the fibre and especially the cross-

fibre direction, the simulated responses also predict a stiffer behaviour than the experimental results, with the simulated results exhibiting slightly lower Green strains for similar magnitudes of Cauchy stresses. There is also an instance in both the fibre and cross-fibre directions where the simulated response deviates from the shape of the general material response curve. The rate of increase in the Cauchy stress sharply increases then slightly decreases over a small portion of Green strain developing a sort of bump on otherwise smooth curves.

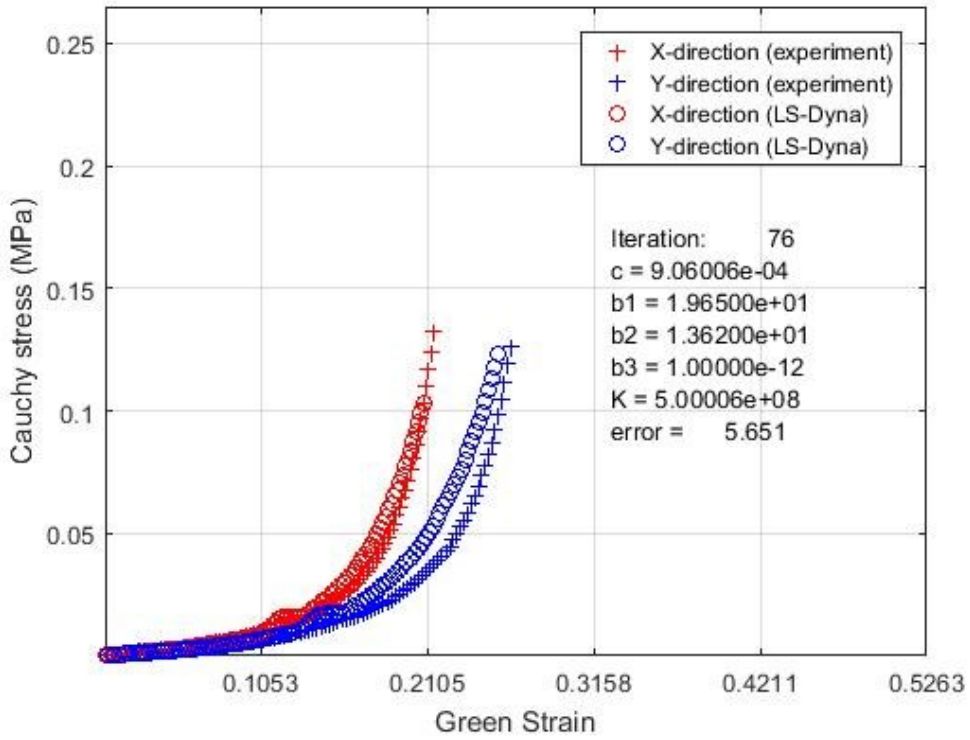

Figure 5.2: Simulated and experimental response of GPP through the optimization of *c* and *K*.

The simulated responses for materials PC and CC display similar characteristics to that of GPP. Their simulated responses show the same exponential shape as the experimental results taken from planar biaxial testing. Like GPP, their simulated responses predict lower Cauchy

stresses than exhibited by the experimental results along the fibre direction. PC's simulated responses also predict a stiffer response in the cross-fibre direction by predicting lower Green strains than seen in the experimental response; this is especially prevalent when the Cauchy stresses begin to rapidly increase. The simulated response for CC predicts a slightly stiffer response along the cross-fibre direction at high Green strain, predicting higher stresses and lower Green strains than exhibited by the experimental results. Both PC and CC have an error of ~1.5 % between the simulated and experimental data.

Although the error for APP is lower than GPP at 3.324%, from Figure 5.3 it can be seen that the shape of the simulated responses are the least resembling the experimental curves out of the two materials. The simulated response predicts lower Cauchy stresses at high Green strains in both the fibre and cross-fibre directions. The simulated curves also predict the rapid increase in the Cauchy stresses at a lower Green strain than the experimental, having the response display higher Cauchy stresses while the experimental Cauchy stresses are maintained at a low value for the period of deformation. There is also an issue where near the end of the response, the simulated material curve for APP appears to begin to change shape. The rate of change of the Cauchy stress begins to decrease in both the fibre and cross-fibre directions. The material response also displays higher Green strains, exceeding the strain values seen in the experimental data.

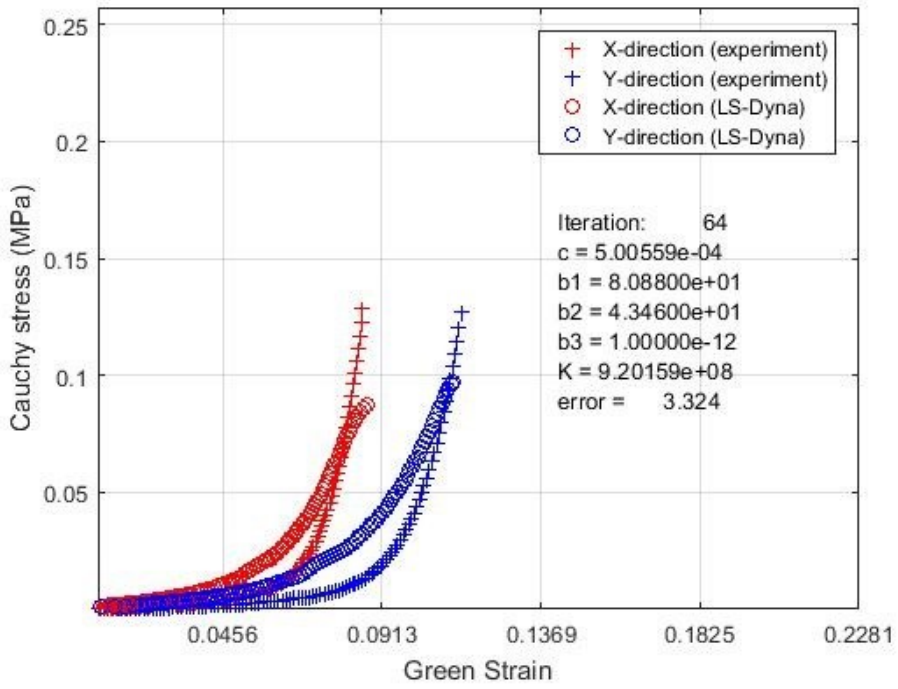

Figure 5.3: Simulated and experimental responses for APP through the optimization of *c* and *K*.

The material SJM had the smallest error out the five biomaterials at 0.831% difference between the simulated and experimental responses. The shapes of the curves were similar for both the simulated and experimental responses, with only slight deviations at the end of the curves. SJM exhibited the same deviation as seen in APP, along the fibre direction. The rate of change of the simulated mechanical response again appears to begin to decrease because the simulated response exhibits higher Green strains than seen in the experimental results. The simulated response along the cross-fibre direction also begins to deviate from the experimental response, as it begins to predict higher Cauchy stresses than the experimental data for the same Green strains.

The optimized *c* parameters for all five materials were within the same range by a factor of 10. PC had the lowest *c* value of all the materials with 3.694×10^{-4} MPa while SJM had the highest magnitude of *c* at 3.290×10^{-3} MPa. These values can be compared with the values of *c* determined analytically, from Labrosse et al [7], which can also be found in Table 5.1. Aside from GPP, where the difference between the analytically determined *c* and the LS-DYNA optimized *c* is less than 1%, the other four materials all have a greater than 30% error between their optimized *c* from this program and analytically determined *c* from the reference. PC had the highest discrepancy, with almost 60% error between the two values. It should also be noted that in all four of these cases the purely analytical model predicted higher values of *c* than was produced through the optimization process of this program. These discrepancies show that transferring an analytical model into a practical FE model cannot be effectively achieved through just the addition of the penalty term *P*. The scaling constant *c*, must also be further optimized along with *K*, where $K=P/c$, to produce a mechanical response that reflects the experimental material response in an FE model. The dimensionless *K* constant for the five materials ranged from 5×10^{8} for GPP to 9.201×10^{8} for APP.

5.1.2 Five-constant Optimization

The simulated mechanical responses of the five biomaterials were also determined through the optimization of all five material parameters. The optimized material parameters and corresponding error can be found in Table 5.2, while the simulated responses compared with the experimental response for all five materials are located in Appendix A.

Table 5.2: Optimized material constants from the five-constant optimization program

Material	GPP	PC	CC	APP	SJM
Optimized c (MPa)	$9.316\text{x}10^{-4}$	$3.378\text{x}10^{-4}$	$1.104\text{x}10^{-3}$	$4.202\text{x}10^{-4}$	$3.128\text{x}10^{-3}$
Optimized b_1	18.04	59.05	59.90	84.22	292.35
Optimized b_2	14.47	26.42	32.94	44.73	149.30
Optimized b_3	$1.435\text{x}10^{-4}$	1.489	$1.188\text{x}10^{-2}$	$1.079\text{x}10^{-5}$	$1.409\text{x}10^{-6}$
K (P=cK)	$5.067\text{x}10^{8}$	$8.880\text{x}10^{8}$	$8.877\text{x}10^{8}$	$8.989\text{x}10^{8}$	$7.085\text{x}10^{8}$
Op Error (with curvature, %)	5.535	1.638	1.440	3.660	0.756

For GPP, the error between the simulated and experimental responses decreased to 5.535% when optimizing all five versus two constants. The optimization of all five constants produced a smoother simulated response curve than when optimizing only c and K. There was no bump in the middle of the data set and the rate of increase in the Cauchy stresses was always increasing, unlike the simulated curves determined through two-constant optimization. However, the simulated response with all five constants optimized still predicted lower Cauchy stresses than exhibited by the experimental response at high Green strains, as well as an overall stiffer material response which was again most prevalent in the cross-fibre direction.

For material CC, the error between the simulated and experimental results decreased from 1.509% to 1.440% through the additional optimization of b_1, b_2, and b_3. The simulated curves from the two-constant optimization and five-constant optimization are visually nearly indistinguishable. The simulated material behaviour still displayed the same discrepancies as seen in the two-constant optimization. The simulated response still predicted lower Cauchy stresses at higher Green strain in the fibre direction, and an overall slightly stiffer response in the

cross-fibre direction. Although the discrepancy in stiffness between the simulated and experimental responses was less than with the two-constant optimization in both directions.

For material PC, the error actually increased from 1.598% to 1.638% when optimizing all five constants compared with optimizing only c and K. The simulated curves for both the five and two constant optimizations maintained the same shapes with the same discrepancies, with the two-constant optimization program producing a slightly smoother curve in the cross-fibre direction. The two-constant optimized simulated response also displayed Cauchy stresses closer to those exhibited by the experimental material behaviour at high Green strains than predicted by the simulated curve from the five-constant optimization program.

The error between the experimental and simulated material behaviours for APP also increased when all five constants were optimized to 3.660%. The five-constant optimization did produce a slightly smoother curve in the cross-fibre direction than the two-constant optimization, with Cauchy stresses closer to those exhibited by the experimental curves for the middle of the data sets. However, this improvement was negated by the five-constant optimization having a larger difference between the predicted values of Cauchy stresses and experimental value at high Green strains, with even lower Cauchy stresses than the two-constant optimization. The simulated curves produced by the five-constant optimization also experienced a slightly larger decrease in the rate of increase for the Cauchy stresses at high Green strains.

For material SJM, the error decreased when optimizing all five constants to 0.756%, however from visually assessing the simulated curves the two-constant optimization still produces a material behaviour that better reflects the experimental response. From Figure 5.4, it can be seen that the simulated curves determined by five-constant optimization developed a greater deviation from the experimental data at high Green strains. There was a significantly

larger decrease in the rate of increase of the Cauchy stress and higher discrepancy in the maximum Green strains in the fibre direction than seen with the two-constant optimization, with the Cauchy stress appearing to plateau if the Green strains were to continue to increase. This deviation was also displayed in the simulated curve in the cross-fibre direction, although not to the same extent, which was absent from the cross-fibre simulated behaviour in the two-constant optimization.

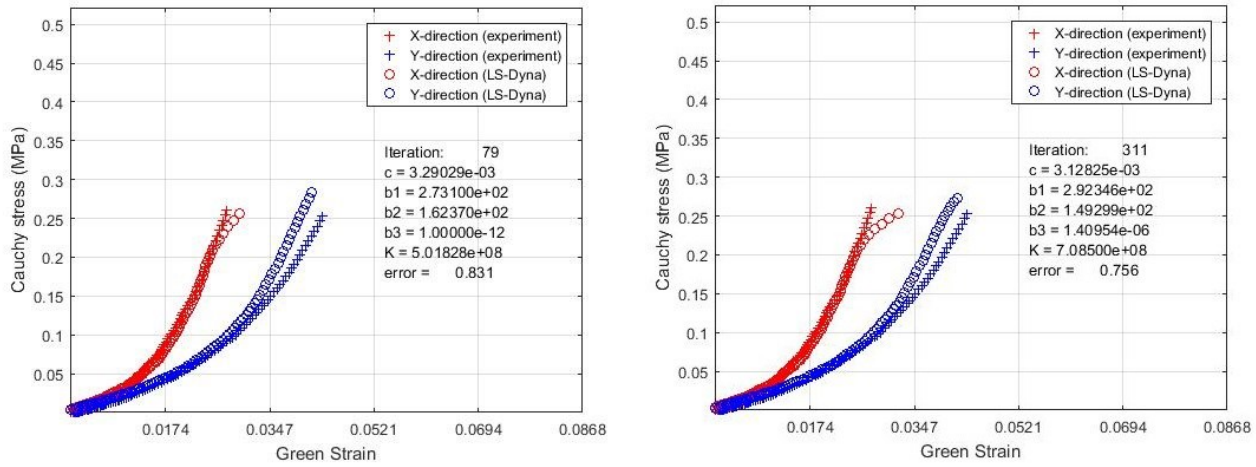

Figure 5.4: Comparison of the simulated response through two-constant (left) and five-constant optimization (right) for SJM.

The material constants determined through five-constant optimizations for all the materials can also be seen to be values close to the constants determined through the two-constant optimization process. For parameters b_1, and b_2, the optimized values were all within a ~8% difference from the analytically determined values. The optimized c and K values also were all within a ~8% difference, aside from the K constant in SJM which had a significantly higher difference at 41.19%. There were large differences in the error between the analytically determined b_3 and the optimized b_3, however this error was skewed as the analytical value for most materials was essentially 0 although the value 10^{-12} was chosen as the input so as to not

conflict with an initial lower boundary for b_3 of 0, this bound value was later changed to negative infinity. Of the materials with a larger than 0 value for b_3, the error difference between the five- and two-constant optimizations was seen to be 2.67% and 18.8% for CC and APP respectively.

Only in three out of the five soft tissue materials did the optimized error between the simulated and experimental responses decrease between the optimization of only two constants and the optimization of all five constants. Even in one of these cases, SJM, the simulated curve determined from the two-constant optimization was seen to better reflect the material's experimental behaviour even with the lower optimized error from the five-constant optimization. The five-constant optimization simulated curves still exhibited the same shortcomings as the two-constant optimization, predicting lower Cauchy stress at high Green strains as well as producing stiffer responses than seen in the experimental data. The five- constant optimization also further amplified the issue in APP and SJM where the simulated curves predicted higher Green strains than seen in the experimental behaviour and exhibited a localized decrease in the rate of increase of the curves. Overall, the positive effects in the simulated curves from optimizing all five constants versus two were small, with only GPP exhibiting a large visible positive change. The computation time for optimizing all five constants compared with two significantly increased with the number of iterations increasing from under 80 (~6 hrs.) for all the materials to 150 to over 350 (over 30 hrs) iterations depending on the material. The machine used was a workstation with two Intel Xeon E5640 2.67 GHz 4-core processors and 6 GB of RAM.

Given that there was not much of a change in the error and material parameter values, nor was there an overall positive effect on the simulated mechanical response, as well as given the significant increase in computation time with the optimization of all five constants, it can be

argued that optimization of only constants, c and K, would be sufficient for producing reasonable simulated responses using the Guccione's strain energy model when implementing analytically determined material parameters as initial guesses.

5.2 Effects of actual sample thickness

As mentioned previously, in optimizing both two and five material constants, the undeformed thickness of the material sample in the FE model was kept constant throughout all the biomaterials at 1 mm. However, the experimental samples varied in thickness ranging from 0.41 mm for CC to 0.20 mm for GPP. The two-constant optimization process was run again with the true thickness of GPP to compare simulated responses. GPP was chosen because it had the largest difference in thickness from the 1 mm and therefore would have the highest chance for discrepancy between the results.

From Figure 5.5, it can be seen that the change in thickness did not have a marked effect on the simulated material behaviour. The shapes of the curves were similar for both thicknesses. However, the discrepancies between the simulated and experimental responses exhibited by GPP with the 1 mm thickness were amplified when using the experimental thickness in the FE analysis. The 0.2-mm thick sample's simulated response predicted lower Cauchy stresses at high Green strain than the 1-mm thick sample in the fibre direction. The simulated response with the lower thickness also displayed stiffer material behaviour in both the fibre and cross-fibre directions than the 1-mm thick sample and the experimental behaviour, with higher Cauchy stresses being predicted in the middle of the curves. The bump in the simulated response caused by a sudden change in the rate the Cauchy stress increases was also larger when the true thickness was taken into account for GPP and shifted from appearing in approximately the middle of the curves for the 1 mm thick sample, to near the beginning at low Green strains.

Although the optimized error was lower for the simulated response with the true experimental thickness, visually, the sample with 1 mm results produced a better response. It could be assumed the same effect could occur when applying a change in thickness to the other materials, whereby the already existing discrepancies between the simulated and experimental behaviour will be amplified although perhaps not to the same extent if the sample's actual thickness is closer to 1mm.

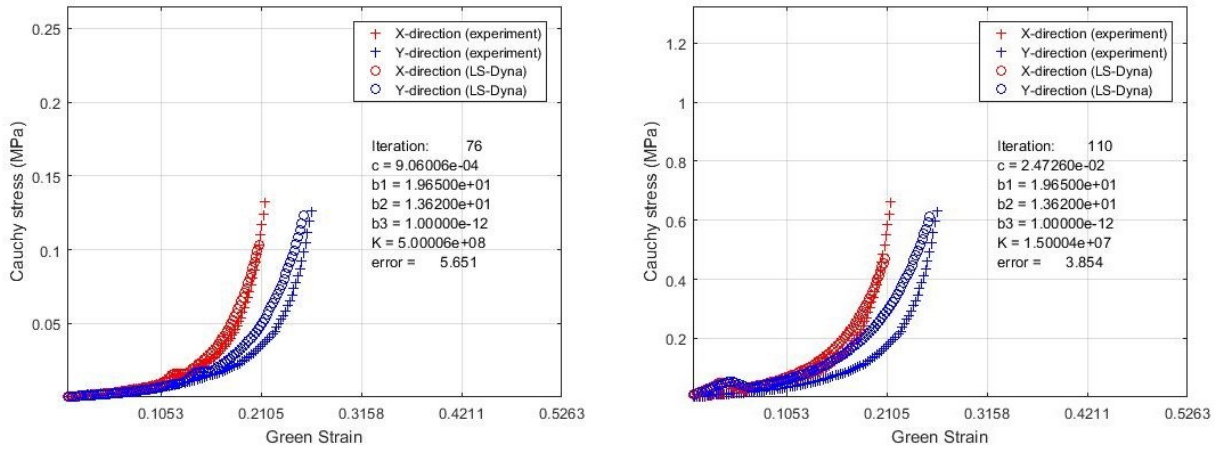

Figure 5.5: Simulated response for GPP using a 1 mm undeformed thickness (left) versus 0.2 mm thickness (right) through the optimization of *c* and *K*.

The change in thickness also had an effect on the optimized *c* and *K* values. The simulated response with the lower thickness's optimized *c* value increased to 2.47×10^{-2} MPa, and in turn decreased the *K* value to 1.5×10^{7} for GPP, possibly limited by the lower bound on *K*. This increase in *c* affected the overall FE stiffness calculation of the material, and the time step size in the LS-DYNA analysis. In this situation the time step dramatically decreased, significantly increasing the computational time for each iteration. However, with the increase in *c*, the issue with low *K* values affecting the time steps was mitigated. Therefore, if the material's *c* range was

known to be at a higher magnitude, the lower limit of $1.5x10^7$ for the *K* values could in turn be lower possibly optimizing to a different *c* and *K* combination that would produce a more accurate simulated response.

GPP produced smoother and closer fitting simulated curves to the experimental responses when all five parameters were optimized. Therefore, it is possible that optimizing all five constants could produce a simulated response that better reflects the experimental data. However, given the long computation time for optimizing just two constants of over 48 hours when implementing true thickness compared to ~6 hours, the optimization of all five would be impractical.

Although the actual thickness of a soft tissue material could be implemented into the optimization program and produce a simulated response that can be representative of the experimental material behavior, there are notable differences when comparing the material response with an FE analysis using a 1-mm thickness. The 1-mm thickness of the sample seems to produce simulated results closer to the response exhibited from the experimental results. If a simulated soft tissue model is needed and accurate thickness is not an issue, such as a membrane problem excluding the bending behaviour, then these results would suggest that using the optimization program with a standard 1-mm thickness would produce results closer to the experimental response exhibited by the material during biaxial testing. More research is needed to explore the effects of the change in thickness of simulated responses and the corresponding optimized constants.

5.3 Analyzing a quarter of the elements in the FE model

When comparing the two-constant and five-constant optimization methods, all the elements in the FE model were used in the analysis. However, elements along the edges can be affected by

the boundary conditions, becoming distorted and producing unrealistic stresses and strains which would be reflected in the simulated response. An option was implemented in the optimization code to allow only the central elements, essentially a quarter of the model, to be selected for the calculation of the Cauchy stresses and Green strains. Figure 5.6 shows the difference in the simulated response for GPP when using a quarter versus all the elements in the FE material model for the two-constant optimization.

The simulated response using only a quarter of the elements produced a smoother curve than when using all the elements for the FE analysis. Similar to the simulated response determined from optimizing all five parameters for GPP, the bump in the middle of the response seen in the two-constant optimization was no longer present when using only the central elements of the model. This implies that the small deviations and bumps in the simulated response curves were most likely related to boundary condition effects.

However, the quarter elements model's simulated response experienced no changes in the other deviations seen between the simulated and experimental responses for GPP. The model still predicted lower Cauchy stresses at high Green strains in the fibre direction and produced a stiffer response in the cross-fibre direction than exhibited by the experimental material behavior. The optimized K parameter was found to be different between the models, with an optimized value of $\sim 9 \times 10^8$ when using a quarter of the elements compared to the whole model's optimized value of 5×10^8. A manual single iteration of the program was implemented using a quarter of the elements for analysis and the optimized K value from the whole model optimization to see if the material response changes from the quarter element analysis could be associated with the change in K. The resulting material response using a quarter of the elements in the model had no significant

differences with the change in the *K* value. Therefore, the change in the simulated responses can be attributed to the use of only central elements in the analysis and not the change in *K*.

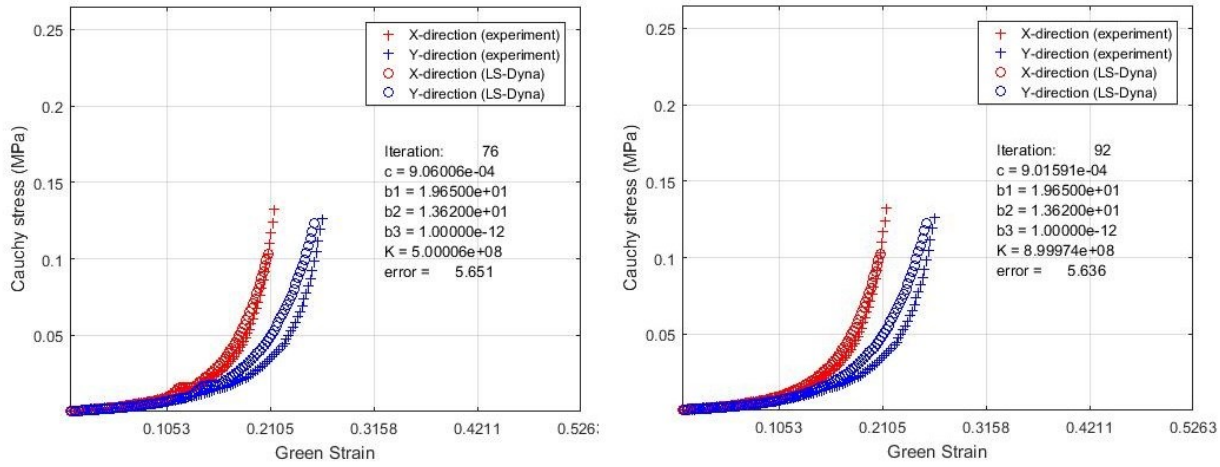

Figure 5.6: Comparison of the simulated responses for GPP using all elements (left) versus only a quarter of the elements (right) through the optimization of *c* and *K*.

From Figure 5.7, the same trend can be seen for APP, with the simulated response using only a quarter of the elements producing a smoother response without the small divots, and bumps seen in the simulated response using all the elements. The deviations between the simulated and experimental response for APP were also present in both the quarter element model and the model using all the elements. Therefore, it can be assumed that using only the elements in the central region will produce smoother simulated response curves for the soft tissue material, as the bumps and small deviations seen in the material behaviour when the whole material sample can be linked to boundary condition effects.

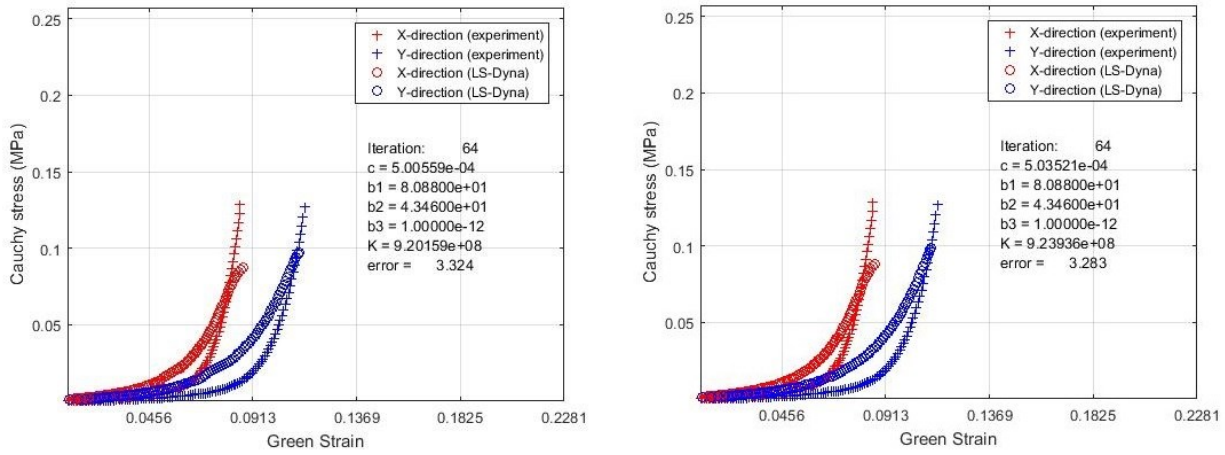

Figure 5.7: Comparison of the simulated responses for APP using all elements (left) versus aquarter of the elements (right) through the optimization of *c* and *K*.

Therefore, using a quarter of the elements in the FE model will generally produce a simulated response that better reflects the experimental material behaviour and may be an option to improve the simulated response when true thickness is essential. The large deviation seen in Figure 5.5 in the simulated response, using the experimental material thickness, at low Green strains could be an effect from the boundary conditions as seen with a similar deviation that was present in the 1-mm thick response. However, the general shape of the curve was not affected by using only a quarter of the elements, and the deviations of the simulated response from the experimental results such as producing a stiffer response will most likely remain unchanged.

5.4 Program capabilities

For all five materials, the optimization programs were able to produce material parameters that predicted simulated material responses that adequately, albeit not perfectly, reflected the experimental material behaviour from planar biaxial testing. However, there were some common discrepancies that were seen in most of the biomaterials' simulated responses. The simulated

response generally predicted lower Cauchy stresses at high Green strains in the fibre direction, and produced a stiffer material behaviour in the cross-fibre direction, especially in the region of rapid increase in the Cauchy stresses. These issues remained present whether all five versus only two material parameters were being optimized, the experimental thickness was implemented, or only a quarter of the elements in the FE model were being analyzed.

The optimization program seemed to have more trouble in producing simulated responses for materials with sharper exponential response, where the Cauchy stress increases slowly at low Green strains then there is a rapid increase at a critical Green strain as seen in the experimental responses of APP, GPP, and PC. This was especially apparent with APP where the experimental Cauchy stresses were maintained at low, almost stagnant, values for the first two thirds of the Green strain values and then rapidly increased at high Green strains. The simulated responses in both the fibre and cross-fibre directions in APP displayed stiffer material behaviour with the largest difference from the experimental behaviour happening when the rate of change of Cauchy stress begins to rapidly increase. Both the fibre and cross-fibre directions for APP predicted lower Cauchy stresses than the experimental response. For PC and GPP, the sudden increase in the Cauchy stresses was not as sharp; therefore, this discrepancy between the experimental and simulated response was not to the same extent. The experimental response for PC in the fibre direction exhibited a sharper increase in the range of change of the Cauchy stress as opposed to the more gradual increase in the cross-fibre direction and the experimental response of GPP. This could be why, like in the simulated responses of APP, the simulated response in the fibre direction of PC predicted a larger discrepancy in Cauchy stresses at high Green strains. The simulated response of GPP in the fibre direction had a more gradual increase in Cauchy stresses and was more similar in shape to the response in the cross-fibre direction. Thus, the discrepancy

between the simulated Cauchy stresses and experimental Cauchy stresses appeared smaller visually. CC and SJM displayed an even more gradual increase in Cauchy stress in both the fibre and cross-fibre directions for the experimental material behaviour than the other three materials, which could be why the simulated responses were closer to the experimental behaviour and the Cauchy stresses in the fibre direction were closer to the experimental Cauchy stresses at high Green strains.

These common discrepancies between the simulated and the experimental responses can be seen to be similar in comparison to the discrepancies between the analytical and experimental behaviours from Labrosse et al [7]. In Figure 5.8, the material response determined analytically for APP is similar to the simulated response with the response predicting a stiffer material behaviour particularly when the Cauchy stresses begin to rapidly increase. Similar to the LS-DYNA simulated response, the analytically determined response also predicts lower Cauchy stresses at high Green strains than exhibited by the experimental material behaviour. Therefore, the discrepancies seen in the simulated responses could be attributed to the limitations of Guccione's strain energy model which was used to determine both the analytical model and FE simulated response. Thus, incorporating the incompressibility penalty term P into an analytical model to have it be functional in FE analysis was a success as the simulated model closely resembles the analytical model.

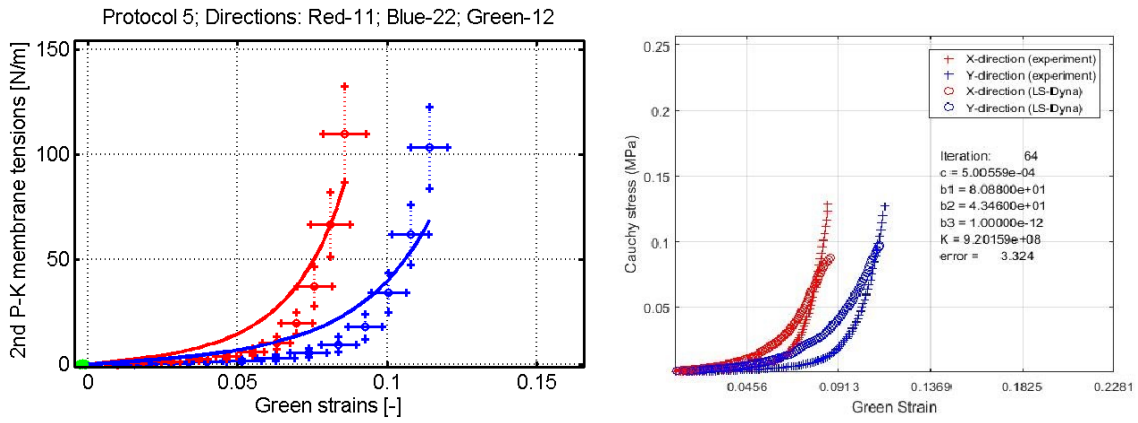

Figure 5.8: Comparison of the experimental and analytically derived responses (left) and the experimental and LS-DYNA simulated responses (right) for APP **[7]**.

Another issue exhibited by the simulated response was seen in the responses of APP and SJM and was further amplified when the optimization of all five constants occurred for both these materials. For SJM, the shape of the simulated response curve began to change, in the fibre direction for the two-constant optimization, and in both directions for the five-constant optimization, with the rate of increase in Cauchy stresses beginning to decrease and the Cauchy stresses even beginning to plateau at high Green strains. The maximum simulated Green strain for SJM was also higher than seen in the experimental behaviour. Displacement was applied to the FE model through stretch ratios which were calculated from the experimental Green strain. Therefore, there should have been no discrepancy between the experimental and simulated Green strains, because the simulated Green strain was derived from the experimental Green strain. This implies that the simulated response at a point during the analysis, is no longer being subjected to the same testing conditions as the experiment and therefore can no longer be used for predicting material behaviour under those test conditions. This deviation from experimental conditions was also seen in APP although not to the same extent. However, these deviations were no longer

present in the simulated responses when the value of *K* increased. Figure 5.9 shows simulated responses of SJM and APP with higher *K* values. For both responses, the maximum Green strains are now aligned with the maximum experimental Green strains. This could imply that a reason for these unrealistic behaviours at high Green strains could come from an incompressibility issue in the FE analysis. For SJM and APP's optimized *c* values, the optimized *K* could not be sufficiently high for the penalty term to enforce $I_3 - 1 = 0$ at these high Cauchy and Green strains. Therefore, when the *K* value is manually raised, causing *P* to also increase, the material behaviour became more in line with the experimental one because *P* was high enough to ensure incompressibility. For the optimization through all five constants, APP and SJM produced lower optimized *c* values which could explain why the issue was amplified with these materials.

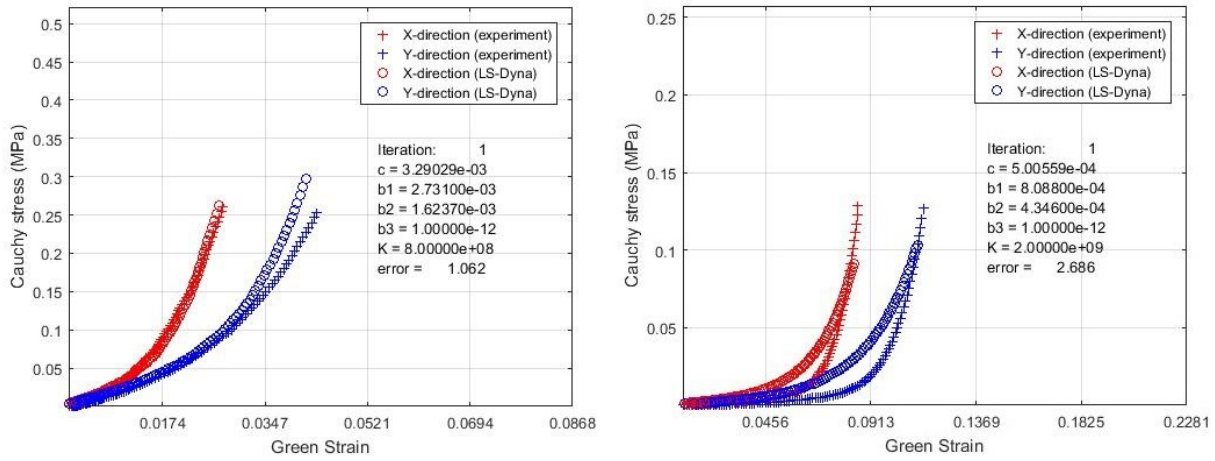

Figure 5.9: Simulated response from two constant optimization with a manual increase in the optimized *K* from ~5x10^8 to 8x10^8 for SJM (left) and ~9x10^8 to 2x10^9 for APP (right).

For the simulated response for SJM, the error was higher than with the originally optimized *K* values probably due to the higher Cauchy stresses being predicted at high Green strains. The current optimization process works just through the minimization of a scalar error

and does not account for unrealistic behaviours if it does not greatly affect the components of the error. Therefore, changes in the error function, or implementing a rule in *fmincon* to reject steps which produce higher maximum Green strains than seen in the experimental results could alleviate this issue.

The optimized K value needed to produce a more realistic response for APP with the two constant optimized c was higher than the upper bounds of the K range given in the optimization program, so the program would not have attempted this combination. Therefore, increasing the range of K could help produce more accurate results for APP and the other materials. The reason behind this change in material behaviour and its possible relation to incompressibility must be further explored before this optimization program is a viable option for predicting soft tissue material behaviour.

5.4.1 Importance of initial guesses

The optimization programs were not fully automatic, as the user needed to supply initial guesses for c, b_1, b_2, and b_3. These initial guesses were the starting material parameters for the optimization process, and the ability of the optimization program to produce an acceptable simulated response relied on these guesses. For the five materials tested in this thesis, the analytically determined b_1, b_2, and b_3 proved to be sufficient without any further optimization to produce an acceptable result. However, if the analytical constants for Guccione's model were unavailable, then it would be unlikely for the programs to produce simulated responses that would reflect the experimental material behaviour given the wide range of b_1 and b_2 across the material samples.

The initial guess of c proved to have a large effect on the determined simulated response. The initial set of twenty-five automatic cycles was introduced before launching the *fmincon*

optimization to account for some possible deviations in the initial *c* guess. However, even with these initial cycles, the *c* chosen as the initial guess for the *fmincon* optimization had to be sufficiently close to the value of the optimized *c* needed to produce an acceptable response. In some cases, the initial guess of *c* taken from the analytically determined *c* had to be readjusted to produce a simulated response which reflected the experimental behaviour. As seen in Figure 5.10, the initial guess of $9x10^{-4}$ MPa which was the analytically determined *c* for APP did not produce a response that resembled the experimental data, but changing the initial guess to $4.09x10^{-3}$ MPa was sufficient to produce a simulated response that reflected the experimental material behaviour.

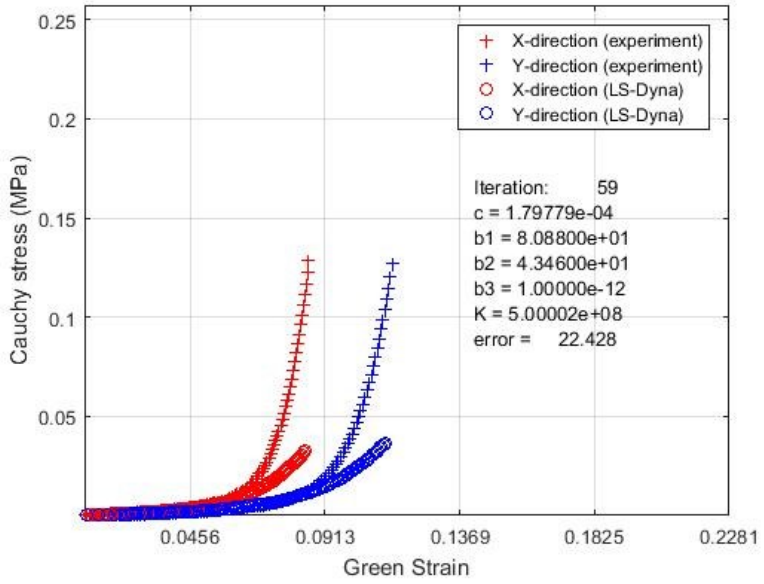

Figure 5.10: Simulated response for APP through two constant optimization from starting c of $9x10^{-4}$ MPa.

A simple solution to this issue would be to readjust the initial cycles to include more variations of *c* to increase the chance of having *c* closer to what the optimized value would be for

an acceptable response. This would in turn increase the computation time because a simulated biaxial analysis must be completed for each combination of c and K, an addition of another c guess would then increase the number of iterations in the initial set of cycles by five. The user could manually change the range of the initial set of cycles and bound limits if expected magnitudes of c and K were known. The better option would be to attempt to make the only user inputs be experimental conditions. If the program could determine the appropriate initial guesses directly from the uploaded experimental material behaviour, it could minimize the range of variation of c and K in the initial set of cycles or alleviate the need of it altogether, decreasing computation time. A totally automated process would make the program more versatile as already known constants would no longer be needed.

5.5 Individual roles of Guccione's strain energy material parameters

The material parameter c in Guccione's strain energy model is considered to be the scaling factor. c dictates the size of the simulated response: the higher the c value the higher the Cauchy stresses will be, while lowering the c value generally lowers the Cauchy stresses in the responses. This can be seen in the optimized material parameters, where SJM has the highest c value out of the soft tissue materials tested, and it also exhibits the highest experimental Cauchy stresses, while PC was determined to have the lowest c value and its experimental response exhibits the lowest Cauchy stresses. If all the materials were ranked from highest maximum simulated Cauchy stresses to least, the c values of the corresponding materials would also be ranked in the same order. SJM is seen to have a significantly higher c value than the rest of the materials simulated, which is reflected in the simulated responses with SJM being significantly stiffer than the other materials. Figure 5.11 shows the effects of a change in c on the simulated response of CC if all other materials parameters are kept constant. With an increase in the c

value, the magnitude of the response does increase with greater simulated Cauchy stresses along with the general stiffness of the material. However, the order of the c values across the five materials does not indicate which materials are stiffer than others, as GPP has a higher c value than APP, but APP is seen to have a generally stiffer response. Therefore, it is a combination of c with the other constants which dictate the stiffness of the response. An increase in c value in CC also produced a response with the discrepancies seen in the simulated responses of APP and SJM, where the shape of the response at high Green strains changes. The rate of increase in the Cauchy stresses begins to decrease with the Cauchy stresses even plateauing and, in the cross-fibre direction, the Cauchy stress even begins to decrease. However, if these unrealistic results had to do with incompressibility issues, then an increase in c values would imply the threshold for a K value to ensure that P was sufficiently high would be lower, yet this discrepancy was seen with a higher c when there was no issue with the previous c and K value. Therefore, it is possible that these unrealistic results could be from the acceptable values of P to ensure $I_3 - 1 \cong 0$ being a range with upper and lower bounds. A certain high c and K value combination could produce a P value higher than the upper bound, therefore affecting the incompressibility of the material and producing unrealistic material responses.

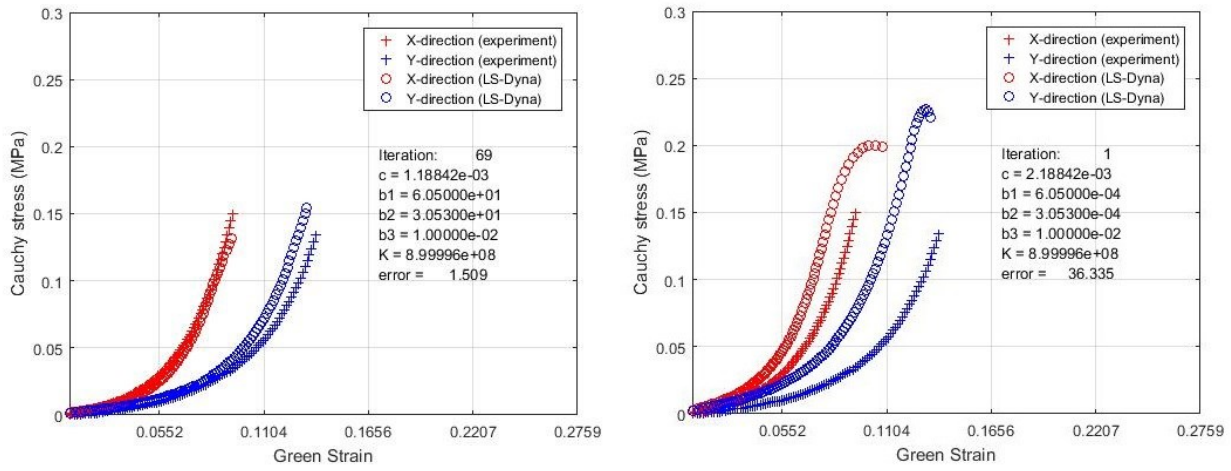

Figure 5.11: Comparison of simulated response of CC with a change of $1x10^{-3}$ in c.

Material parameters b_1 and b_2 are thought to dictate the stiffness of the simulated material, with b_1 affecting the stiffness in the fibre direction and b_2 affecting the cross-fibre direction. This relationship can again be seen in the simulated responses of the material. SJM is by far the stiffest material in both the fibre and cross-fibre directions, thus having markedly higher b_1 and b_2 values than the other materials. GPP has the lowest b_1 and b_2 values, and its simulated response exhibits the largest deformation. The b_1 values of CC and PC are similar, 60.50 and 58.19 respectively. The material responses in the fibre direction of the two materials have close maximum Green strain with PC having a slightly lower Green strain, CC on the other hand has a higher maximum Cauchy stress than PC. These characteristics would give CC a higher overall stiffness than PC. In the cross-fibre materials direction, there is a larger difference between the two with PC having a larger maximum Green strain as well as a lower maximum Cauchy stress thus the materials have a larger difference in the b_2 values of 30.53 for CC and 26.39 for PC. From Figure 5.12, an increase in b_1 in CC resulted in a slightly stiffer response in the fibre direction, as expected. However, there also seemed to be a larger effect on the stiffness

in the cross-fibre direction. This increase in stiffness for both directions resulted from predicting higher Cauchy stresses. The increase in b_1 also produced a change in the increase of the Cauchy stresses in both the fibre and cross-fibre directions as seen also with the increase in c, with a much larger simulated maximum Green strain in the fibre direction than the experimental maximum strain. If these unrealistic results were again to be associated with incompressibility and insufficient P values, then this would mean that the P value needed also fluctuates with changes in b_1.

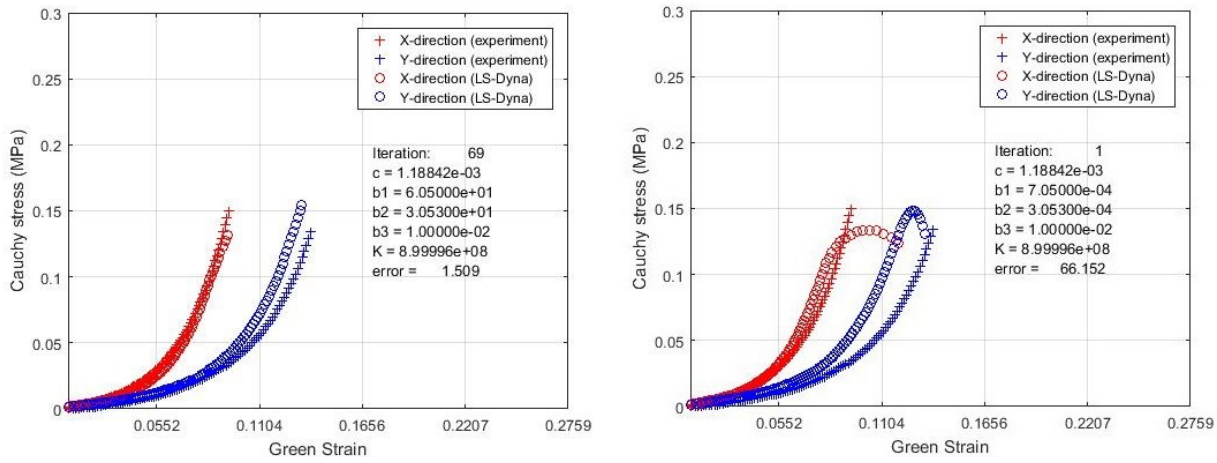

Figure 5.12: Comparison between simulated response of CC for different b_1.

The change in the simulated response of CC when increasing b_2 can be seen in Figure 5.13. As with the change in b_1, both the fibre and cross-fibre directions were affected, each predicting a stiffer response. There was more of an effect in the cross-fibre direction, which explains why b_2 is associated with the stiffness in that direction. However, unlike the changes in c and b_1, increasing b_2 did not produce the unrealistic results of the high Cauchy stresses decreasing or maximum Green strain being higher than the experimental. The Cauchy stresses at

high Green strains were still aligned with the simulated material response just being higher in magnitude.

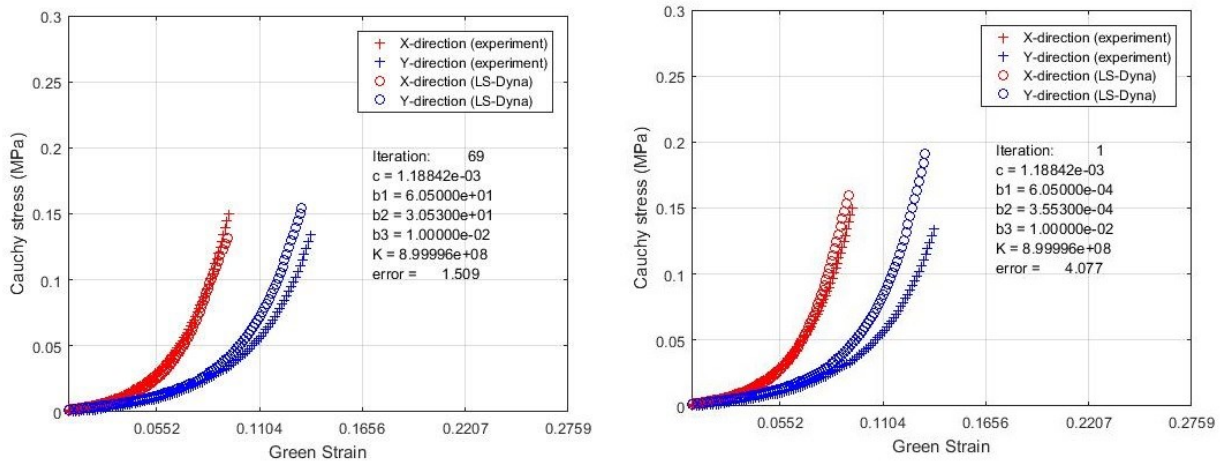

Figure 5.13: Comparison between simulated response of CC for different b_2.

Material constant b_3 is supposed to affect the material's response to shearing between the fibre and cross-fibre directions. The experimental results and simulated planar biaxial testing were taken from an equibiaxial test with the reference directions being aligned with the fibre directions. Therefore, there should theoretically be no effects from shear. Constant b_3 should effectively be zero for all the materials and should have no effect on the responses because if there was in-plane shear it would not be along the fibre or cross-fibre direction. This lack of an effect on the responses can be seen in Figure 5.14 where there is minimal change to the simulated responses in either direction with an increase in magnitude of b_3 from 10^{-12} to 100. To minimize computation time, when using an equibiaxial testing protocol, only the other four constants need to be optimized if optimizing all the material parameters.

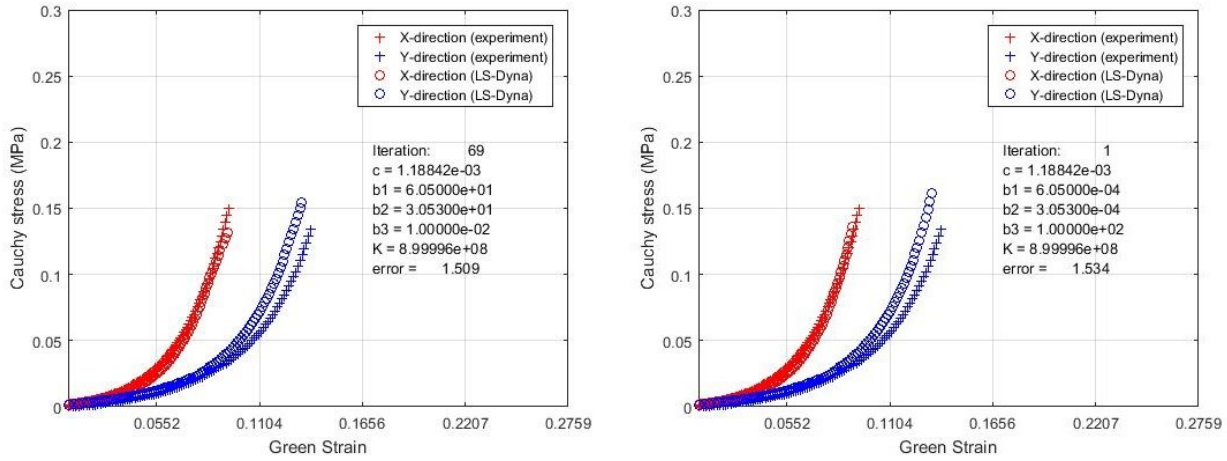

Figure 5.14: Comparison of simulated responses of CC with a change in b_3.

Finally, material parameter K is associated with the penalty term for ensuring incompressibility in FE programs. The values of K are dependent on c because K is defined such that $P=cK$. Figure 5.15 shows the difference in the simulated response of c when K is decreased. The simulated responses have the same shape, except for one significant change: in the fibre direction, at high Green strains, the response with the lower K begins to display unrealistic material behaviour where the rate of increase for Cauchy stresses begins to decrease with the Cauchy stresses remaining constant while the Green strains continue to increase and far exceed the experimental Green strains. In the cross-fibre direction, this effect also happens although for a smaller set of Cauchy stresses, and in this case, the Cauchy stresses even begin to decrease, but the maximum Green strain is the same as the experimental one. As mentioned, these effects would appear to make sense if they were related to incompressibility. With the decrease in the K value, the penalty term is no longer sufficiently high given CC's current c value to enforce incompressibility at these high Cauchy stress and Green strain values hence the unrealistic material behaviour.

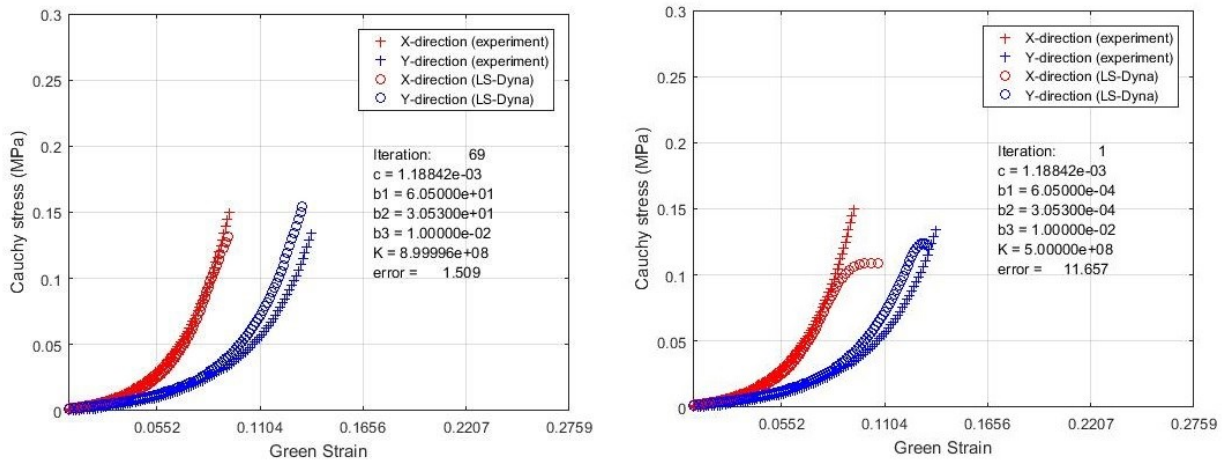

Figure 5.15: Comparison of the simulated response through two constant optimization of CC with a change in *K*.

As mentioned earlier, the generally accepted range of *K* for *P* to be sufficiently high is 10^3-10^4 [12]. However, the range of *K* found to produce acceptable results for the five biomaterials considered in this study was between approximately $5x10^8$- $9x10^8$ with this range increasing to up to $5x10^9$ for the manually determined *K* value of APP. This range is far above the current accepted range in the literature. Even with the implementation of the material's actual thickness which decreased the *K* value, GPP still had an optimized *K* of $1.5x10^7$. If the thickness was kept at 1mm, LS-DYNA would not even be able to produce a simulated response using the *K* from the literature because of the time step issue. There is no specific solution for these simulated responses; however, because the combination of constants is not unique, and many combinations may produce a similar simulated response, it is conceivable that there could be a range of *c* values that could produce acceptable simulated results with the range of *K* from the literature. More research could be done in developing the range combinations of constants *c* and *K*.

6 Conclusion and Future Work

In this thesis, the challenge of producing a simulated material response that will accurately predict the experimental planar biaxial behaviour of soft tissue was addressed. The issues that were explored included the effects of the incorporation of the penalty term to ensure incompressibility in FE programs, changes in the material parameters, and change in thickness on the simulated responses.

6.1 Summary of findings

The objective of this thesis was to develop a process to determine the optimized values for the five materials constants c, b_1, b_2, b_3, and K that would produce a simulated material response that would accurately predict soft tissue behaviour under a planar biaxial test with an equibiaxial protocol. The simulated response was implemented using a combination of MATLAB and LS-DYNA, using Guccione's strain energy function (LS-DYNA's MAT_HEART_TISSUE) with the incorporation of the penalty term such that $P=cK$. This optimization process required the input of the experimental behaviour of a material from planar biaxial testing as well as initial material parameters and experimental test conditions from the user. These initial parameters were implemented in LS-DYNA to determine a simulated response which was compared with the user provided experimental response using an error function. The constants were then optimized until the error function was minimized. Two optimization programs were developed, one optimized all five of the material parameters while the other only optimized two constants c and K. Five biomaterials were tested using each optimization process.

For all five biomaterials, the two-constant optimization program produced acceptable simulated responses that reflected the material's experimental behaviour. Two materials

produced unrealistic material behaviour at high Green strains. However, this issue was found to be removed by a manual increase in the optimized K value. There were some common discrepancies between the simulated and experimental responses across all the materials, such as predicting lower Cauchy stresses at high Greens strains and producing an overall stiffer material behaviour. These discrepancies remained present in the simulated responses with the optimization of all five constants, change in thickness, and when performing an FE analysis using only the central elements in the sample. It was seen that these discrepancies appeared in comparison of analytically determined and experimental material behaviour and were most likely linked to the shortcomings of the Guccione strain energy model itself. The simulated models displayed similar responses to analytically optimized responses for the same material when using the same experimental data for optimization and the analytically determined constants as initial guesses. This finding suggested that this optimization process successfully incorporated the penalty term into an already determined analytical model to develop an effective and functional FE material model.

The two-constant program was found to be sufficient in determining an acceptable simulated response when using analytically determined constants as initial guesses, and in some cases even produced better material behaviours than the five-constant optimization. Implementing a change in thickness of the material sample did have an effect on the simulated response, the corresponding material parameters with the original set thickness of 1 mm producing a better response than the response using the experimental thickness. However, the simulated response determined from the experimental thickness was still close enough that it could be used to predict material behaviour if true thickness was essential for the simulation. When processing the stress and strain results from only the central elements in the sample, the

material response was found to be slightly better producing a smoother curve than seen when using the whole model for the analysis. The optimized K values of the five materials were also found to be largely higher than the acceptable K range given in the literature with a range of approximately $5x10^8$-$5x10^9$.

6.2 Future work

There are several possibilities for future work to advance this research. As mentioned, the simulated responses only reflect the material's behaviour under planar equibiaxial testing (i.e. in the fibre and cross-fibre directions). Looking at effects from bending loads and incorporating them into the optimization program would be beneficial to determine a more robust material model for in vivo simulations. However, bending test results are very scarce in the literature, which would justify a full-blown experimental campaign after a robust testing protocol applicable to flimsy biomaterials has been devised.

Developing the program to be fully automatic, with the initial guesses for the material parameter being determined directly from the experimental responses and not user-determined, would also be an area that would be beneficial for future in-vivo simulations and the development of soft tissue material models. More research can also be done incorporating the true thickness of a material sample and the effects of thickness on computation times and material parameters.

The value of K and the incorporation of P into strain energy models have not been sufficiently studied given that they are essential for producing accurate simulated models. This thesis only discussed the effects of K on the Guccione strain energy model. More research into the effects of K and determining appropriate K values for other strain energy models would be beneficial.

The capabilities of various material models in simulating human soft tissue in vivo, healthy or otherwise, should also be evaluated. An experimental testing method which would allow the determination of mechanical properties while the tissue is still in vivo would significantly contribute to the accuracy and practically of these material models. As mentioned, indentation testing may allow for this capability to be implemented in the future, with minimal invasiveness. However, it is currently only capable of providing material properties in one direction. Further improvements in the design of the indenter and material model determined from this type of testing are needed. This would also allow for the development of patient specific soft tissue material models, thus providing a base, when paired with patient-specific geometry through FE models, for developing patient specific healthcare solutions.

References

[1] United Nations, "World Population Aging 2015," United Nations, New York, 2015.

[2] M. R. Labrosse and C. J. Beller , "Aortic valve leaflet sizer: a new device for aortic valve sparing," *Journal of Heart Valve Disease,* no. 16, pp. 145-147, 2007.

[3] Merriam-Webster, "Medical Definition of Soft Tissue," [Online]. Available: https://www.merriam-webster.com/medical/soft%20tissue. [Accessed 22 March 2107].

[4] G. A. Holzapfel , "Biomechanics of Soft Tissue," November 2000. [Online]. Available: https://biomechanics.stanford.edu/me338/me338_project02.pdf. [Accessed 20 March 2017].

[5] R. J. Minns, P.D. Soden, and D. S. Jackson, "The role of the fibrous components and ground substance in the mechanical properties of biological tissues: A preliminary investigation," *J. Biomech,* vol. 6, pp. 153-165, 1973.

[6] C. N. Maganaris and J. P. Paul, "In vivo human tendon mechanical properties," *The Journal of Physiology,* vol. 521, pp. 307-313, 1999.

[7] M. R. Labrosse et al, "Planar biaxial testing of heart valve cusp replacement biomaterials: Experiments, theory, and material constants," *Acta Biomaterialia,* vol. 45, pp. 303-320, 2016.

[8] J. D. Humphrey, Cardiovascular Solid Mechanics Cells, Tissues, and Organs, New York: Springer-Verlag New York, Inc., 2002.

[9] A. Aggarwal, "An improved parameter estimation and comparison for soft tissue constitutive models constaining exponential fuction," *Biomechanics and Modeling in Mechanobiology,* pp. 1-16, 2017.

[10] K. Miller et al, "Total Lagrangian explicit dynamics finite element algorithm for computing soft tissue deformation," *Communications in Numerical Methods in Engineering,* vol. 23, pp. 121-134, 2006.

[11] K. J. Bathe and M. M. I. Baig, "On a composite implicit time integration procedure for nonlinear dynamics," *Computers and Structures,* vol. 83, pp. 2513-2524, 2005.

[12] R. D. Wood and J. Bonet, Nonlinear continuum mechanics for finite element analysis, New York: Cambridge University Press, 1997.

[13] R. M. Bowen, Introduction to Continuum Mechanics for Engineers, New York: Plenum Press, 1989.

[14] Y. C. Fung, Biomechanics: Mechanical Properties of Living Tissue, 2nd ed., New York: Springer Verlag, 1993.

[15] W. Sun et al, "Biaxial mechanical response of bioprosthetic hear valve biomaterials to high in-plane shear," *J Biomech Eng,* vol. 112, no. 2, pp. 372-380, 2003.

[16] S. Wei and M. Sacks, "Finite element implemantion of a generalized Fung-elastic constitutive model for planar soft tissue," *Biomechanics and Modeling in Mechanobiology,* vol. 4, pp. 190-199, 2005.

[17] J. M. Guccione, A. D. McCulloch, and L. K. Waldman , "Passive material properties of intact ventricular myocardium determined from a cylindrical model," *ASME J. biomech. Engng,* vol. 113, pp. 42-55, 1991.

[18] G. A. Holzapfel, T. C. Gasser, and R. W. Ogden, "A new constitutive framework for arterial wall mechanics and a comparative study of material models," *Journal of Elasticity,* vol. 61, pp. 1-48, 2000.

[19] R. M. Delaine-Smith, et al, "Experimental validation of a flat punch indentation methodology calibrated against unconfined compression tests for determination of soft tissue biomechanics," *Journal of the Mechanical Behaviour of Biomedical Materials,* vol. 60, pp. 401-415, 2016.

[20] C. Valero et al, "Finite element simulation for the mechanical characterization of soft biological materials by atomic force microscopy," *Journal of the Mechanical Behavior of Biomedical Materials,* vol. 62, pp. 222-235, 2016.

[21] C. Lee et al, "An inverse modeling approach for the stress estimation in mitral valve anterior leaflets valvuloplasty for in-vivo valvular biomaterials assessments," *Journal of Biomechanics,* vol. 47, pp. 2055-2063, 2014.

[22] A. Wittek et al, "A finite element updating approach for identification of an anisotropic hyperelastic properties of normal and diseased aortic walls from 4D ultrasound strain imaging," *Journal of the mechanical behaviour of biomedical materials,* vol. 58, pp. 122-138, 2016.

[23] MathWorks, "fmincon," 2017. [Online]. Available: https://www.mathworks.com/help/optim/ug/fmincon.html. [Accessed 24 February 2017].

[24] W. Sun and M. S. Sacks, "Finite element implementation of a generalized Fung-elastic constitutive model for planar soft tissue," *Biomech. Model Mechanobiol.,* vol. 4, pp. 190-199, 2005.

[25] F. B. Hildebrand, Advance Calculus for Applications, Prentice-Hall, 1962.

[26] M. Hazewinked et al, "Positive-definite Form," in *Encyclopedia of Mathematics*, Springer, 2001.

[27] MathWorks, "Constrained Nonlinear Optimization Algorithms," 2017. [Online]. Available: https://www.mathworks.com/help/optim/ug/constrained-nonlinear-optimization-algorithms.html#brnpd5f. [Accessed 30 January 2017].

[28] MathWorks, "Optimization Options Reference," 2017. [Online]. Available: https://www.mathworks.com/help/optim/ug/optimization-options-reference.html. [Accessed 30 January 2017].

Appendix A: Simulated Material Responses

From the two-constants optimization:

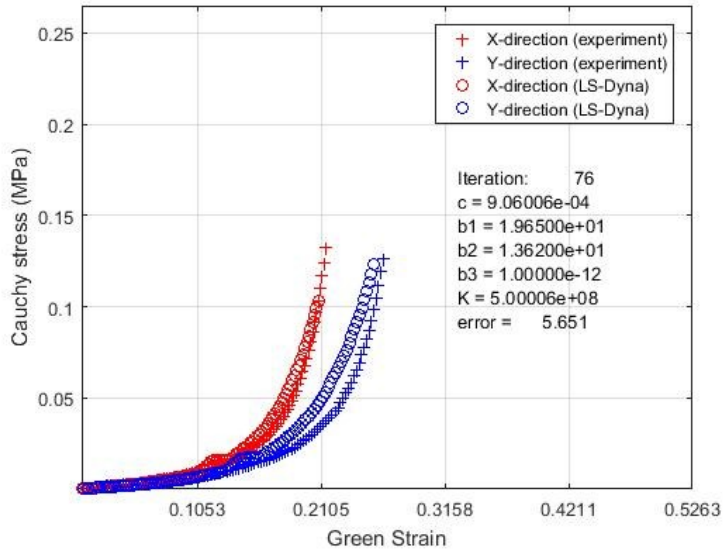

Figure A.1: Simulated response for GPP through the optimization of *c* and *K*.

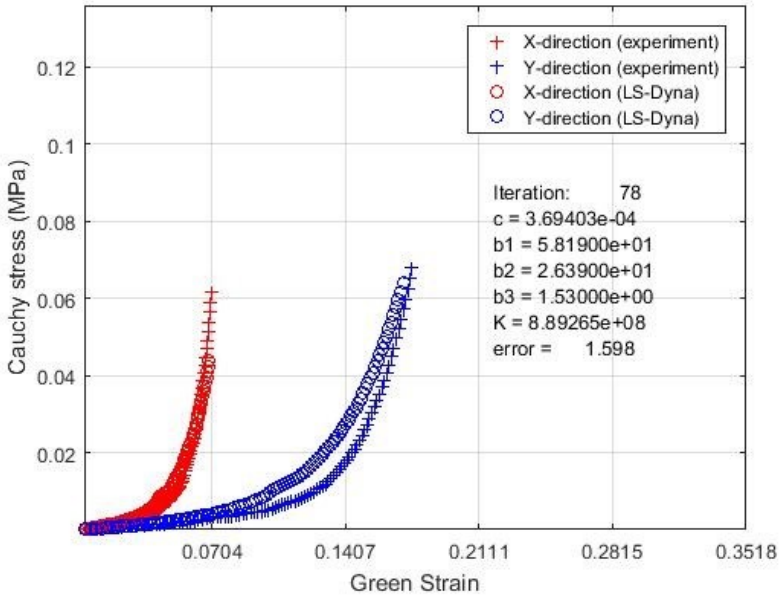

Figure A.2: Simulated response for PC through the optimization of *c* and *K*.

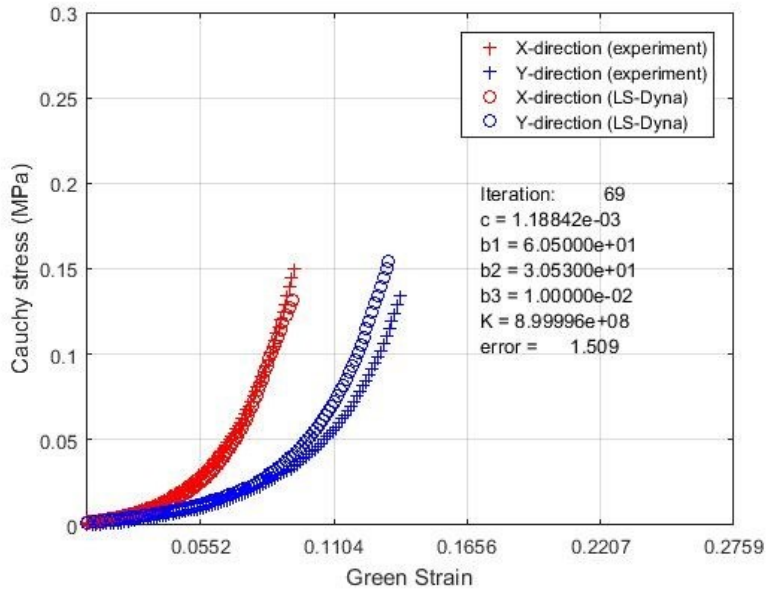

Figure A.3: Simulated response for CC through the optimization of *c* and *K*.

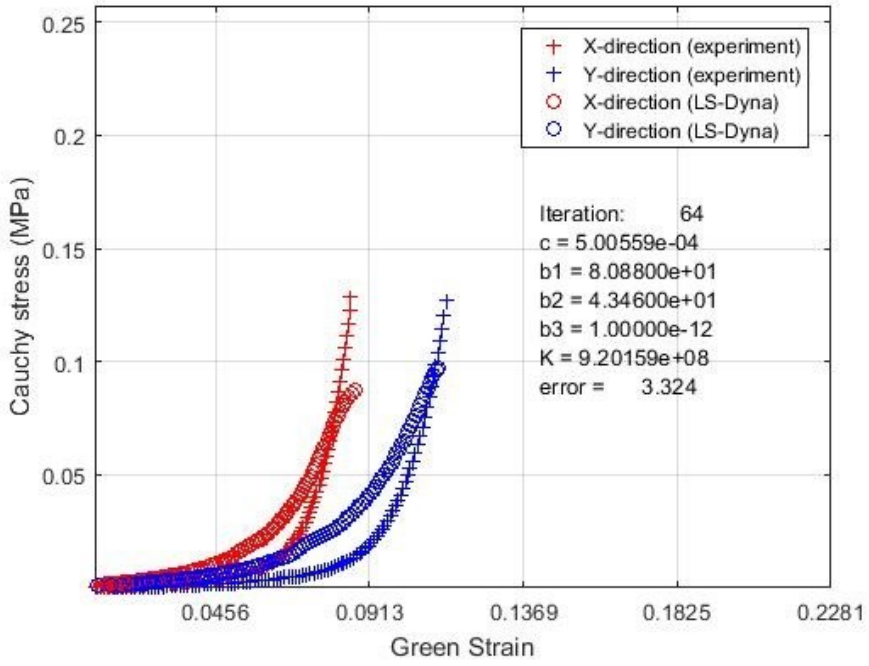

Figure A.4: Simulated response for APP through the optimization of *c* and *K*.

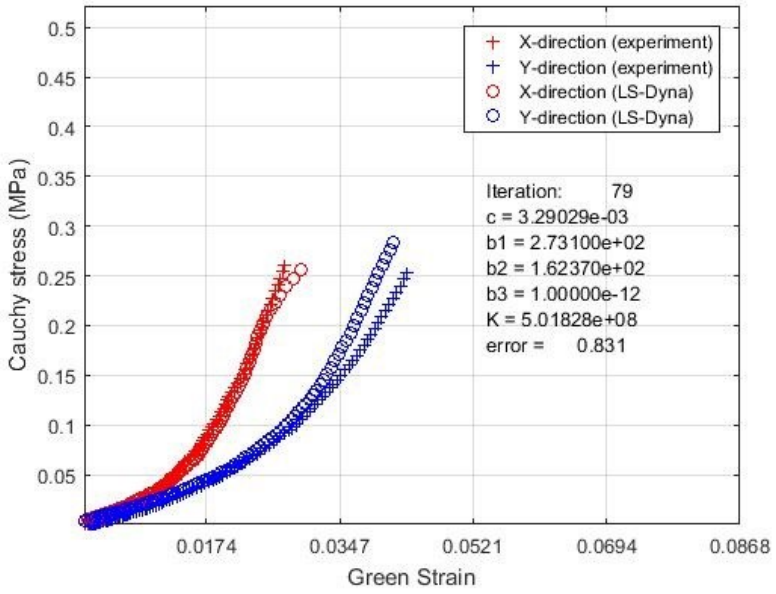

Figure A.5: Simulated response for SJM through the optimization of *c* and *K*.

From the five-constant optimizations:

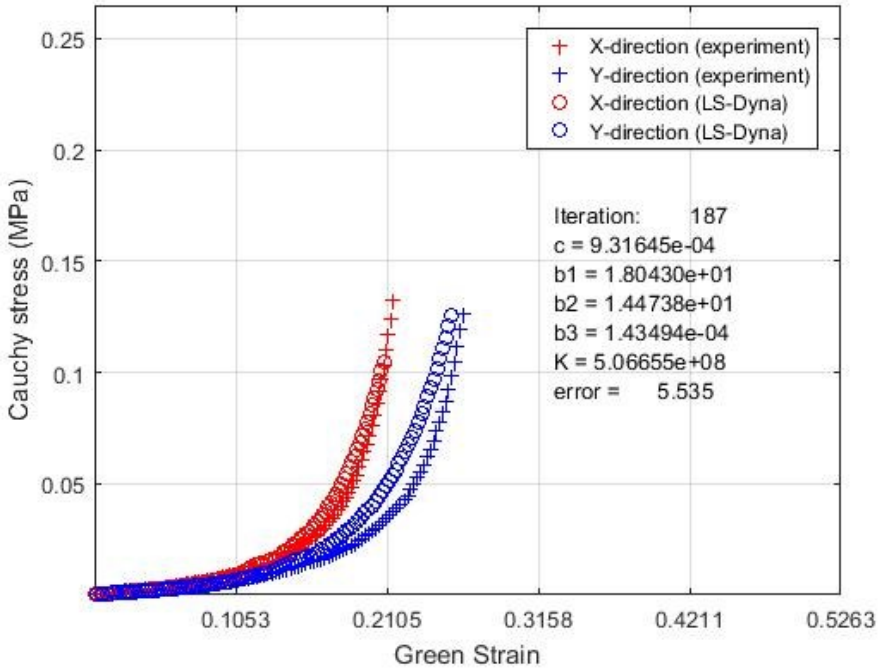

Figure A.6: Simulated response for GPP through the optimization of all five parameters.

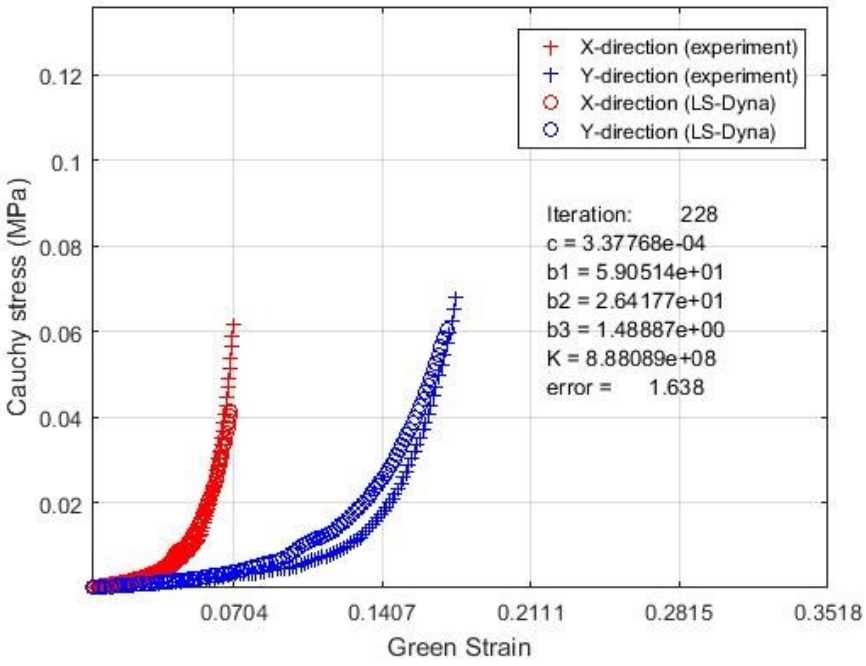

Figure A.7: Simulated response for PC through the optimization of all five parameters.

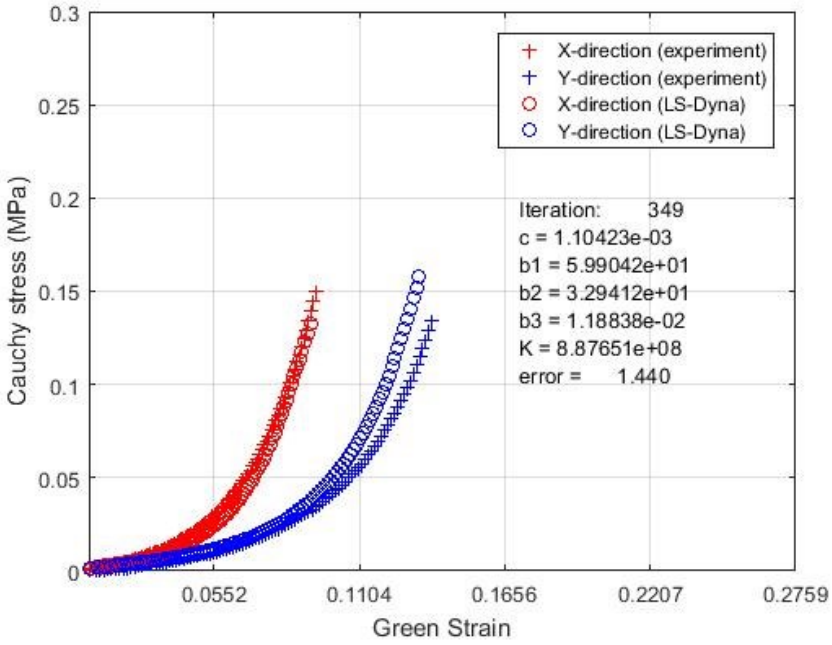

Figure A.8: Simulated response for CC through the optimization of all five parameters.

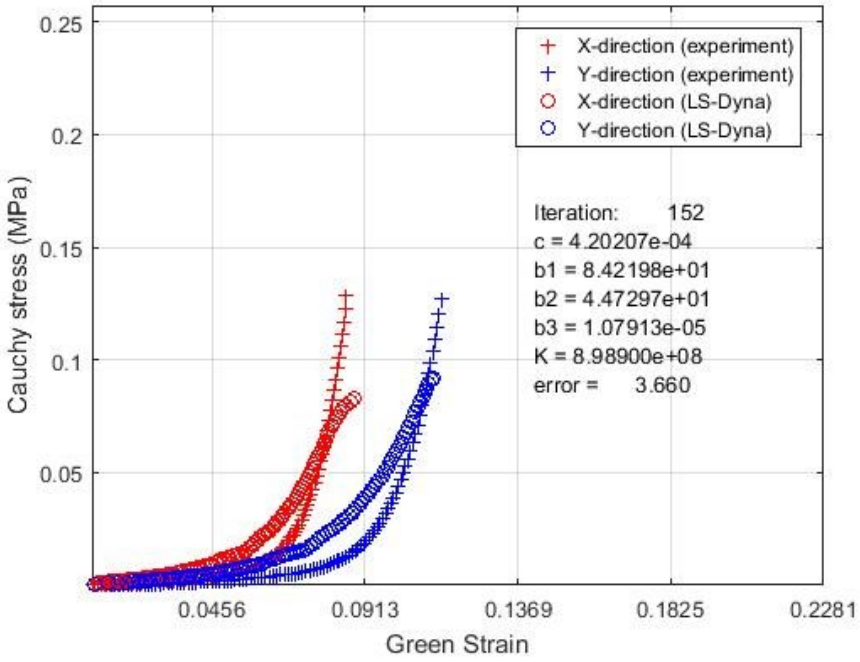

Figure A.9: Simulated response for APP through the optimization of all five parameters.

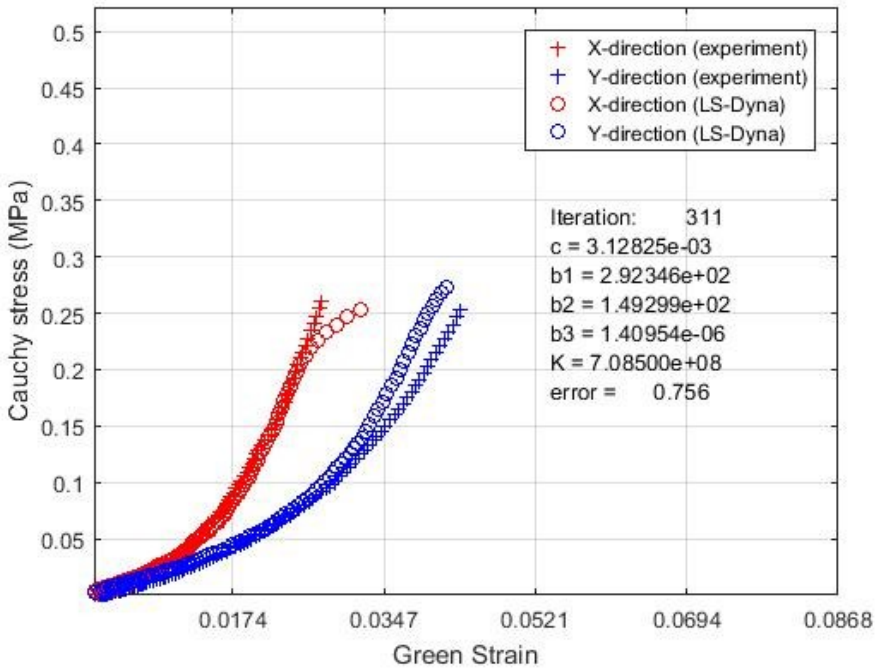

Figure A.10: Simulated response for SJM through the optimization of all five parameters.

Appendix B: MATLAB Programs

```
function computesLSDynaHeartTissueConstantsFromBiaxialTestingData_5const()

clc
clear

E11ave = [];
E22ave = [];
T11Save = [];
T22Save = [];

Constants = zeros(1,5);

% Load experimental data from bixial testing (SPG material)
load('TSvsE_SJM.mat','E11ave','E22ave','T11Save','T22Save');


nChar = 90;  % Default number of characters in input dialog

go_on = 'Y';
while strcmp(go_on,'Y')
    dlg_title = 'Parameters for analysis';
    prompt = {'Enter new parameters, (Y)ES or (N)O:?'};
    def = {'Y'};
    answer0 = inputdlg(prompt,dlg_title,[1 nChar],def);
    if isempty(answer0)
        return
    else
        go_on = answer0{1};
        if strcmp(go_on,'Y')
            dlg_title = 'Input of material constants';
    prompt = {...
    'Enter value for constant c (scales overall response), in MPa:';...
    'Enter value for constant b1 (~ stiffness in x-direction), [-]:';...
    'Enter value for constant b2 (~ stiffness in y-direction), [-]:';...
    'Enter value for constant b3 (~ stiffness in xy-direction), [-]:';...
    'Enter sample x-y dimensions, in mm:';...
    'Enter sample thickness (in z-direction), in mm';...
    'Enter duration of loading , in seconds:';...
    'Enter number of elements in x- and y-directions:';...
    'Enter number of elements z-direction:'};
            if Constants(1) == 0
    def = {'2.126e-2','273.10','162.37','1e-12','5','1','0.01','10','2'};
            else
    def = {num2str(Constants(1),'%10.5e'),...
           num2str(Constants(2),'%10.2e'),...
           num2str(Constants(3),'%10.2e'),...
           num2str(Constants(4),'%10.1e'),...
           num2str(Dim.X,'%10.1f'),...
           num2str(Dim.Z,'%10.2f'),...
           num2str(Dim.endTime,'%10.4f'),...
           num2str(Dim.MeshX-1,'%3i'),...
           num2str(Dim.MeshZ-1,'%3i')};
```

```
end
answer1 = inputdlg(prompt,dlg_title,...
[1 nChar;1 nChar;1 nChar;1 nChar;1 nChar;...
 1 nChar;1 nChar;1 nChar;1 nChar],def);
if isempty(answer1)
    return
else
    for i = 1:4
        Constants(i) =  str2double(answer1{i});
    end
    Dim.X = str2double(answer1{5});
    Dim.Z = str2double(answer1{6});
    Dim.endTime = str2double(answer1{7});
    Dim.MeshX = str2double(answer1{8})+1;
    Dim.MeshZ = str2double(answer1{9})+1;
end


Dim.Y = Dim.X;
Dim.MeshY = Dim.MeshX;
Dim.nStates = 20;     % number of saves during analysis
weightc=1e2;
weightb=1e5;
weightk = 1e14;

% Data from Protocol 5 (~ equibiaxial)
Dim.nDataPoints = size(E11ave,1);

% experimental Green strain in x-direction
Dim.GSXexp = E11ave(:,5);
% experimental Green strain in y-direction
Dim.GSYexp = E22ave(:,5);

% In-plane stretch ratios
Dim.lambdaX = sqrt(2.*Dim.GSXexp + 1);
Dim.lambdaY = sqrt(2.*Dim.GSYexp + 1);

% experimental Cauchy stress in x-direction, in MPa
Dim.CSXexp = T11Save(:,5).*Dim.lambdaX.^2*1e-3/Dim.Z;
% experimental Cauchy stress in y-direction, in MPa
Dim.CSYexp = T22Save(:,5).*Dim.lambdaY.^2*1e-3/Dim.Z;
% experimental Cauchy stress in xy-direction, in MPa


% Part definition
npart = 1;
part = cell(1,npart);
part(1) = cellstr('Membrane Sample');

% Nodes
x = 0:Dim.X/(Dim.MeshX-1):Dim.X;
y = 0:Dim.Y/(Dim.MeshY-1):Dim.Y;
z = 0:Dim.Z/(Dim.MeshZ-1):Dim.Z;
Dim.Nnodes = Dim.MeshX*Dim.MeshY*Dim.MeshZ;
Nodes = zeros(Dim.Nnodes,4);
```

```
for i = 1:Dim.MeshZ
    for j = 1:Dim.MeshY
        for k = 1:Dim.MeshX
Nodes(k+Dim.MeshX*(j-1)+Dim.MeshX*Dim.MeshY*(i-1),:) = ...
[k+Dim.MeshX*(j-1)+Dim.MeshX*Dim.MeshY*(i-1);x(k);y(j);z(i)];
        end
    end
end

% Brick elements
Dim.Nelems = (Dim.MeshX-1)*(Dim.MeshY-1)*(Dim.MeshZ-1);
Elements = zeros(Dim.Nelems,9);
for i = 1:(Dim.MeshZ-1)
    for j = 1:(Dim.MeshY-1)
        for k = 1:(Dim.MeshX-1)
 Elements(k+(Dim.MeshX-1)*(j-1)+...
     (i-1)*(Dim.MeshX-1)*(Dim.MeshY-1),:) = ...
[k+(Dim.MeshX-1)*(j-1)+(i-1)*(Dim.MeshX-1)*(Dim.MeshY-1);...
 k+(j-1)*Dim.MeshX+(i-1)*Dim.MeshX*Dim.MeshY;...
 k+(j-1)*Dim.MeshX+i*Dim.MeshX*Dim.MeshY;...
 k+1+(j-1)*Dim.MeshX+i*Dim.MeshX*Dim.MeshY;...
 k+(j-1)*Dim.MeshX+(i-1)*Dim.MeshX*Dim.MeshY+1;...
 k+j*Dim.MeshX+(i-1)*Dim.MeshX*Dim.MeshY;...
 k+j*Dim.MeshX+i*Dim.MeshX*Dim.MeshY;...
 k+1+j*Dim.MeshX+i*Dim.MeshX*Dim.MeshY;...
 k+1+j*Dim.MeshX+(i-1)*Dim.MeshX*Dim.MeshY];
        end
    end
end

% Nodes that have boundary conditions
% corner nodes
count = 0;
for k = 1:Dim.MeshZ
    count = count+1;
    BC.Cnode(count) = 1+(k-1)*Dim.MeshX*Dim.MeshY;
end
BC.nCnode = count;

% Side 1 nodes
count = 0;
for k = 1:Dim.MeshZ
    for i = 2:Dim.MeshX
        count = count+1;
        BC.S1node(count) = i+(k-1)*Dim.MeshX*Dim.MeshY;
    end
end
BC.nS1node = count;

% Side 2 nodes
count = 0;
for k = 1:Dim.MeshZ
    for j = 1:Dim.MeshY
        count = count+1;
        BC.S2node(count) = ...
        Dim.MeshX+(j-1)*Dim.MeshX+(k-1)*Dim.MeshX*Dim.MeshY;
```

```
            end
        end
        BC.nS2node = count;

        % Side 3 nodes
        count = 0;
        for k = 1:Dim.MeshZ
            for i = 1:Dim.MeshX
                count = count+1;
                BC.S3node(count) = ...
                i+(Dim.MeshY-1)*Dim.MeshX+(k-1)*Dim.MeshX*Dim.MeshY;
            end
        end
        BC.nS3node = count;

        % Side 4 nodes
        count = 0;
        for k = 1:Dim.MeshZ
            for j = 2:Dim.MeshY
                count = count+1;
                BC.S4node(count) = ...
                1+(j-1)*Dim.MeshX+(k-1)*Dim.MeshX*Dim.MeshY;
            end
        end
        BC.nS4node = count;

        %scale constants for optimization
        Constants(1)=Constants(1)/weightc;
        Constants(2)=Constants(2)/weightb;
        Constants(3)=Constants(3)/weightb;

         %intial cycle error calc
        initalc =[Constants(1), (Constants(1)*1e-1), (Constants(1)*1e1),
(Constants(1)/(1e1/2)), ((Constants(1)*1e1)/(1e1/2))];
        initalk= [2e7/weightk, 1e8/weightk, 6e7/weightk, 5e8/weightk,
9e8/weightk];
        count=0;
        initalerror=zeros(20,1);
        finalerror=inf;
        for k = 1:5
            Constants(1)=initalc(k);
            for i=1:5
            count=count+1;
            Constants(5)=initalk(i);
            initalerror(count)
=computesError(Constants,part,npart,Nodes,Elements,Dim,BC,weightc,weightb,wei
ghtk);
            if initalerror(count)< finalerror
               finalerror=initalerror(count);
               finalc=initalc(k);
               finalk=initalk(i);
            end
            end
        end
        Constants(1)=finalc;
        Constants(5)=finalk;
```

```
            % Launches simulation and computes error between curves
        options = optimset('Algorithm','interior-
point','Display','iter','MaxFunEvals',5000,'FinDiffType','central','TolFun',1
e-6);
        x0=Constants;
        A=[0,-weightb,-weightb,0,0;0,-weightb,-3*weightb,-1,0;];
        b=[0;0];
        Aeq=[];
        beq=[];
        lb=[1e-5/weightc 0 0 -inf (1.5e7/weightk)];
        ub=[9e-2/weightc inf inf inf (1e9/weightk)];

x=fmincon(@(Constants)computesError(Constants,part,npart,Nodes,Elements,Dim,B
C,weightc,weightb,weightk),x0,A,b,Aeq,beq,lb,ub,@(Constants)nonlinconstraints
(Constants,weightb),options);
        Constants=x;
        error =
computesError(Constants,part,npart,Nodes,Elements,Dim,BC,weightc,weightb,weig
htk);

        end % end if strcmp(go_on,'Y')
    end % end if isempty(answer0)
end % end while strcmp(go_on,'Y')

end

function error =
computesError(Constants,part,npart,Nodes,Elements,Dim,BC,weightc,weightb,weig
htk)

fprintf(['c = %-10.5e\n',....
                'b1 = %-10.2e\n',....
                'b2 = %-10.2e\n',....
                'b3 = %-10.1e\n',....
                'K = %-10.0e'],...
(Constants(1)*weightc),(Constants(2)*weightb),(Constants(3)*weightb),Constant
s(4),...
(Constants(5)*weightk));

persistent iterationCount plotHandle

runLSDyna(Constants,part,npart,Nodes,Elements,Dim,BC,weightc,weightb,weightk)
;
[CSXnum,CSYnum,GSXnum,GSYnum] = LSpostprocessing(Dim);

CSXnum = resamplesVector(CSXnum,Dim.nDataPoints,'spline');
CSYnum = resamplesVector(CSYnum,Dim.nDataPoints,'spline');
GSXnum = resamplesVector(GSXnum,Dim.nDataPoints,'spline');
GSYnum = resamplesVector(GSYnum,Dim.nDataPoints,'spline');


scale = norm(Dim.CSXexp.^2 + Dim.GSXexp.^2 + ...
        Dim.CSYexp.^2 + Dim.GSYexp.^2);
```

```
error = norm((CSXnum - Dim.CSXexp).^2 + (GSXnum - Dim.GSXexp).^2 + ...
        (CSYnum - Dim.CSYexp).^2 + (GSYnum - Dim.GSYexp).^2);



% comparing ratios in curvature

%first for experimental

straightLengthXexp = sqrt((Dim.GSXexp(Dim.nDataPoints) - ...
                           Dim.GSXexp(round(Dim.nDataPoints/1.5)))^2 + ...
                          (Dim.CSXexp(Dim.nDataPoints) - ...
                           Dim.CSXexp(round(Dim.nDataPoints/1.5)))^2);
straightLengthYexp = sqrt((Dim.GSYexp(Dim.nDataPoints) - ...
                           Dim.GSYexp(round(Dim.nDataPoints/1.5)))^2 + ...
                          (Dim.CSYexp(Dim.nDataPoints) - ...
                           Dim.CSYexp(round(Dim.nDataPoints/1.5)))^2);

curveLengthXexp = 0;
for i = round(Dim.nDataPoints/1.5):Dim.nDataPoints-1
    curveLengthXexp = curveLengthXexp + ...
                      sqrt((Dim.GSXexp(i+1) - Dim.GSXexp(i))^2 + ...
                           (Dim.CSXexp(i+1) - Dim.CSXexp(i))^2);
end
curveLengthYexp = 0;
for i = round(Dim.nDataPoints/1.5):Dim.nDataPoints-1
    curveLengthYexp = curveLengthYexp + ...
                      sqrt((Dim.GSYexp(i+1) - Dim.GSYexp(i))^2 + ...
                           (Dim.CSYexp(i+1) - Dim.CSYexp(i))^2);
end

% for simulated
straightLengthXnum = sqrt((GSXnum(Dim.nDataPoints) - ...
                           GSXnum(round(Dim.nDataPoints/1.5)))^2 + ...
                          (CSXnum(Dim.nDataPoints) - ...
                           CSXnum(round(Dim.nDataPoints/1.5)))^2);
straightLengthYnum = sqrt((GSYnum(Dim.nDataPoints) - ...
                           GSYnum(round(Dim.nDataPoints/1.5)))^2 + ...
                          (CSYnum(Dim.nDataPoints) - ...
                           CSYnum(round(Dim.nDataPoints/1.5)))^2);
curveLengthXnum = 0;
for i = round(Dim.nDataPoints/1.5):Dim.nDataPoints-1
    curveLengthXnum = curveLengthXnum + ...
                      sqrt((GSXnum(i+1) - GSXnum(i))^2 + ...
                           (CSXnum(i+1) - CSXnum(i))^2);
end
curveLengthYnum = 0;
for i = round(Dim.nDataPoints/1.5):Dim.nDataPoints-1
    curveLengthYnum = curveLengthYnum + ...
                      sqrt((GSYnum(i+1) - GSYnum(i))^2 + ...
                           (CSYnum(i+1) - CSYnum(i))^2);
end

error = (100*error/scale)+ ...
         100*abs(curveLengthXnum/straightLengthXnum - ...
```

```
                curveLengthXexp/straightLengthXexp) + ...
          100*abs(curveLengthYnum/straightLengthYnum - ...
                curveLengthYexp/straightLengthYexp);
display(error)

if ishandle(plotHandle)
    iterationCount = iterationCount + 1;
else
    iterationCount = 1;
end

plotHandle = plot(Dim.GSXexp,Dim.CSXexp,'+r',...
     Dim.GSYexp,Dim.CSYexp,'+b',...
     GSXnum,CSXnum,'or',...
     GSYnum,CSYnum,'ob');
set(gca,'XTick',...
    0:2*max([Dim.GSXexp;Dim.GSYexp])/5:2*max([Dim.GSXexp;Dim.GSYexp]))
axis([min([Dim.GSXexp;Dim.GSYexp]) 2*max([Dim.GSXexp;Dim.GSYexp]) ...
      min([Dim.CSXexp;Dim.CSYexp]) 2*max([Dim.CSXexp;Dim.CSYexp])])
ylabel('Cauchy stress (MPa)')
xlabel('Green Strain')
legend('X-direction (experiment)','Y-direction (experiment)',...
       'X-direction (LS-Dyna)','Y-direction (LS-Dyna)');
grid on;
str = sprintf(['Iteration: % 10i\n',...
               'c = %-10.5e\n',....
               'b1 = %-10.5e\n',....
               'b2 = %-10.5e\n',....
               'b3 = %-10.5e\n',....
               'K = %-10.5e\n',...
               'error = %10.3f'],...
iterationCount,Constants(1)*weightc,Constants(2)*weightb,...
Constants(3)*weightb,Constants(4),Constants(5)*weightk,error);
text(6.2*max([Dim.GSXexp;Dim.GSYexp])/5,max([Dim.CSXexp;Dim.CSYexp]),str);

end

function
runLSDyna(Constants,part,npart,Nodes,Elements,Dim,BC,weightc,weightb,weightk)
savefile = 'LSDynaInputDeck.dyn';
fid = fopen(savefile, 'wt');
fprintf(fid, '*KEYWORD\n');
fprintf(fid, '$---+----1----+----2----+----3----+----4----+----5----+----6---
-+----7----+----8\n');
fprintf(fid, '$                    TITLE CARD\n');
fprintf(fid, '$---+----1----+----2----+----3----+----4----+----5----+----6---
-+----7----+----8\n');
fprintf(fid, '*TITLE\n');
fprintf(fid, 'In-plane biaxial simulation\n');
fprintf(fid, '$---+----1----+----2----+----3----+----4----+----5----+----6---
-+----7----+----8\n');
fprintf(fid, '$                    CONTROL CARDS\n');
fprintf(fid, '$---+----1----+----2----+----3----+----4----+----5----+----6---
-+----7----+----8\n');
fprintf(fid, '*CONTROL_TERMINATION\n');
fprintf(fid, '$   ENDTIM    ENDCYC     DTMIN    ENDNEG    ENDMAS\n');
```

```
fprintf(fid, '%10f         0       0.0       0.0       0.0\n', Dim.endTime);
fprintf(fid, '*CONTROL_TIMESTEP\n');
fprintf(fid, '$   DTINIT      SCFT      ISDO    TSLIMT      DTMS      LCTM
ERODE     MS1ST\n');
fprintf(fid, '      0.00       0.9         0\n');
fprintf(fid, '*CONTROL_HOURGLASS\n');
fprintf(fid, '$      IHQ        QH\n');
fprintf(fid, '         1       0.1\n');
fprintf(fid, '*CONTROL_BULK_VISCOSITY\n');
fprintf(fid, '$       Q2        Q1\n');
fprintf(fid, ' 0.150E+01 0.600E-01\n');
fprintf(fid, '*CONTROL_OUTPUT\n');
fprintf(fid, '$    NPOPT    NEECHO    NREFUP    IACCOP     OPIFS    IPNINT
IKEDIT\n');
fprintf(fid, '         0         0         0         0 0.000E+00         0
0\n');
fprintf(fid, '*CONTROL_ENERGY\n');
fprintf(fid, '$     HGEN      RWEN    SLNTEN     RYLEN\n');
fprintf(fid, '         1         2         1         1\n');
fprintf(fid, '$---+----1----+----2----+----3----+----4----+----5----+----6---
-+----7----+----8\n');
fprintf(fid, '$                    DATABASE CONTROL CARDS FOR BINARY
FILE\n');
fprintf(fid, '$---+----1----+----2----+----3----+----4----+----5----+----6---
-+----7----+----8\n');
fprintf(fid, '*DATABASE_BINARY_D3PLOT\n');
fprintf(fid, '%40i \n',Dim.nStates);
fprintf(fid, '*DATABASE_EXTENT_BINARY\n');
fprintf(fid, '         0         0         3         0         1         1
1         1\n');
fprintf(fid, '         0         0         0         0         0
0\n');
fprintf(fid, '$---+----1----+----2----+----3----+----4----+----5----+----6---
-+----7----+----8\n');
fprintf(fid, '$                    DEFINE PARTS CARDS\n');
fprintf(fid, '$---+----1----+----2----+----3----+----4----+----5----+----6---
-+----7----+----8\n');
for i = 1:npart
   fprintf(fid, '*PART\n');
   fprintf(fid, '$ HEADING\n');
   fprintf(fid, '  PART PID =      %2i PART NAME : %s\n', i,char(part(i)));
   fprintf(fid, '$      PID       SID       MID     EOSID      HGID      GRAV
ADPOPT      TMID\n');
   fprintf(fid, '%10i %9i %9i\n', i,i,i);
end
fprintf(fid, '$---+----1----+----2----+----3----+----4----+----5----+----6---
-+----7----+----8\n');
fprintf(fid, '$                    MATERIAL CARDS\n');
fprintf(fid, '$---+----1----+----2----+----3----+----4----+----5----+----6---
-+----7----+----8\n');
for i = 1:npart
   fprintf(fid, '*MAT_HEART_TISSUE +\n');
   fprintf(fid, '$ MATERIAL NAME :%s\n', char(part(i)));
   fprintf(fid, '$      MID        RO         C        B1        B2        B3
P\n');
   fprintf(fid, '%20i %19.12E %19.12E %19.12E %19.12E %19.12E %19.12E \n',
i,0.1E-
```

```
8,(Constants(1)*weightc),(Constants(2)*weightb),(Constants(3)*weightb),Consta
nts(4),((Constants(5)*weightk)*(Constants(1)*weightc)));
   fprintf(fid, '$     AOPT\n');
   fprintf(fid, '         0\n');
   fprintf(fid, '$       XP        YP        ZP        A1        A2
A3\n\n');
   fprintf(fid, '$       V1        V2        V3        D1        D2        D3
BETA\n\n');
end
fprintf(fid, '$---+----1----+----2----+----3----+----4----+----5----+----6---
-+----7----+----8\n');
fprintf(fid, '$                     SECTION CARDS\n');
fprintf(fid, '$---+----1----+----2----+----3----+----4----+----5----+----6---
-+----7----+----8\n');
for i = 1:npart
   fprintf(fid, '*SECTION_SOLID\n');
   fprintf(fid, '$    SECID    ELFORM       AET\n');
   fprintf(fid, '%10i %9i\n', i,1); % 1 means constant stress elements; 2
would mean constant pressure elements
end
fprintf(fid, '$---+----1----+----2----+----3----+----4----+----5----+----6---
-+----7----+----8\n');
fprintf(fid, '$                      (8) NODAL POINT CARDS\n');
fprintf(fid, '$---+----1----+----2----+----3----+----4----+----5----+----6---
-+----7----+----8\n');
fprintf(fid, '*NODE\n');
fprintf(fid, '$   NODE               X               Y               Z
TC      RC\n');
for i = 1:Dim.Nnodes
    fprintf(fid, '%8i %15.9f %15.9f
%15.9f\n',Nodes(i,1),Nodes(i,2),Nodes(i,3),Nodes(i,4));
end
fprintf(fid, '$---+----1----+----2----+----3----+----4----+----5----+----6---
-+----7----+----8\n');
fprintf(fid, '$                      (11) SOLID ELEMENT CARDS\n');
fprintf(fid, '$---+----1----+----2----+----3----+----4----+----5----+----6---
-+----7----+----8\n');
fprintf(fid, '*ELEMENT_SOLID\n');
fprintf(fid, '$    EID     PID      N1      N2      N3      N4      N5
N6      N7      N8\n');
for i = 1:Dim.Nelems
    pid = 1;
    fprintf(fid, '%8i %7i %7i %7i %7i %7i %7i %7i %7i %7i\n',...

Elements(i,1),pid,Elements(i,2),Elements(i,3),Elements(i,4),Elements(i,5),Ele
ments(i,6),Elements(i,7),Elements(i,8),Elements(i,9));
end
fprintf(fid, '$---+----1----+----2----+----3----+----4----+----5----+----6---
-+----7----+----8\n');
fprintf(fid, '$                     BOUNDARY CONDITION CARDS\n');
fprintf(fid, '$---+----1----+----2----+----3----+----4----+----5----+----6---
-+----7----+----8\n');
% Restrict motions at specific nodes
fprintf(fid, '*BOUNDARY_SPC_NODE\n');
fprintf(fid, '$ NID/NSID       CID      DOFX      DOFY      DOFZ     DOFRX
DOFRY     DOFRZ\n');
```

```
fprintf(fid, '%10i %9i %9i %9i %9i \n',BC.Cnode(1),0,1,1,1);          % no x,
y or z displacements at origin
for i = 2:Dim.MeshZ
   fprintf(fid, '%10i %9i %9i %9i %9i \n',BC.Cnode(i),0,1,1,0);       % no x
or y displacements for corner nodes
end
for i = 1:BC.nS1node
    fprintf(fid, '%10i %9i %9i %9i %9i \n',BC.S1node(i),0,0,1,0);     % no y
displacements for Side 1 nodes
end
for i = 1:BC.nS4node
    fprintf(fid, '%10i %9i %9i %9i %9i \n',BC.S4node(i),0,1,0,0);     % no x
displacements for Side 4 nodes
end
% Imposes motions at specific nodes
fprintf(fid, '*BOUNDARY_PRESCRIBED_MOTION_NODE\n');
fprintf(fid, '$      NID       DOF       VAD      LCID        SF       VID
DEATH     BIRTH\n');
%   displacement in x-direction
for i = 1:BC.nS2node
    fprintf(fid, '%10i %9i %9i %9i\n',BC.S2node(i),1,2,1);
end
%   displacement in y-direction
for i = 1:BC.nS3node
    fprintf(fid, '%10i %9i %9i %9i\n',BC.S3node(i),2,2,2);
end
% Define edge node displacement load curves
fprintf(fid, '*DEFINE_CURVE\n');
fprintf(fid, '$     LCID      SIDR      SCLA      SCLO      OFFA
OFFO\n');
fprintf(fid, '%10i %9i\n',1,0);
fprintf(fid, '$                A1                  O1\n');
fprintf(fid, '      0.00000000E+00      0.00000000E+00\n');
for i = 1:Dim.nDataPoints
fprintf(fid, '      %14.9f
%14.9f\n',i*Dim.endTime/Dim.nDataPoints,Dim.X.*(Dim.lambdaX(i)-1));
end
fprintf(fid, '      %14.9f
%14.9f\n',1.01*Dim.endTime,Dim.X.*(Dim.lambdaX(Dim.nDataPoints)-1));
fprintf(fid, '*DEFINE_CURVE\n');
fprintf(fid, '$     LCID      SIDR      SCLA      SCLO      OFFA
OFFO\n');
fprintf(fid, '%10i %9i\n',2,0);
fprintf(fid, '$                A1                  O1\n');
fprintf(fid, '      0.00000000E+00      0.00000000E+00\n');
for i = 1:Dim.nDataPoints
fprintf(fid, '      %14.9f
%14.9f\n',i*Dim.endTime/Dim.nDataPoints,Dim.Y.*(Dim.lambdaY(i)-1));
end
fprintf(fid, '      %14.9f
%14.9f\n',1.01*Dim.endTime,Dim.Y.*(Dim.lambdaY(Dim.nDataPoints)-1));
fprintf(fid, '*END\n');
fclose(fid);
command = strcat('C:\LSDYNA\program\ls-dyna_smp_d_R810_winx64_ifort131.exe
I="C:\Users\miriam\Documents\MATLAB\LSDynaInputDeck.dyn" S="intfor"');
system(command);
pause(1);
```

```
list = 'disk8';
while strcmp('disk8',list) == 1
    list = ls('disk8');
    pause(1);
end
fprintf(['c = %-10.5e\n',....
                'b1 = %-10.2e\n',....
                'b2 = %-10.2e\n',....
                'b3 = %-10.1e\n',....
                'K = %-10.0e'],...
(Constants(1)*weightc),Constants(2)*weightb,Constants(3)*weightb,Constants(4)
,...
(Constants(5)*weightk));
end

function [CSXnum,CSYnum,GSXnum,GSYnum] = LSpostprocessing(Dim)
PathName='C:\Users\miriam\Documents\MATLAB\';
filename = strcat(PathName,'lspostResults_processing.cfile');

state=num2str(Dim.nStates);
fid = fopen(filename, 'wt');
fprintf(fid,'open d3plot %sd3plot\n',PathName);
fprintf(fid,'state %s\n',state);
fprintf(fid,'fringe 1\n');
fprintf(fid,'pfringe\n');
fprintf(fid,['output %sCauchyStressX.txt 1:',state,' 1 0 1 0 0 0 0 1 0 0 0 0
0 0\n'],PathName);
fprintf(fid,'fringe 2\n');
fprintf(fid,'pfringe\n');
fprintf(fid,['output %sCauchyStressY.txt 1:',state,' 1 0 1 0 0 0 0 1 0 0 0 0
0 0\n'],PathName);
fprintf(fid,'fringe 201\n');
fprintf(fid,'pfringe\n');
fprintf(fid,['output %sGreenStrainX.txt 1:',state,' 1 0 1 0 0 0 0 1 0 0 0 0 0
0\n'],PathName);
fprintf(fid,'fringe 202\n');
fprintf(fid,'pfringe\n');
fprintf(fid,['output %sGreenStrainY.txt 1:',state,' 1 0 1 0 0 0 0 1 0 0 0 0 0
0\n'],PathName);
fprintf(fid,'exit\n');
fclose(fid);
system(strcat('C:\LSDYNA\program\lsprepost.exe
c=',PathName,'lspostResults_processing.cfile &'));

keep = 1; % if keep = 1: all elements are kept;
          % if keep = 2: 1/2 of elements are kept, etc.
n = ceil((Dim.MeshX-1)/keep)*ceil((Dim.MeshY-1)/keep)*(Dim.MeshZ-1);
Elnum = zeros(1,n);
CSX = zeros(Dim.nStates,n);
CSY = zeros(Dim.nStates,n);
GSX = zeros(Dim.nStates,n);
GSY = zeros(Dim.nStates,n);
CSXnum = zeros(Dim.nStates,1);
CSYnum = zeros(Dim.nStates,1);
GSXnum = zeros(Dim.nStates,1);
GSYnum = zeros(Dim.nStates,1);
```

```
for state = 1:1:Dim.nStates
    readfile = strcat(PathName,'CauchyStressX.txt');
    fid2 = fopen(readfile, 'rt');
    c = textscan(fid2, '%f %f','HeaderLines', (state-1)*(Dim.Nelems+8)+8);
    pause(1);
    tempel = 0;
    for kk = 1:(Dim.MeshZ-1)
        for jj = 1:ceil((Dim.MeshY-1)/keep)
            for ii = 1:ceil((Dim.MeshX-1)/keep)
                tempel = tempel+1;
            El =ii+(jj-1)*(Dim.MeshX-1)+(kk-1)*(Dim.MeshX-1)*(Dim.MeshY-1);
            CSX(state,tempel) = c{2}(El);
            end
        end
    end
    fclose(fid2);

    readfile = strcat(PathName,'CauchyStressY.txt');
    fid2 = fopen(readfile, 'rt');
    c = textscan(fid2, '%f %f','HeaderLines', (state-1)*(Dim.Nelems+8)+8);
    tempel = 0;
    for kk = 1:(Dim.MeshZ-1)
        for jj = 1:ceil((Dim.MeshY-1)/keep)
            for ii = 1:ceil((Dim.MeshX-1)/keep)
                tempel = tempel+1;
            El=ii+(jj-1)*(Dim.MeshX-1)+(kk-1)*(Dim.MeshX-1)*(Dim.MeshY-1);
            CSY(state,tempel) = c{2}(El);
            end
        end
    end
    fclose(fid2);

    readfile = strcat(PathName,'GreenStrainX.txt');
    fid2 = fopen(readfile, 'rt');
    c = textscan(fid2, '%f %f','HeaderLines', (state-1)*(Dim.Nelems+8)+8);
    tempel = 0;
    for kk = 1:(Dim.MeshZ-1)
        for jj = 1:ceil((Dim.MeshY-1)/keep)
            for ii = 1:ceil((Dim.MeshX-1)/keep)
                tempel = tempel+1;
            El=ii+(jj-1)*(Dim.MeshX-1)+(kk-1)*(Dim.MeshX-1)*(Dim.MeshY-1);
            GSX(state,tempel) = c{2}(El);
            end
        end
    end
    fclose(fid2);

    readfile = strcat(PathName,'GreenStrainY.txt');
    fid2 = fopen(readfile, 'rt');
    c = textscan(fid2, '%f %f','HeaderLines', (state-1)*(Dim.Nelems+8)+8);
    tempel = 0;
    for kk = 1:(Dim.MeshZ-1)
        for jj = 1:ceil((Dim.MeshY-1)/keep)
            for ii = 1:ceil((Dim.MeshX-1)/keep)
                tempel=tempel+1;
            El=ii+(jj-1)*(Dim.MeshX-1)+(kk-1)*(Dim.MeshX-1)*(Dim.MeshY-1);
```

```
            GSY(state,tempel) = c{2}(El);
            end
        end
    end
    fclose(fid2);


end
% Mean values over the elements kept
for state = 1:1:Dim.nStates
    CSXnum(state,1) = mean(CSX(state,:));
    CSYnum(state,1) = mean(CSY(state,:));
    GSXnum(state,1) = mean(GSX(state,:));
    GSYnum(state,1) = mean(GSY(state,:));

end

end

% Function resamplesVector creates a vector that spans the same range as
% VectorInput and resamples the data in it according to mode
% ('spline' or 'spline'). The vectors may be horizontal or vertical.
% Parameter outputSize is the dimension of VectorOutput.
function VectorOutput = resamplesVector(VectorInput,outputSize,mode)

    points = 1:outputSize;
    [nRows,nCols] = size(VectorInput);
    if nRows == 1
        xi = zeros(1,outputSize);
        xi(1,:) = 1 + (points - 1)*(nCols-1)/(outputSize-1);
        X = 1:1:nCols;
    elseif nCols == 1
        xi = zeros(outputSize,1);
        xi(:,1) = 1 + (points - 1)*(nRows-1)/(outputSize-1);
        X = 1:1:nRows;
        X = X';
    else
        errordlg('Input is not a vector');
    end
    VectorOutput = interp1(X,VectorInput,xi,mode);

end

function [c,ceq] = nonlinconstraints(Constants,weightb)
c=[((-1*((Constants(3)*weightb)^2))-
(2*(Constants(2)*weightb)*(Constants(3)*weightb)));(-
1*((Constants(3)*weightb)^2))-
(2*(Constants(2)*weightb)*(Constants(3)*weightb)-
((Constants(2)*weightb)*Constants(4))-
(3*(Constants(3)*weightb)*Constants(4)));(-
1*Constants(4)*((Constants(3)*weightb)^2))-
(2*(Constants(2)*weightb)*(Constants(3)*weightb)*Constants(4))];
ceq=[];
end
```